Universidade de Santiago de Compostela

PhD Thesis

Groundwater influence on soil moisture memory and land-atmosphere interactions over the Iberian Peninsula

Tésis Doctoral

Influencia de las aguas subterráneas en la memoria de la humedad de suelo y las interacciones tierra-atmósfera en la Península Ibérica

Autor:
Alberto Martínez de la Torre

Director:
Gonzalo Miguez Macho

Documento realizado para optar al título de Doctor
Grupo de Física No Lineal (*Non Linear Physics Group*)
Departamento de Física de la Materia Condensada

Santiago de Compostela, Marzo 2014

Declaración de autoría

Dr. Gonzalo Miguez Macho, docente e investigador titular de la Universidade de Santiago de Compostela, en el Departamento de Física de la Materia Condensada (Grupo de Fśica No Lineal),

CERTIFICA

El presente documento, *Groundwater influence on soil moisture memory and land-atmosphere interactions over the Iberian Peninsula*, fue realizado por **Alberto Martínez de la Torre** bajo su dirección, concluyendo de esa manera la Tésis Doctoral para optar al tt́ulo de Doctor

Firmado:

Santiago de Compostela, 28 de Marzo de 2014

UNIVERSIDADE DE SANTIAGO DE COMPOSTELA

Abstract

Departamento de Física de la Materia Condensada
Non Linear Physics Group

Groundwater influence on soil moisture memory and land-atmosphere interactions over the Iberian Peninsula

by Alberto Martínez de la Torre

Land-atmosphere coupling is a key factor in climate modeling research. This thesis is intended as a step forward in the model representation of groundwater influence on the land-atmosphere system. The Land Surface and Groundwater Model LEAFHYDRO is presented and evaluated. The model represents groundwater dynamics through 3 different interactions; *1*) two-way groundwater-soil fluxes, *2*) groundwater lateral flow, and *3*) two-way groundwater-streams exchange. 10-year simulations (WT run, with the groundwater scheme switched on, and FD run, with the groundwater scheme switched off) are performed over the Iberian Peninsula in order to study the influence of groundwater dynamics on soil moisture and evapotranspiration (ET) fluxes at seasonal and interannual timescales. The model is forced with daily analysis precipitation (0.2° spatial resolution). The model WT simulation is validated with observational water table depht (*wtd*) data; it captures well the shallow water table zones, the mean water table positions and the seasonal and interannual evolution. The simulation of the streamflow seasonal cycle in the WT run improves the simulation in the FD run when comparing with observations. The main results on groundwater influence on soil moisture and land-atmosphere fluxes are: *1*) the groundwater recharge presents positive patterns (upward capillary flux) over river valleys and shallow water table regions, the upward flux is maximal in summer; *2*) over the shallow water table regions ($wtd \leq 8$ m) the upward flux results in soil moisture increase (with a new shallow water table wet pattern in soil moisture fields) and reduces partly seasonality, since the soil moisture increase is stronger in spring and summer, when the surface balance $P - ET$ (precipitation minus evapotranspiration) is lower; *3*) the higher soil water availability results in ET enhancement (positive ET difference, WT-FD runs) over the shallow water table regions, seasonally the ET enhancement is greater in summer (34.4% increase, 0.54 mm dαy^{-1}) and spatially when analysing the different Iberian basins, the ET increase is more important in southern semiarid basins (21.4% yearly ET increase in the Guadalquivir basin and 28.4% in the Segura basin) and less significant in the northern Miño basin where ET is not water limited but energy limited (13.3%); *4*) the water table presents strong seasonal and interannual persistence, its time evolution responds slowly to long-term climatic conditions but not to seasonal or annual peaks and lows in precipitation; *5*) the water table persistence induces soil moisture memory over the shallow water table regions where soil and groundwater are hydraulically connected, and therefore the soil moisture "remembers" past wet years (buffering drought effects) and past dry years (making drought effects last longer); *6*) the soil moisture memory passes to the atmosphere as ET memory, and the yearly ET enhancement depends not only on the previous wet season (slow drainage by the presence of the water table keeps the soil wetter in the WT run and therefore there is more soil water availability during the ET season to cover ET demands) but also on the *wtd* long-term trend. This results will have important impacts on seasonal forecast when using fully coupled groundwater-soil-atmosphere models (precipitation recycling, summer temperature decrease).

Acknowledgements

Thanks in the first place to my thesis director, Dr. Gonzalo Miguez Macho, for the chance he gave me to work in modeling research, for his guidance, for all the things I have learnt from him and for his friendship. Thanks to the researchers that invited me to do research stays abroad: Gianpaolo Balsamo from the ECMWF, Ying Fan and Haibin Li from Rutgers University, and Pedro Viterbo and Pedro M. Soares from the Universidade de Lisboa. Thanks to the *Supercomputing Centre of Galicia* (CESGA), that gave me and my colleagues priceless tools to carry out our research. Thanks to MeteoGalicia, the *Agencia Estatal de METeorología* (AEMET, Spain), the *Instituto Portugues do Mar e da Atmosfera* (IPMA), the Spanish *Ministery of Narutal Environment*, the *Instituto Geográfico y Minero de España* (IGME), several Spanish *Confederaciones Hidrográficas*, and the *Sistema Nacional de Informaçao de Recursos Hídricos* (SNIRH) for the data provided. Thanks to the Spanish *Ministery of Education and Science* and the *European Commission* for they financed this research.

Aprovecho también para agradecer por su trabajo, su compañerismo, su apoyo, su sentido del humor y su amistad a mis compañeros del Grupo de Física No Lineal. A los que están; Dani Garaboa somos todos, Dáário, Xaco Guiu, Jorge 24/7, Breo el nuevo, y Carlos (el hombre que ostenta el título de persona más buena del mundo). Y a los que se fueron; Alexandre que ha compartido todo el viaje conmigo, Lucía que se marcho a medio camino pero dejo su huella, Dani Cuiñas que me enseño todo lo que sé, a Florian y Alexandra que me invitaron a la mejor boda, a Jorge Carballeira, a Guillermo que de vez en cuando se deja ver, a Alberto Pérez Muñunzuri, que no sé si se fué o se quedó, y a Vicente Pérez Muñunzuri que está pero no está.

Gracias a todos los amigos de Santiago, que me han hecho sentir como uno más desde que llegué, Nuria, Marcos, Consu-Quique-Teo-Antón, Olalla, Iria, Roberto, Raquel, los compaẽros del fútbol, los del comunio,...

Gracias a mis amigos de casa, que no han dejado de subir a verme y de paso ponerse moraos, Miguel, Luis, Laura, Cristina, Gálvez, Carlos, Raúl, el otro Carlos,....

Gracias a mi familia, que estaba esperando a que leyese para subir (ya no teneis escusa), Papa, Mama, Pili y Antonio. Y al resto de familia de Jaén que siempre preguntaba para cuando...

Gracias a miniña, que siempre está ahí conmigo y sin la cual no podría haber hecho este trabajo, ni muchas otras cosas.

Contents

Abstract iii

Acknowledgements iv

List of Figures vii

Summary xi

Resumen xvii

1 Introduction 1
- 1.1 Natural Water Cycle . . . 1
- 1.2 Climate variability in the Iberian Peninsula . . . 3
  - 1.2.1 Precipitation variability in the Iberian Peninsula . . . 5
  - 1.2.2 Droughts in the Iberian Peninsula . . . 8
- 1.3 The groundwater link to the land-atmosphere system . . . 9
  - 1.3.1 The soil moisture link to the atmosphere . . . 9
  - 1.3.2 The groundwater link to soil moisture and land-atmosphere fluxes . . . 11
  - 1.3.3 The groundwater link to streamflow . . . 12
  - 1.3.4 The importance of a correct representation of groundwater interactions in the Iberian Peninsula . . . 13

2 LEAFHYDRO Land Surface and Groundwater Model description 17
- 2.1 Land surface and soil layers formulation . . . 20
  - 2.1.1 Soil formulation . . . 20
  - 2.1.2 Snow and temporary surface water formulation . . . 22
  - 2.1.3 Surface vegetation formulation . . . 24
  - 2.1.4 Surface bare ground formulation . . . 26
  - 2.1.5 Canopy-atmosphere fluxes . . . 27
  - 2.1.6 Precipitation fluxes . . . 28
  - 2.1.7 Radiative fluxes . . . 28
  - 2.1.8 Surface balances . . . 30
- 2.2 Dynamic groundwater scheme . . . 31
  - 2.2.1 Groundwater recharge formulation . . . 32
  - 2.2.2 Groundwater lateral flow formulation . . . 35
  - 2.2.3 Groundwater-streams exchange formulation: Gaining and losing streams . . . 37
- 2.3 River flow scheme . . . 40

3 LEAFHYDRO simulation settings. Initial conditions and forcings 43
- 3.1 10-year simulations . . . 43
- 3.2 Initial conditions . . . 44

3.2.1 Land, vegetation and soil parameters . . . 44
3.2.1.1 Topography . . . 44
3.2.1.2 Vegetation parameters . . . 45
3.2.1.3 Soil parameters . . . 46
3.2.2 Equilibrium Water Table Depth . . . 46
3.2.3 Soil moisture initialization . . . 49
3.2.4 River parameters . . . 50
3.3 Atmospheric forcings . . . 52

4 LEAFHYDRO 10-year simulation validation 53
4.1 Water table depth and time evolution: validation with observations . . . 55
4.1.1 Observational *wtd* data . . . 55
4.1.2 Model performance . . . 56
4.2 Modeled streamflow: validation with streamflow observations . . . 58
4.2.1 River flow scheme in the FD simulation . . . 59
4.2.2 Observational streamflow data . . . 60
4.2.3 Validation and WT-FD streamflow comparison . . . 61
4.2.4 Winter streamflow underestimation . . . 65
4.3 Discussion . . . 67

5 Water table effects on the land-atmosphere system. Spatial and seasonal variability 69
5.1 Water table control on soil moisture . . . 69
5.2 Water flux across the water table: Recharge . . . 74
5.2.1 Long-Term Recharge . . . 74
5.2.2 Seasonal variability . . . 76
5.3 Enhanced Evapotranspiration (ET) . . . 77
5.4 Discussion . . . 80

6 Soil moisture memory induced by the water table 83
6.1 Water table seasonal and interannual persistence . . . 84
6.2 The effects of water table persistence on soil moisture memory . . . 86
6.2.1 Analysis over the Iberian Peninsula . . . 86
6.2.2 A closer look: *La Mancha Húmeda* . . . 90
6.2.2.1 Soil moisture memory induced over the localized shallow water table zone . . . 90
6.2.2.2 The effects of soil moisture memory on evapotranspiration (ET) . . . 93
6.3 Discussion . . . 95

7 Water table integrated effects over the main Iberian river basins 97
7.1 Main Iberian basins . . . 97
7.2 Seasonal and long-term time evolution . . . 99
7.2.1 Atlantic basins . . . 99
7.2.2 Mediterranean basins . . . 104
7.3 Discussion . . . 106

8 Conclusions 109

Bibliography 113

List of Figures

1.1 Natural water cycle sketch . . . 2
1.2 Koppen-Geiger classification climates for the Iberian Peninsula and the Balearic Islands . . . 4
1.3 Mean yearly precipitation for the period 1950-2007 in the Iberian Peninsula. Division of 7 pluviometric regions with different precipitation regimes . . . 6
1.4 Trends of the mean yearly precipitation at the pluviometric regions . . . 7
1.5 Fraction of natural flow in the Iberian rivers . . . 15

2.1 LEAFHYDRO storage reservoirs and water and energy fluxes sketch . . . 19
2.2 LEAFHYDRO soil column layers sketch . . . 21
2.3 LEAFHYDRO groundwater balance in a model cell . . . 31
2.4 LEAFHYDRO double scenario to calculate groundwater recharge . . . 33
2.5 LEAFHYDRO double scenario to calculate groundwater lateral flow . . . 36
2.6 Gaining and losing streams sketch. Representation of the cases in nature (left) and in LEAFHYDRO (right) . . . 38
2.7 Typical river in nature (left) and its representation with the surface water balance fluxes in LEAFHYDRO (right) . . . 41

3.1 Topography used in the LEAFHYDRO simulations . . . 44
3.2 Vegetation type . . . 45
3.3 Initial Iberian Peninsula Equilibrium Water Table Depth . . . 47
3.4 Iberian Peninsula groundwater recharge recharge . . . 48
3.5 Iberian Peninsula Equilibrium Water Table Depth, calculated with a LEAFHYDRO 10-year test run recharge . . . 49
3.6 Sketch for the methodology to calculate river parameters . . . 51

4.1 Water table depth validation . . . 57
4.2 River streamflow stations . . . 60
4.3 Forcing precipitation, observed streamflow and natural streamflow at the Alcalá del Río Station for the period with observed data availability (Jan/1989-Sep/1995) . . . 61
4.4 River streamflow validation . . . 62
4.5 LEAFHYDRO streamflow simulation skill scores . . . 65
4.6 Observed daily drecipitation at 4 stations from the MeteoGalicia observation network and IB02 analysis precipitation . . . 66

5.1 Soil soisture difference (WT-FD) and water table depth patterns . . . 70
5.3 Seasonal soil moisture difference (WT-FD) averaged over shallow water table zones . . . 73
5.4 Long-Term Recharge and mean precipitation forcing . . . 75
5.5 Mean seasonal recharge . . . 76
5.6 Mean seasonal evapotranspiration . . . 78
5.7 Mean seasonal evapotranspiration difference (WT and FD) . . . 79

6.1 Seasonal anomaly plots for precipitation and *wtd* 85
6.2 Hydrological year anomaly plots for precipitation, *wtd* and soil moisture difference (WT-FD) 87
6.3 Yearly anomalies time series correlations for the Iberian Peninsula (precipitation vs. soil moisture and *wtd* vs. soil moisture) 89
6.4 Anomalies spatial correlations for the Iberian Peninsula (precipitation vs. soil moisture and *wtd* vs. soil moisture) along the 9 complete hydrological years simulated and total yearly precipitation 90
6.5 Zoomed hydrological year anomaly plots for precipitation, soil moisture and *wtd* 92
6.6 Zoomed hydrological year anomaly plots for precipitation and ET 94

7.1 Main river basins in the Iberian Peninsula (left) and mean seasonal precipitation (right) 98
7.2 Atlantic basins time evolution (precipitation, *wtd*, soil moisture difference and enhanced ET). Spectrum analysis (*wtd* and soil moisture) . . . 100
7.3 Atlantic basins time evolution (continuation) 101
7.4 Mean yearly enhanced ET and ET increase in the WT simulation, Atlantic basins 103
7.5 Time series for yearly Enhanced ET, Atlantic basins 103
7.6 Mediterranean Basins Time Evolution (precipitation, *wtd*, soil moisture difference and enhanced ET). Spectrum analysis (*wtd* and soil moisture) 105
7.7 Time series for yearly Enhanced ET, Mediterranean basins 106

Al tito Rafa

Summary

Motivation

Climate change can only be assessed with Earth System Models. It is essential to understand how well the models represent the processes and feedbacks that take part in the climate system that couples the atmosphere, the ocean and the land surface. It is in this context, that this thesis attempts to contribute in the model representation of climate.

Groundwater is 30.1% of the total fresh water on Earth [107]. In the global hydrological cycle, water fluxes from soil storage to groundwater reservoir are estimated to be 46,000 km^3 yr^{-1}, and from the groundwater reservoir to the rivers and lakes 43,800 km^3 yr^{-1} [34]. These figures reveal the importance of the groundwater reservoir within the Earth fresh water. It is well known that groundwater interacts with the soil above, with surface water and with the ocean. But, ***1)*** **how does groundwater affect climate?**, *2)* is groundwater a player in land-atmosphere coupling?, *3)* can groundwater interactions with the land-atmosphere system be represented in land surface models?, *4)* in semiarid regions of the interior Iberian Peninsula, for instance, where land-atmosphere coupling plays an important role in precipitation recycling [93] and there are measured evidences of shallow water tables during dry years due to previous wet episodes [80], will a model representation of the groundwater interactions with the land-atmosphere system make a difference in climate simulations?

The working hypothesis is that **YES** answers Questions *2*, *3* and *4*. Testing the hypothesis and seeking an answer to **Question *1*** motivate this thesis work in the USC *Non Linear Physics Group*.

Thesis structure and brief resume

This thesis is understood as self contained modelling research experiment. It is organised in eight chapters. It begins with a general introduction of the problem: assessing the groundwater influence on the land-atmosphere system over the Iberian

Peninsula (Chapter 1), a description of the main modeling tool: LEAFHYDRO, a Land Scheme and Groundwater Model (Chapter 2), and a description of the experimental settings; simulations, initial conditions and forcings (Chapter 3). Then a validation of the main simulation with observational water table depth and streamflow data is performed to support the thesis findings (Chapter 4). The results are divided in three different categories of the water table effects; water table effects on the land-atmosphere system and their spatial and seasonal variability (Chapter 5), soil moisture memory induced by the water table (Chapter 6) and water table integrated effects over the main Iberian river basins (Chapter 7). Finally, the general conclusions and future efforts in the line of research are presented (Chapter 8).

A brief resume of the thesis is presented next:

Chapter 1 presents a general introduction in order to contextualise this research. Firstly, a brief description of the natural water cycle and its main reservoirs and processes is given. The groundwater reservoir plays an important role in the natural water cycle; *a*) interacting with the unsaturated zone of the soil through gravitational drainage and capillary rise (groundwater recharge), *b*) transporting groundwater within the saturated zone, driven by topography (lateral groundwater flow), and *c*) interacting with the rivers and lakes, receiving infiltration and feeding the baseflow (groundwater-streams exchange). Secondly, an Iberian Peninsula climate variability description, including long-term precipitation analysis, introduces the area of study. The need to be cautious investigating hydrological processes in the peninsula is pointed out, dividing it into basins or hydrological zones and studying long-term periods, since the pluviometric regimes differ greatly within the peninsula and several-year long droughts occur all over it. Finally, an overview of recent efforts in assessing the groundwater link to soil moisture, land-atmosphere fluxes and surface streams concludes the chapter, focussing on the importance of considering groundwater dynamics in Iberian Peninsula modeling research.

In **Chapter 2**, the main tool used in this thesis to assess the role of groundwater dynamics in the Iberian Peninsula soil moisture and land-atmosphere fluxes is presented and described: the Land Surface and Groundwater Model LEAFHYDRO. The model represents energy and water storages and vertical exchanges in the land surface based on the original Land Surface Model LEAF (*Land Ecosystem-Atmosphere Feedback*) [63, 64], and also represents the groundwater reservoir based on a dynamic groundwater scheme first presented by *Miguez-Macho et al.* (2007) [83], that has been continuously developed and reviewed since then as part of an ongoing collaborative work between the USC *Non-Linear Physics Group* and the *Rutgers University Department of Environmental Sciences*.

The first section of the chapter introduces LEAFHYDRO methodology for the land surface and the unsaturated soil layers (up to 4 m deep), consisting of the calculation of incoming and outgoing water and heat fluxes for each layer and surface represented, and the prognosis of temperature and moisture values through water

mass and energy balances once the fluxes are known. A review of these calculations is presented, starting by the unsaturated soil formulation and following up through snowcover and temporary surface water, vegetation, bare ground, canopy air, precipitation and radiation. The second section of the chapter is a complete presentation of the LEAFHYDRO dynamic groundwater scheme, where the groundwater interactions and their model representation are detailed: two-way groundwater-soil fluxes, groundwater lateral flow and two-way groundwater-streams exchange. The chapter concludes with a description of the river flow scheme that closes the water cycle in the model.

In **Chapter 3**, the main experiment carried out in this thesis is described first. The experiment consists of two LEAFHYDRO 10-year period simulations with a 2.5 × 2.5 km grid; *1*) the WT (Water-Table) run with the dynamic groundwater scheme switched on, that closes the Iberian Peninsula long-term water cycle accounting for the groundwater interactions with the soil and the land surface, and *2*) the FD (Free-Drain) run with the dynamic groundwater scheme switched off, that uses the commonly adopted free-drain approach, where soil water is allowed to drain out of the soil column at a rate set by the bottom soil layer hydraulic conductivity. Comparing the WT and FD runs, the influence of groundwater can be isolated.

Then, the model initial topography, vegetation and soil parameters are shown. For the water table and soil moisture initialization, an initial Iberian Peninsula Equilibrium Water Table Depth estimation by *Gestal-Souto et al.* (submitted) [47] is used, based on a two-dimensional groundwater model [42] that finds a balance between the atmospheric influence in the form of groundwater recharge and the topographic influence in the form of gravity-driven lateral convergence. The process to obtain a more realistic initial water table condition using the yearly groundwater recharge from a LEAFHYDRO 10-year test run is described, as is the calculation of the initial soil moisture conditions using Richards' Equation for soil water movement and the water table initial position. The initial river parameters origin and processing, as well as the use of surface atmospheric forcings from ERA-Interim reanalysis and Iberian Peninsula precipitation analysis (0.2° spatial resolution), are detailed.

In **Chapter 4**, water table depth (*wtd*) and streamflow observational data are used to validate the LEAFHYDRO simulations and hence support the results in following chapters. The chapter is introduced with a discussion about the model parameterization of local lateral groundwater flow, which resolves subgrid internal drainage and results in a baseflow consistent with topography and climate, and not solely dependant on vertical fluxes or the water table position. A realistic water table spatial distribution and time evolution is essential to assess the groundwater-soil link, and model performance validation with observational *wtd* data at 623 stations shows; *1*) the model captures shallow water table positions ($wtd \leq 8$ m; greater connection to the land surface), as 66.0% of the observational shallow points are also shallow in the model; *2*) the model captures the mean water table positions, as 33.0%

of the shallow water table stations present less than 2 m difference between simulated and observed *wtd* means (14.0% when all stations are considered); and *3*) the seasonal cycle and long-term trends are realistically represented in the model, as 32.3% of the observed time series present a correlation coefficient greater than 0.5 with the simulated time series.

The representation of streamflow, as the last player in the water cycle discharging ultimately to the ocean, closes the water budget in the model. From validation with observational streamflow data and comparison between the FD and WT runs, the streamflow seasonal cycle is found to be differently represented by both runs; winter higher and closer to observations streamflow in the FD run, better representation of summer baseflow in the WT run, and faster recovery of streamflow when the autumn precipitation begins (September-October) following observations in the WT run. Correlation coefficients between observed and simulated streamflow time series indicate the better simulation of the seasonal cycle and interannual variability by the WT run. Nevertheless, a clear underestimation of the wet season (especially by the WT run) constrains the model performance at simulating streamflow. The chapter concludes with a discussion on future efforts to better represent the model streamflow and therefore strengthen the line of research of this thesis; improvement of the deeper soil-groundwater linkage, improvement of surface runoff triggered by heavy rainstorms or snowcover depletion, and improvement of subgrid scale geological features representation.

In **Chapter 5**, a study of the groundwater effects on the land-atmosphere system and their seasonal and spatial variability is carried out, using the WT and FD simulations. Soil moisture shows that the water table makes the soil wetter over shallow water table regions, introducing a new pattern in soil moisture fields different to the climatic conditions and soil texture patterns. Analysing seasonal means, the water table influence on soil moisture is found to reduce partly seasonality, since soil wetness increase over the shallow water table regions is greater at water scarcity seasons (24.4% in spring, when evapotranspiration – ET – reaches the maximum rates, and 23.8% in summer, when soil moisture is at a minimum due to the lack of precipitation and high ET rates), and lower in autumn and winter ($\sim$ 20%), when the surface water balance ($P - ET$, precipitation minus evaporation) is higher. The Long-Term Recharge is presented as the mean yearly water table flux, showing a positive pattern (upward recharge via capillary flux), as a result of lateral groundwater convergence and river infiltration, over extended shallow water table regions and river valleys. Groundwater recharge seasonal variability is found to respond to the surface precipitation and ET with two different cycles: *1*) the *negative recharge* (downward drainage) is stronger during winter and spring, responding to drainage of infiltrated precipitation from the wet season, and weaker during summer and autumn after the dry season; *2*) the *positive recharge* is strong in spring and maximal in summer (ET season in the Iberian Peninsula), due to the gradual decrease of the surface water balance, then during autumn it weakens significantly due to

the decrease of ET demands, and finally it reaches the minimum in winter, when precipitation presents the highest rates and ET the lowest.

The soil moisture increase by the water table presence via upward capillary fluxes translate to the atmosphere as ET enhancement. The ET difference between the WT and FD simulations present the spatial pattern induced in soil moisture by the water table (reaching significant differences over river valleys and shallow water table regions in the semiarid interior Iberia). The enhanced ET averaged over the Iberian Peninsula is 0.54 mm day^{-1} in summer, when precipitation is the lowest and ET demands are high, 0.24 mm day^{-1} in spring, when ET demands are the highest, 0.14 mm day^{-1} in autumn and 0.05 mm day^{-1} in winter, when the ET demands are very low. To conclude the chapter, convective precipitation enhancement and summer temperature decrease are discussed as potential effects of these water table dynamics results on fully coupled groundwater-land-atmosphere modeling research.

The choice of a 10-year simulation period including dry and wet episodes allows a deeper look into the water table influence on soil moisture, and in **Chapter 6** the water table seasonal and interannual persistence and soil moisture memory that it induces is studied over the peninsula. The time evolution of the water table does not respond immediately to seasonal or yearly peaks and lows in precipitation, but it responds to long-term climatic conditions with 1-2 years delay. When the water table enters the soil-atmosphere system in the WT simulation, its persistence passes to the soil as soil moisture memory, and the soil "remembers" past dry and wet conditions, buffering drought effects on soil moisture and delaying the recovery after the drought in spite of wetter conditions.

The soil moisture memory induced by water table persistence is stronger over shallow water table regions, where soil and groundwater are hydraulically connected. Analysing hydrological year (September-August) anomalies for precipitation, soil moisture and water table depth over a well known shallow water table region in the upper Guadiana basin (*La Mancha Húmeda*), the water table influence on soil moisture memory is inferred. Moreover, soil moisture memory is passed to the atmosphere as ET memory over this shallow water table region.

In **Chapter 7**, the groundwater effects on soil moisture and land-atmosphere fluxes, analysed in previous chapters at seasonal and interannual timescales, are studied as area average over the main Iberian river basins, as the basins integrate the groundwater influence through lateral flow convergence. This allows to investigate the groundwater role in the land-atmosphere system under different climatic conditions. At basin scale, the water table presence, through slow drainage and soil moisture accumulation during the wet season and upward capillary rise during the dry season, induces ET enhancement during spring and summer in the WT simulation. This groundwater influence on ET is more significant in southern basins of semiarid climates of water limited ET (yearly ET increases 28.4% in the Mediterranean Segura basin and 21.4% in the Atlantic Guadalquivir basin), but as the ET is

less water limited towards the northern basins, the groundwater is less influential on ET fluxes (13.3% in the northern Miño basin, where ET is energy limited).

The time evolution of ET increase (WT-FD) follows the long-term trends of the *wtd* evolution, caused by consecutive dry and wet years. Hence, the water table persistence is passed to the atmosphere as ET memory at basin scale, and the yearly ET enhancement in the WT run depends not on only the previous wet season but also on the long-term *wtd* evolution. This is observed clearly over the Atlantic basins. Over the Mediterranean basins, that present moderate wet season and variable dry season, the ET memory is constrained by the intensity of the dry season (less memory when the summer precipitation is especially low because the ET enhancement is high, and when the dry season is especially high because the ET enhancement is low, in both cases the intensity of the dry season takes over the *wtd* trend).

Finally, in **Chapter 8**, a summary of the main conclusions drawn through the investigation is presented, where an attempt to answer the initial Questions is produced. A review of future efforts in this line of research concludes the thesis.

Early stage results of this investigation have been published in the article "*The role of groundwater on the Iberian climate, precipitation regime and land-atmosphere interactions*" [47]. However, the main results are in preparation to be submitted for publication in the article "*Groundwater influence on soil moisture memory and land-atmosphere interactions over the Iberian Peninsula*" [26]. A high resolution estimation for the Iberian Peninsula Equilibrium Water Table Depth, from the a long-term recharge estimation obtained from LEAFHYDRO simulations is also in preparation to complete and submit the article "*Water Table Depth and Potential Capillary Flux to the Land Surface in the Iberian Peninsula*" [48].

Resumen

Motivación

El cambio climático sólo se puede evaluar con el uso de "Earth System Models". Por tanto, es esencial conocer en que medida los modelos representan los procesos e interacciones que tienen lugar en el sistema climático, que conecta la atmósfera con los océanos y la superficie terrestre. En este contexto, esta tésis doctoral contribuye a la representación del clima en modelización.

Las aguas subterráneas constituyen un 30.1% del total de agua dulce en la Tierra [107]. Dentro del ciclo hidrológico global, los flujos de agua desde el suelo hacia las aguas subterráneas está estimado en 46,000 km^3 $año^{-1}$, y desde las aguas subterráneas hacia los ríos y lagos en 43,800 km^3 $año^{-1}$ [34]. Estas cifras hablan de la importancia de las aguas subterráneas dentro del sistema global de agua dulce. Es bien sabido que las aguas subterráneas interactúan con las capas de suelo sobre ellas, con las aguas superficiales y con los oceános. Pero, ***1) ¿cómo afectan las aguas subterráneas al clima?***, *2)* ¿afectan las aguas subterráneas al acoplamiento tierra-atmósfera?, *3)* ¿pueden los modelos de suelos representar las interacciones de las aguas subterráneas con el sistema tierra-atmósfera?, *4)* en zonas de clima semiárido del interior de la Península Ibérica, por ejemplo, donde el acoplamiento tierra-atmósfera desempeña un papel importante en el reciclaje de precipitatción [93] y existen evidencias observadas de capa freática cerca de la superficie durante años secos debido a previos episodios húmedos [80], ¿supondrá un valor añadido la representación de las interacciones de las aguas subterráneas con el sistema tierra-atmósfera en simulaciones climáticas?

La hipótesis de trabajo de esta tésis es que las Preguntas *2*, *3* y *4* tienen **SI** como respuesta. Probar la hipótesis y buscar una respuesta a la **Pregunta *1*** son las motivaciones para el desarrollo de esta investigación en el *Grupo de Física No Lineal* de la Universidad de Santiago de Compostela.

Estructura y breve resumen de la tésis

Este trabajo de tésis doctoral se entiende como una investigación experimental autocontenida. Se organiza en ocho capítulos, comenzando con una introducción del problema científico: evaluación de la influencia de las aguas subterráneas en el sistema tierra-atmósfera de la Península Ibérica (Capítulo 1), una descripción de la herramienta de trabajo principal: el Modelo de Suelos y Aguas Subterráneas LEAFHYDRO (Capítulo 2), y una descripción del experimento; simulaciones, condiciones iniciales y forzamientos (Capítulo 3). Después se lleva a cabo una validación de la simulación principal con datos de observación de profundidad de capa freática y caudal de ríos, para apoyar los resultados de la investigación (Capítulo 4). Los resultados se dividen en tres tipos de efectos de las aguas subterráneas analizadas; efectos de la capa freática en el sistema tierra-atmósfera y su variabilidad espacial y estacional (Capítulo 5), memoria de la humedad de suelo inducida por la capa freática (Capítulo 6) y efectos integrados de la capa freática en las principales cuencas ibéricas (Capítulo 7). Finalmente, se presentan las conclusiones generales y planes futuros en esta línea de investigación (Capítulo 8).

A continuación se presenta un breve resumen de la tésis:

El **Capítulo 1** presenta una introducción general con el objeto de contextualizar este trabajo de investigación. En primer lugar, se ofrece un breve descripción del ciclo hidrológico y sus principales componentes y procesos. Las aguas subterráneas desempeñan una función importante en el ciclo hidrológico; *a*) interacción con el suelo no saturado a través de drenaje por gravedad y flujo capilar ascendente (recarga), *b*) transporte de agua dentro de la zona saturada, inducido por la topografía (flujo lateral de aguas subterráneas), y *c*) interacción con los ríos y lagos, recibiendo infiltración y manteniendo el caudal base (intercambio entre aguas subterráneas y superficiales). En segundo lugar, se introduce la región de estudio (Península Ibérica) con una descripción de la variabilidad climática, usando datos de análisis de precipitación. Se insiste en la necesidad de ser minuciosos cuando se afronta investigación hidrológica en la Península Ibérica, debido a la diversidad de regímenes pluviométricos que presenta y la ocurrencia frecuente de sequías. En último lugar, se realiza un repaso sobre esfuerzos recientes en la comunidad científica para investigar el acoplamiento entre las aguas subterráneas y la humedad de suelo, los flujos tierra-atmósfera y las aguas superficiales. Finalmente, se cierra el capítulo, centrándose en la importancia de tener en cuenta las interacciones de las aguas subterráneas cuando se abordan trabajos de investigación con modelos hidrológicos y atmosféricos en la Península Ibérica.

En el **Capítulo 2**, se presenta y describe la herramienta principal que se va a usar en la evaluación del papel de las aguas subterráneas, en la humedad de suelo y los flujos tierra-atmósfera en la Península Ibérica: el Modelo de Suelos y Aguas Subterráneas LEAFHYDRO. El modelo representa los principales componentes de la superficie terrestre que almacenan energía y agua, y los flujos verticales entre ellos,

basándose en el Modelo de Suelos LEAF original [63, 64]. Pero además representa las aguas subterráneas basándose en una implementación de dinámica de aguas subterráneas presentada inicialmente por *Miguez-Macho et al.* (2007) [83], y que ha sido desarrollada y revisada de forma continuada desde entonces, como parte de un trabajo de colaboración entre el *Grupo de Física No Lineal* de la Universidad de Santiago de Compostela y el *Departamento de Ciencias Ambientales* de Rutgers University (EEUU).

La primera sección del capítulo describe la metodología que usa LEAFHYDRO para la superficie terrestre y la zona no saturada del suelo (entre la superficie y 4 m), que consiste en el cálculo de flujos de agua y calor entrantes y salientes en cada superficie y capa de suelo representada, y el pronóstico de temperatura y humedad a través de balances de masa y energía una vez que los flujos son conocidos. Se repasan las formulaciones para estos cálculos, empezando por las capas de suelo y siguiendo hacia arriba; nieve y aguas superficiales temporales, vegetación, superficie no cubierta por vegetación, canopía, precipitación y radiación. La segunda sección del capítulo es una presentación completa de la implementación de dinámica de aguas subterráneas de LEAFHYDRO, donde las interacciones y sus representaciones en el modelo son detalladas: flujo bimodal entre las aguas subterráneas y el suelo, flujo lateral dentro de las aguas subterráneas y flujo bimodal entre las aguas subterráneas y superficiales (ríos y lagos). El capítulo concluye con una descripción de la implementación de caudeles de ríos que cierra el ciclo hidrológico en el modelo.

En el **Capítulo 3** se describe primero el experimento principal de la tésis, que consiste en dos simulaciones de un periodo de 10 años con LEAFHYDRO en una malla de 2.5 km de resolución horizontal; *1*) la simulación WT (WaterTable) con la implementación de dinámica de aguas subterráneas conectada, que cierra el ciclo hidrológico a largo plazo en la Península Ibérica considerando las interacciones entre las aguas subterráneas, el suelo y la superficie terrestre, y *2*) la simulación FD (FreeDrain) con la implementación de aguas subterráneas desconectada, que usa la técnica comunmente adoptada "free-drain", con la que el agua que llega a la última capa de suelo resuelta por el modelo drena fuera del sistema a una velocidad marcada por la conductividad hidraúlica de la última capa. La influencia de las aguas subterráneas en el sistema tierra-atmósfera se puede aislar y evaluar comparando las simulaciones WT y FD.

Después se muestran los condiciones iniciales de topografía, vegetación y parámetros del suelo. Para la inicialización de profundidad de la capa freática y humedad de suelo, se usa una estimación de la Profundidad de Capa Freática de Equilibrio, elaborada por *Gestal-Souto et al.* (submitted) [47] mediante el uso de un modelo bidimensional de aguas subterráneas [42] que encuentra una profundidad de equilibrio entre la influencia atmosférica en forma de recarga climatológica y la influencia topográfica en forma de convergencia lateral inducida por gravedad. El proceso llevado a cabo para obtener una capa freática inicial más realista mediante

el uso de recarga anual obtenida de una simulación "test" con LEAFHYDRO es descrito a continuación, así como el calculo de la humedad de suelo inicial mediante la Ecuación de Richards para el movimiento de agua y la profundidad de capa freática inicial. Se describe el origen de los parámetros de ríos y el preprocesado para su obtención. Finalmente se describen los datos de forzamiento de la base de reanálisis ERA-Interim y una base de análisis de precipitación en la Península Ibérica de 0.2° de resolución espacial.

En el **Capítulo 4** se usan datos de observación de profundidad de capa freática (*wtd*) y caudal de ríos para validar las simulaciones y sustentar así los resultados en próximos capítulos. El capítulo comienza con una reflexión sobre la parametrización de flujo lateral de aguas subterráneas a escala local del modelo, que resuelve implícitamente el drenaje interno de las celdas y resulta en un caudal base consistente con la topografía y el clima, y no exclusivamente dependiente de flujos verticales o la posicitón de la capa freática, como sucede en otros modelos. Para la evaluación del acoplamiento entre el suelo y las aguas subterráneas, son esenciales tanto una distribución espacial de capa freática como una evolución temporal realistas, y la validación del modelo con 623 estaciones de observación de profundidad de capa freática concluye que; *1*) el modelo captura las zonas de capa freática superficial ($wtd \leq 8$ m; mayor conexión hidraúlica con el suelo), ya que el 66.0% de los puntos de observación superficiales son indentificados como tales en el modelo; *2*) el modelo captura las posiciones medias de capa freática, ya que el 33.0% de las estaciones de capa freática superficial presentan una diferencia menor de 2 m entre las *wtd* medias simuladas y observadas (14.0% si se consideran todas las estaciones); y *3*) el ciclo estacional y las tendencias a largo plazo son representadas de forma realista en el modelo, ya que el 32.3% de las series temporales observadas presentan una correlación mayor de 0.5 con las series simuladas.

La representación de los caudales como último participante en el ciclo hidrológico, descargando hacia los oceános, cierra el balance hidrológico en el modelo. A partir de la validación con observaciones y comparación entre los caudales simulados en WT y FD, se concluye que el ciclo estacional representado por el modelo es muy diferente en ambas simulaciones; caudal más alto y cercano a las observaciones en invierno con la simulación FD, mejor representación del flujo base de verano con la simulación WT, y recuperación más rápida de caudal cuando comienzan las lluvias de otoño (Septiembre-Octubre) en la simulacón WT, siguiendo a las observaciones. Los coeficientes de correlación entre series temporales de caudal observado y simulado indican la mejor simulación del ciclo estacional y la variabilidad interanual en la simulación WT. Sin embargo, hay que apuntar una clara subestimación del caudal invernal (especialmente en la simulación WT) que condiciona la actuación del modelo. El capítulo finaliza con una explicación de posibles causas de la subestimación de caudal invernal y planes para mejorar la representación del caudal en el modelo; mejora de la representación de la conexión entre capas profundas de suelo y las aguas subterráneas cuando la capa freática es profunda, mejora de la escorrentía superficial amplificada por tormentas de lluvia o fundimiento de nieve

en zonas montañosas, y mejora de la representación de características geológicas del suelo a mayor resolución que la del modelo.

En el **Capítulo 5** se estudian los efectos de las aguas subterráneas en el sistema tierra-atmósfera y su variabilidad espacial y estacional, usando las salidas de las simulaciones WT y FD. La humedad del suelo revela un patrón más húmedo en zonas de capa freática superficial, que se suma a los patrones de tipo de suelo y condiciones climáticas. Analizando medias estacionales, se observa que la influencia de la capa freática en la humedad de suelo reduce parcialmente la estacionalidad, ya que el aumento humedad de suelo en las zonas de capa freática superficial ($wtd \leq 8$ m) es mayor en estaciones de escasez de agua (24.4% en primavera, cuando la evapotranspiración – ET – alcanza valores máximos, y 23.8% en verano, cuando la humedad de suelo es mínima debido a la ausencia de precipitación y alta ET, y menor en otoño e invierno ($\sim$ 20%), cuando el balance de agua en superficie ($P - ET$, precipitación menos evapotranspiración) es más alto. Se presenta la Recarga Climatológica, calculada como el flujo medio anual a través de la capa freática, que muestra un patrón de recarga positiva (flujo capilar ascendente), como resultado de la convergencia lateral de aguas subterráneas e infiltración desde los ríos, extendido sobre regiones de capa freática superficial y valles. La variabilidad estacional de la recarga responde a la precipitación y ET en la superficie con dos ciclos diferenciados: *1*) la *recarga negativa* (drenaje gravitacional) es más fuerte durante invierno y primavera, drenando precipitación infiltranda durante la estación húmeda, y más débil durante verano y otoño tras la estación seca; *2*) la *recarga positiva* es fuerte en primavera y máxima en verano (la temporada de mayor ET en la Península Ibérica), debido a un descenso gradual del balance de agua en superficie, después en otoño se debilita de forma significativa debido a la caída de demanda de ET, y finalmente alcanza el mínimo en invierno, cuando la precipitación presenta los valores más altos y la ET los más bajos.

El aumento de humedad de suelo inducido por la presencia de la capa freática a través de recarga positiva, repercute en la atmósfera en forma de aumento de ET. Las diferencia en ET entre las simulaciones WT y FD presenta el patrón espacial inducido en la humedad de suelo por la capa freática (alcanzando valores significativos en valles y regiones de capa freática superficial en zonas semiáridas del interior de la península). El aumento en ET promediado sobre la península es de 0.54 mm día en verano, cuando la precipitación es más baja y la demanda de ET es alta, 0.24 mm día en primavera, cuando la demanda de ET es más alta, 0.14 mm día en otoño y 0.05 mm día en invierno, cuando la demanda de ET es muy baja. Al final del capítulo, la posible potenciación de precipitación convectiva y el descenso de la temperatura en verano son argumentados como efectos potenciales de la introducción de estos resultados de dinámica de aguas subterráneas en modelización climática totalmente acoplada con la superficie y las aguas subterráneas.

La elección de una simulación de 10 años incluyendo periodos secos y húmedos permite un estudio a largo plazo de la influencia de las aguas subterráneas en la

humedad de suelo. En el **Capítulo 6** se evalúa la persistencia estacional e interanual de la capa freática, y la memoria que ésta induce en la humedad de suelo. La evolución temporal de la capa freática no responde inmediatamente a picos o bajas estacionales o anuales de precipitación, sino que responde a la evolución de las condiciones climáticas con un cierto retraso de 1-2 años. Cuando la capa freática entra en el sistema tierra-atmósfera en la simulación WT, su persistencia pasa al suelo como memoria en la humedad de suelo, y el suelo "recuerda" condiciones secas y humedas de años pasados, suavizando así los efectos de las sequías en la humedad de suelo pero también retrasando la recuperación después de las sequías a pesar de que lleguen condiciones más húmedas.

La memoria inducida en la humedad de suelo es más fuerte en zonas de capa freática superficial, donde el suelo está conectado hidraúlicamente a las aguas subterráneas. Analizando anomalías en años hidrológicos (Septiembre-Agosto) de precipitación, humedad de suelo y profundidad de capa freática en una región de documentada capa freática superficial en el Alto Guadiana (*La Mancha Húmeda*), la influencia de la capa freática induciendo memoria en la humedad de suelo es observada. Además, se observa cómo la memoria de la humedad de suelo pasa a la atmósfera como memoria de la ET en zonas de capa freática superficial.

En el **Capítulo 7**, se estudian los efectos integrados (promediados) en las principales cuencas de la Península Ibérica de las aguas subterráneas en la humedad de suelo y los flujos tierra-atmósfera. Las cuencas integran la influencia de las aguas subterráneas a través de convergencia de flujo lateral. Así se puede investigar el papel de las aguas freáticas en el sistema tierra-atmósfera bajo diferentes condiciones climáticas. A escala de cuencas, la presencea de la capa freática causa aumento de ET durante primavera y verano en la simulación WT, a través de drenaje lento y acumulación de agua en el suelo durante la estación húmeda y flujo capilar ascendente durante la estación seca. Esta influencia de la capa freática en el aumento de ET es más significativa en las cuencas del sur de climas semiáridos donde la ET está muy limitada por la existencia de agua (aumento anual de ET del 28.4% en la cuenca mediterránea del Segura y del 21.4% en la cuenca atlántica del Guadalquivir), pero a medida que la ET pasa a ser menos limitada por el agua en cuencas más al norte, la capa freática tiene menor influencia (13.3% en la cuenca del Miño donde la ET está más limitada por la energía).

La evolución temporal del aumento de ET (simulación WT – simulación FD) sigue las tendencias a largo plazo de la evolución de la capa freática, que responde a su vez a periodos de años secos y húmedos consecutivos. Por tanto, la persistencea de la capa freática pasa a la atmósfera como memoria de la ET a escala de cuencas, y el aumento anual de ET en la simulación WT no depende sólo de la estación húmeda previa, sino que también depende de la tendencia a largo plazo de la profundidad de la capa freática. En las cuencas mediterráneas, que presentan estación húmeda moderada y estación seca variable, la memoria de la ET está condicionada por la

intensidad de la estación seca (se pierde memoria cuando el verano es especialmente seco porque el aumento de ET es muy alto, imponiéndose a la evolución de la capa freática, y también cuando el verano es especialmente lluvioso y no hay estación seca, porque el aumento de ET es muy bajo, imponiéndose de nuevo a la evolución de la capa freática).

Finalmente, el **Capítulo 8** repasa las conclusiones más importantes de la investigación, intentando así ofrecer respuestas a las preguntas planteadas inicialmente. La tesis concluye con planes de trabajo futuro en esta línea de investigación.

Algunos resultados de las primeras etapas de esta investigación han sido publicados en el artículo "*The role of groundwater on the Iberian climate, precipitation regime and land-atmosphere interactions*" [47]. Sin embargo, los principales resultados ofrecidos en esta tésis están siendo preparados para ser publicados en el artículo "*Groundwater influence on soil moisture memory and land-atmosphere interactions over the Iberian Peninsula*" [26]. La estimación de una Profundidad de la Capa Freática de Equlibrio de alta resolución para la Península Ibérica, obtenida a partir de recarga climatológica resultante de simulaciones con LEAFHYDRO está además en preparación para completar el artículo "*Water Table Depth and Potential Capillary Flux to the Land Surface in the Iberian Peninsula*" [48].

Chapter 1

Introduction

1.1 Natural Water Cycle

Water on Earth never stops; it is continuously and cyclically moving and transferring between different reservoirs in the atmosphere, land and sea; and it is continuously changing states between liquid, gas and ice. In space, these processes take place at planetary, continental, regional and local scales. In time, they occur at timescales of seconds, days, seasons, years and over millions of years. All these movements and processes are energetically driven by the sun and the Earth gravitation, and constitute the natural water cycle.

The main reservoirs and processes of the natural water cycle are illustrated in Figure 1.1. The basic processes of the cycle are: evapotranspiration, precipitation, infiltration, recharge and runoff. Evapotranspiration is the combination of two fluxes; evaporation of water at the surface of the sea, rivers, lakes and land, and transpiration from living beings, especially plants, at the land surface.

The evapotranspirated water passes to the atmosphere as water vapour, then it is transported by atmospheric circulation and, under appropriate circumstances, it can condensate into liquid or solid water and fall back to the surface as precipitation. Precipitated water over the oceans or surface water reservoirs can reinitialize the cycle being evaporated back to the atmosphere, and precipitated water over land can be transported by gravitational forces towards rivers as surface runoff or infiltrate into the soil. Infiltrated water become then part of the soil moisture and can be evapotranspirated back to the atmosphere or percolate through the soil and into the groundwater reservoir as groundwater recharge.

The groundwater reservoir is the volume of water contained in the pores, fissures and fractures of the water-saturated strata of the Earth's crust. The water table is

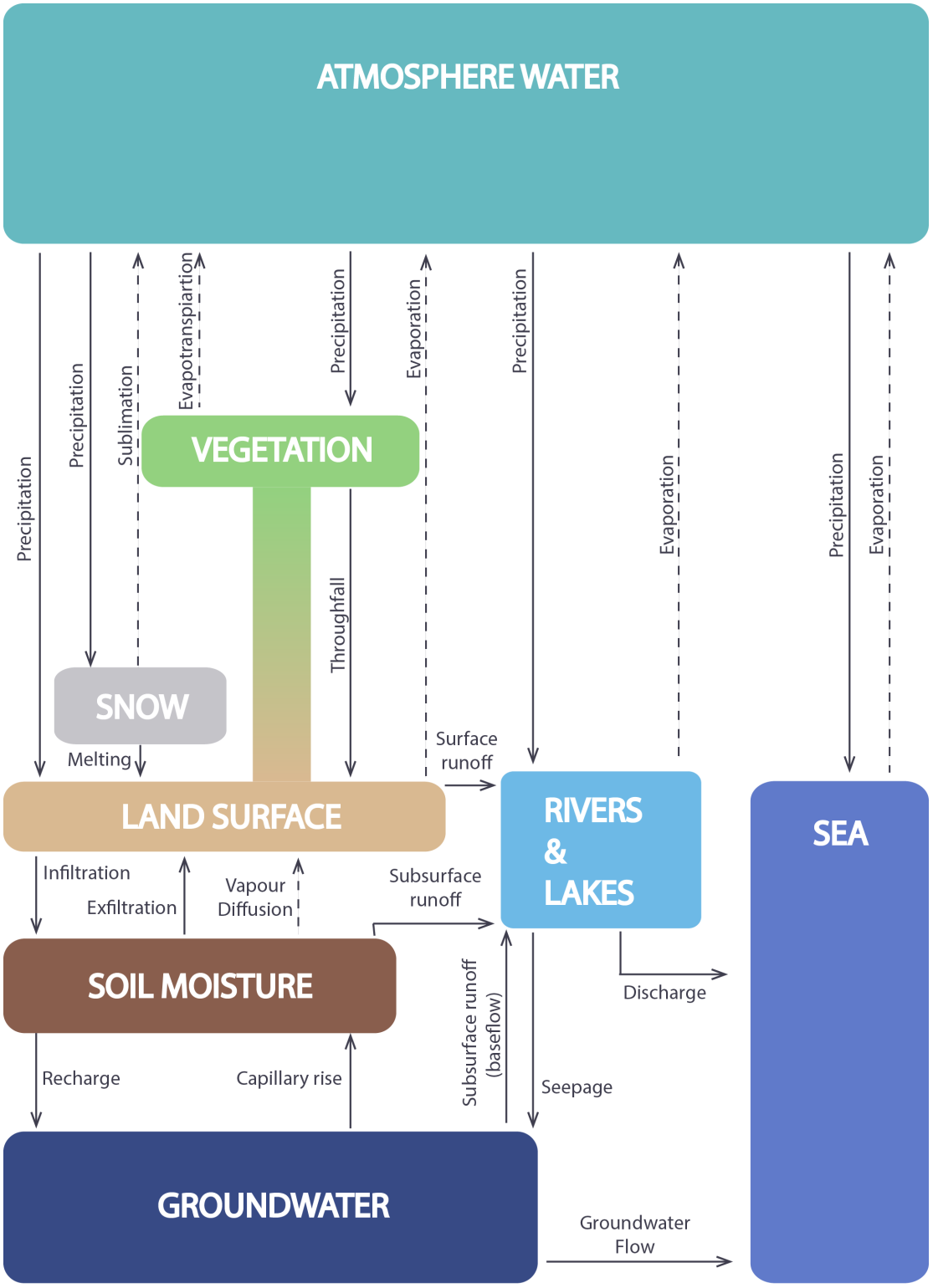

Figure 1.1: Natural Water Cycle sketch.

the surface that limits the saturated and non-saturated zones of the soil. Groundwater near the water table plays an important role in the natural water cycle through different interactions (see Figure 1.1):

- It can move up to the soil via capillary rise, or collect soil moisture drainage provoking a water table rise.
- It can be transported as groundwater flow within the saturated zone, discharging ultimately to the oceans.
- It can receive lake and river infiltration (seepage), or feed the rivers as part of the baseflow.

The water cycle is not a single mechanical circuit. It is necessary to understand and evaluate it a as a compound of different interconnected processes and cycles at different scales in time and space. The spatial scales for these interconnected circuits is continental, like the come and go of water evaporating from an ocean and falling back as rain, regional and local, like the circuits of water in river basins that characterize the region giving it a distinctive biological composition. Water participates in the different circuits and also can be transferred from one to another, like for instance evaporated water from the Pacific Ocean can be transported eastward by atmospheric dynamics, fall as rain on the Rocky Mountains, be transported eastward through the continent by the Mississippi River and end up in the Atlantic Ocean.

The residence times of water in the different reservoirs vary very much. For example, the period of renewal is 9700 years for polar ice, 2500 years for ocean water, 17 years for lake water, 1 year for soil moisture, 8 days for atmospheric moisture or only hours for biological water [107]. The time variability of the natural water cycle is introduced by its dependence on the atmospheric circulation and weather factors. Such dependence on atmospheric dynamics makes it very important to understand the behaviour, variability and connection with the climatic elements of the water cycle reservoirs in climate modeling studies.

1.2 Climate variability in the Iberian Peninsula

The climate in the Iberian Peninsula is defined by its geographical situation (35N-40N, 10W-4E), its continentality and the stratospherical circumpolar vortex dynamics. The stratospherical circumpolar vortex is a large scale closed cyclical circulation around the Arctic Pole whose seasonal, annual or decadal changes in form and intensity influence the climate and weather in the Northern Hemisphere midlatitudes, and therefore the Iberian climatology is linked to the circumpolar vortex dynamics.

Due to the Iberian Peninsula location at the gates of Europe, very different types of air masses can reach it: cold and wet northern maritime Arctic (*mA*) masses from the Greenland Sea; cold and wet northern or northwestern maritime Polar (*mP*)

masses from the Islandic region; cold and dry continental Polar or Arctic (*cP*, *cA*) masses from Escandinavia or the north of Russia; warmer but still wet sourthwestern maritime Tropical (*mT*) masses from the Azores High; warm and dry southern or southeastern continental Tropical (*cT*) masses from the north of Africa. This variability of air masses that can reach the Iberian Peninsula and the continentality that the orography gives to most of the peninsula result in a high climate variability, as the peninsula become a meeting point for different air masses.

Such climate variability is illustrated using the Koppen-Geiger climate classification. This classification system uses series of monthly mean air temperature and precipitation, and defines distinct types of climate based on ranges of these values and their influence on the distribution of vegetation and human activity [38]. The map in Figure 1.2 was published by the AEMET (*Spanish State Agency of Meteorology*) and the IPMA (*Meteorology Institute of Portugal*) [8] using the Koppen-Geiger classification — with the only amendment being that the threshold temperature to separate temperate *C* and cold *D* climates was 0°C instead of –3°C, used in the original classification — for the Iberian Peninsula and the Balearic Islands and up to 12 different types of climate are found.

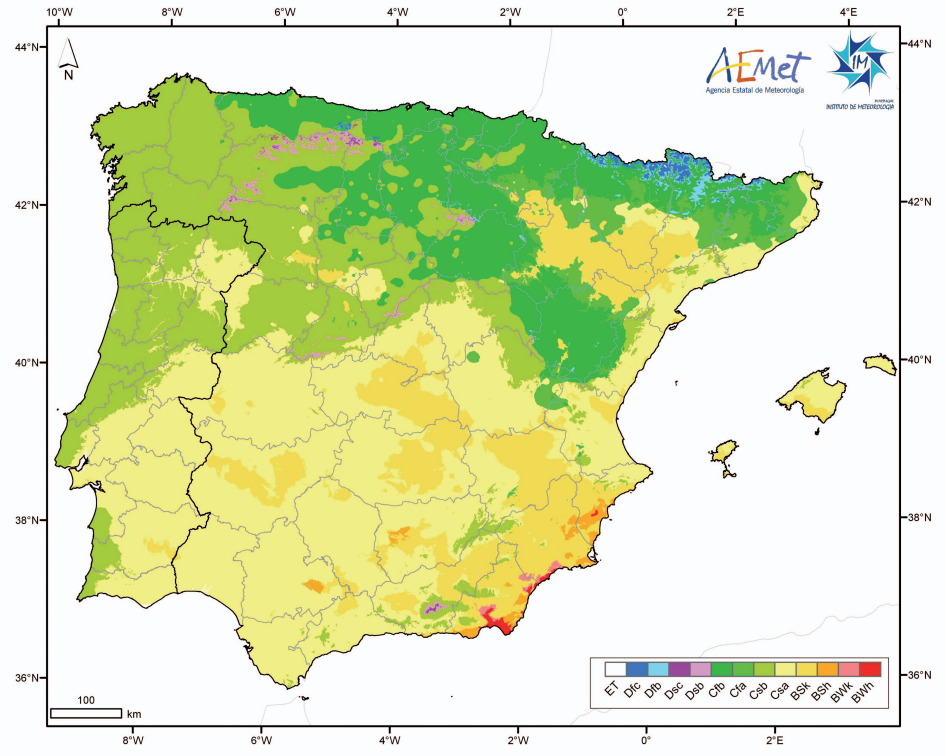

Figure 1.2: Koppen-Geiger classification climates for the Iberian Peninsula and the Balearic Islands.

Temperate climates (type *C*) are dominant in the peninsula. *Csa* climate means dry and hot summer and occupies most of the centre and south of the peninsula, as well as the central and northern Mediterranean coast regions and the Balearic Islands. *Csb* also means dry summer but the hottest month temperature is below

22°C; some mountain regions in the centre and most of the northwestern region and the western Portuguese coast present this type. *Cfb* means no dry season and temperate summer; it covers part of the northern central plateau and the northern mountain ranges (Cantabrian Mountains, Iberian System and most of the Pyrenees). When the hottest month is above 22°C but there is still no dry season the climate is type *Cfa*; it appears surrounding the Pyrenees and the Iberian System (areas of medium altitude).

Arid and semiarid climates (type *B*, defined by the not reaching of a threshold for annual precipitation) also have an important presence in the peninsula, mainly in the southeastern region. *BSk* and *BSh* (cold steppe and hot steppe) mean that the annual rainfall reaches half the threshold established for the *B* climates; *BSk* climate spreads over the south-west of the peninsula and the Ebro river basin, and in a lesser extent it is found in the Inner Plateau (southern subregion), Extremadura (southwestern region of Spain), a small region in Baixo Alentejo (south of Portugal) and the Balearic Islands, limiting *BSh* presence to small regions in the southeastern coast and central Andalusia (vast southern region of Spain). *BWk* and *BWh* (cold dessert and hot dessert) mean that the annual rainfall does not reach half the threshold for *B* climates, and in the peninsula it is found over small regions in the southeastern corner, where the minimum precipitation values are registered.

Cold climates (type *D*) are limited to high altitudes in the peninsula. Hence, in the highest zones of the Pyrenees, Cantabrian Mountains, Central Ranges, Iberian System and Sierra Nevada, 4 different type *D* climates (*Dsb*, *Dsc*, *Dfb* and *Dfc*) are found, depending on whether summer is the dry season (second letter *s*) or there is no dry season (second letter *f*), and whether the temperature is mild (third letter *b*) or cold (third letter *c*). Finally, only in very small high locations of the Pyrenees the polar type *ET* is found; *ET* means average monthly temperature below 10 C all throughout the year.

1.2.1 Precipitation variability in the Iberian Peninsula

Precipitation variability in time and space is a revealing factor to understand climate variability in the Iberian Peninsula.

About the seasonal regime, summer is the drier season and winter is the wetter, but autumn and spring are also wet seasons depending on the region studied inside the peninsula, and there is no dry season over the northern mountain ranges (type *Cfb* climate, Figure 1.2). Using a complete and homogeneous 60-year series of observed precipitation over Spanish territory stations, *de Luis et al.* (2010) [27] found that winter was the dominant precipitation season in 51.1% of the Peninsula during the period 1946–1975 and in 42.7% during the period 1976-2005, whereas the territory percentage where autumn is the dominant season increased from 10.8% in the first period to 41.4% during the second 30-year period and spring, on the other hand, changed from being dominant in 36.1% to only 15.1% of the peninsula.

About the atmospheric circulation systems that affect precipitation in Spain, it is well known that over the west, centre and south, precipitation regimes in the Peninsula are linked to the NAO (*North Atlantic Oscillation*) in early spring [90] and during the wettest October-March period [74]. However, other low frequency patterns specific to the Mediterranean region, like the WeMO (*Western Mediterranean Oscillation*), are needed to explain precipitation in the eastern coast (far from the Atlantic influence) and the eastern half of the Cantabrian coast [74].

In order to analyse the spatial and interannual precipitation variability, the publicly available analysis daily precipitation gridded dataset IB02 (~ 20 km spatial resolution) presented by *Herrera et al.* (2010) [54] and *Belo-Pereira et al.* (2011) [16] is used here. Figure 1.3 shows the mean yearly precipitation (l m^{-2}, hereafter mm) for the period 1950-2007.

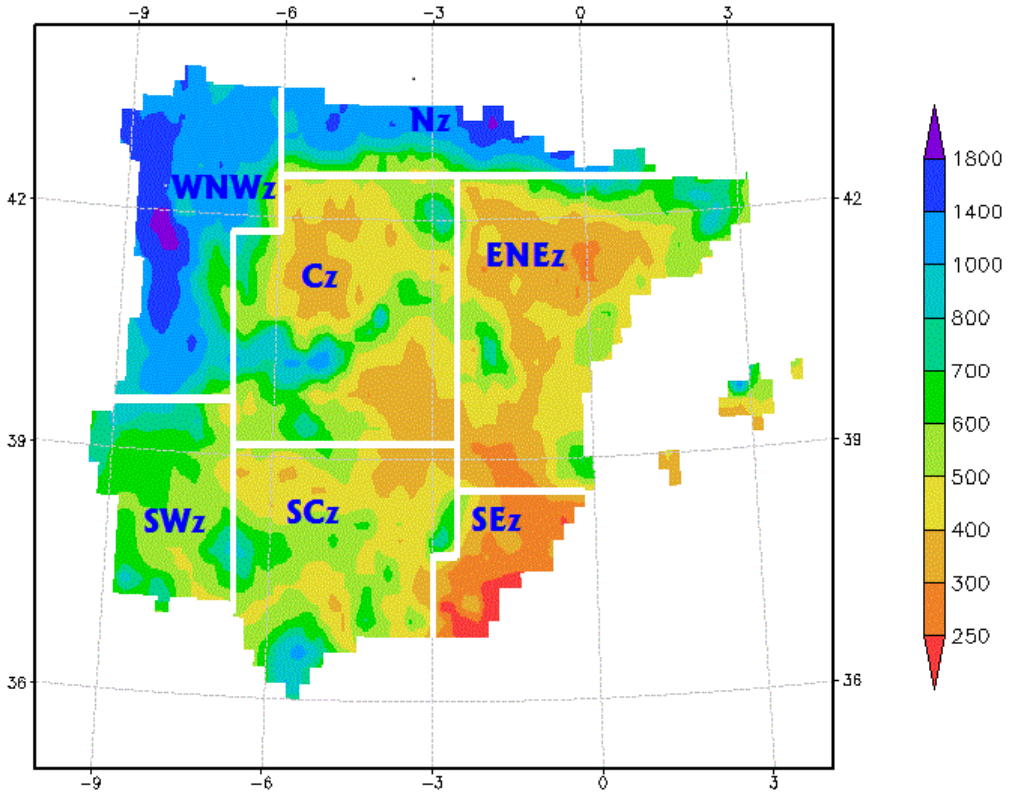

Figure 1.3: Mean yearly precipitation (mm) for the period 1950-2007 in the Iberian Peninsula. Division of 7 pluviometric regions with different precipitation regimes.

The spatial range of variation is very wide, from around 200 mm in the southeastern corner (arid and semiarid type *B* climates) to values over 1500 mm in extended areas of the north-west and in the Basque Country (region in the western Pyrenees by the Cantabrian Sea, at the Spanish-French border). This spatial variability makes it necessary to divide the Iberian Peninsula into different pluviometric regions (as showed in the map) or river basins (as done in Chapter 7) when hydrological or climatic studies are carried out.

Using the highlighted division into pluviometric zones in Figure 1.3, a study of the interannual variability and wet/dry trends is performed. The zones are:

- West-North-West zone (*WNWz*): 1187 mm mean annual precipitation
- North zone (*Nz*): 990 mm mean annual precipitation
- East-North-East zone (*ENEz*): 1461 mm mean annual precipitation
- Centre zone (*Cz*): 519 mm mean annual precipitation
- South-West zone (*SWz*): 688 mm mean annual precipitation
- South-Centre zone (*SCz*): 523 mm mean annual precipitation
- South-East zone (*SEz*): 301 mm mean annual precipitation

The next set of plots in Figure 1.4 represent the five year centred rolling average of the yearly precipitation unitary deviation for the 7 pluviometric zones, as well as for the whole domain (Iberian Peninsula and Balearic Islands) in the last plot. These plots are very useful to visualize trends of increasing and decreasing annual precipitation.

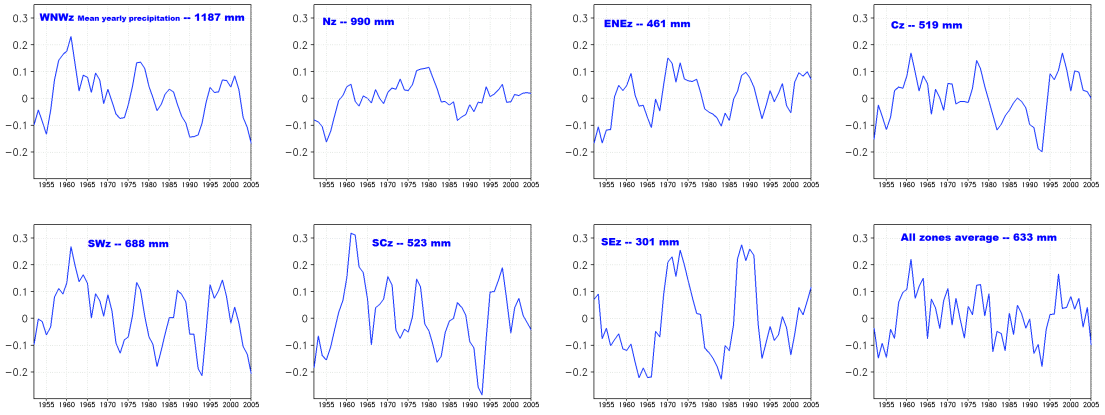

Figure 1.4: Trends of the mean yearly precipitation at the 7 pluviometric zones highlighted in Figure 1.3 and for the whole domain (Iberian Peninsula and Balearic Islands), from the 5-year centred rolling average of the yearly unitary deviation.

Three main conclusions are drawn from Figure 1.4:

1. Even though some cycles are repeated in most of the zones, like the increasing trend from 1955 to 1960, the overall behaviour is different for the different pluviometric zones. Using the correlations between the series, three main patterns are found:
    - The northern zone *Nz* by the Cantabrian Sea has an independent signal, and its correlation with the rest is around or below 0.5.
    - Mediterranean zones *EWWz* and *SEz* present a correlation of 0.7 but are not significantly correlated with the rest.
    - Zones *WNWz*, *Cz*, *SWz* and *SCz* are significantly correlated (values from 0.63 to 0.88) and reflect the main precipitation trends in the Peninsula.

2. There are marked decreasing trends in every pluviometric zone. Sometimes they can take as long as 10 years of continuous rainfall decrease, like the 1973–1983 period in the driest zone *SEz*. These periods may result in severe droughts. Apart from the *Nz*, all zones coincide signalling a drought period in the early 1990s followed by a quick recovery from the middle of the decade. This makes it a very interesting period to be included in long-term coupled land-atmosphere modeling studies.

3. The plot averaging data for the whole domain appears much more jagged than the rest, not reflecting the real behaviour at located regions. This calls for caution when analysing hydrological processes in the Iberian Peninsula, since Iberian average data may lead to mistaken conclusions.

1.2.2 Droughts in the Iberian Peninsula

Vast regions of the Iberian Peninsula register yearly precipitation values under 500 mm (Figure 1.3). Moreover, as analysed in Section 1.2.1, the irregularity in time and space is a main characteristic of the rainfall distribution in the peninsula. Therefore, frequent drought periods occur. Over the cereal cultivated lands, like the basins of the rivers Ebro, Tajo, Guadiana and Guadalquivir, droughts are of greater importance. In addition, when the lack of rainfall comes in hot years, the reductions in river discharge and groundwater recharge are significantly more important due to a reduction of the precipitation hydrological efficiency, as the evapotranspiration from soil and plants increases with respect to temperate years.

A characterization of the Iberian Peninsula through the study of spatial and temporal variabllity of drougths is important for a proper development of management plans for risk mitigation. The need to divide the Peninsula into specific regions as well as the asynchronicity in hydrological patterns between these regions was pointed out by *Vicente-Serrano* (2006) and *Lorenzo-Lacruz et al.* (2013), when they studied spatio-temporal variability of Iberian droughts using 1910-2000 precipitation series [112] and 1945-2005 streamflow series [69], respectively.

As was pointed out in Section 1.2.1 and also according to the hydrological report *Libro Blanco del Agua* (2010) [6], published by the Spanish *Ministery of Natural Environment*, the most severe drought in the Iberian Peninsula during the last 60 years took place in the period 1990/91–1994/95. This drought caused a very important reduction in the interannual river discharge: 50–70% in the centre and southern basins discharging to the Atlantic Ocean and 20–40% in the northern and western Mediterranean basins [6].

The increase in water demands during the last decades, as a consecuence of an increase in irrigated land, and urban and tourist growth have made the Iberian Peninsula more vulnerable to droughts [84]. Furthermore, the Mediterranean region, and especially the Iberian Peninsula, have been recently marked as a *hotspot* by

Prudhomme et al. (2013) [92] when they analysed a likely increase in the global severity of drought occurrence by the end of 21st century, using an ensemble of global hydrological and climate models.

There is not a commonly accepted definition for droughts [62], but depending on the system affected and the impacts timescale they can be classified into 4 categories [116]: meteorological, agricultural, hydrological and socioeconomic. The criteria to define a drought differ from one public administration to the next, depending on local experiences. They take into consideration different thresholds of annual precipitation registered, longer or shorter periods, relations between water demands and resources or similarities with historical droughts. However, since groundwater reservoirs are less affected by lack of precipitation than by river discharge, indicators on the state of groundwater reservoirs are not normally accounted for. In basins where the connection between the streamflow and the natural discharge from aquifers (baseflow) is strong, it can be observed how lack of precipitation periods of 1-3 years (meteorological droughts) are not translated into hydrological droughts when analysing volumes of water in rivers or wetlands connected to the aquifers. A different problem altogether appears when the groundwater reservoirs are used for irrigation of cultivated lands or town water supply due to bad public planifications.

The groundwater reservoirs role as a mitigator of drought effects is one of the factors studied in this work (Chapter 6).

1.3 The groundwater link to the land-atmosphere system

The groundwater interactions with the land-atmosphere system are factors to be taken into consideration when climate and ecosystem modeling studies are performed. Hence, the inclusion of a dynamic water table as the lower boundary condition of the soil column constitutes an important step to improve the land surface representation in climate models. There has been a growing interest in the scientific community to represent goundwater-land-atmospher interactions in recent years at different spatial and temporal scales. Some such efforts and the key aspects of the problem are summarized in this section.

1.3.1 The soil moisture link to the atmosphere

Soil moisture is a key player in climate. Evapotranspiration is highly water-limited, and hence the availability of soil moisture constrains evapotranspiration to the atmosphere [39]. Many efforts have been made in the community to address the climate models sensitivity to land processes and the importance of a consistent

soil moisture initialization given the lack of measurements [95]. Using the ECMWF (*European Centre for Medium-Range Weather Forecasts*) GCM (*General Circulation Model*) model, *Betts* (2004) [17] showed the link between soil moisture and surface fluxes, running 2 seasonal simulations (wet and dry soil initialization) and obtaining greater precipitation and evapotranspiration in the wet simulation. In a case study long before that, *Beeljars et al*. (1996) [15] obtained greater (up to 4 mm day^{-1}) and closer to observations forecasted precipitation for the July 1993 Mississippi flood with the ECMWF model when initialized with wet soil. *Seneviratne et al*. (2006) [105] studied the land-atmosphere coupling in climate models and found that the increase in interannual summer temperature variability expected over Europe [50, 100, 113] is mainly due to feedbacks between the land surface and the atmosphere. Furthermore and affecting the region of interest for the present work, in *Seneviratne et al*. (2006b) [104] they found, through analysis of different GCMs simulations, that the Mediterranean region presents high land-atmosphere coupling.

Regional precipitation recycling constitutes a measurement of the soil moisture link to the atmosphere and the controlling role of soil moisture and evapotranspiration fluxes on regional rainfall regimes. Many studies show how a large portion of the atmospheric moisture is supplied through recycling processes and comes from land interactions [19–21, 36]. For instance, using Lagrangian back-trajectory methods, *Dirmeyer & Brubaker* (2007) [35] obtained a 4.5% average annual precipitation recycling ratio for all land areas of the globe. In a more recent regional study, also using a back-trajectory method, *Harding et al.* (2013) [53] concluded that 60% of summer evaporated water from irrigated areas in the Ganges basin comes back through river flow after being recycled as Himalayan rainfall.

Analytical bulk recycling models [36, 99] have been used here in the USC *Non-Linear Physics Group* by *Rios-Entenza & Miguez-Macho* (2013) [93] to analyse, based on RCM (*Regional Circulation Model*) WRF (*Weather Research and Forecasting*) simulations, the spring precipitation peak in the Iberian Peninsula. These authors found recycling ratios over 20% in some interior areas.

Other studies point out a tendency of land surface models to dry out the soil and the need of including artificial soil moisture nudging, as discussed by *Roads & Betts* (1999) [94] when they compared the NCEP-NCAR (*National Centers for Environmental Prediction - National Center for Atmospheric Research*, USA) and ECMWF Reanalysis Surface Water and Energy Budgets for the Mississippi river basin.

This clear soil moisture coupling with atmosphere processes leaves the scientific community the task of representing correctly land-atmosphere interactions and storages in climate and climate change simulations.

1.3.2 The groundwater link to soil moisture and land-atmosphere fluxes

Soil moisture fields are linked to the groundwater reservoir where the water table appears relatively shallow, and the water table depth is the main indicator of the intensity of groundwater-soil coupling. The water table is linked to the unsaturated zone above by two-way fluxes: the downward gravitational flux and the upward capillary flux. The net flux is downward in the wet season and some time afterwards, when groundwater receives recharge, but upward capillary fluxes can dominate in the dry season if the water table is sufficiently shallow to provide water to meet evapotranspiration demands.

The water table depth time variability is weak as compared to the surface hydrology time variability [42], and hence it might explain partly soil moisture memory. Soil moisture memory refers to the longer persistence of a dry or wet anomaly in the soil, as compared to the atmosphere. In turn, if there is high land-atmosphere coupling, that is, if the conditions of the soil can have a sizeable impact on atmospheric dynamics; then soil moisture memory can translate to weather conditions and have major implications for seasonal and long-term forecasting. As pointed out in Section 1.3.1, *Seneviratne et al*. (2006b) [104] concluded that the Mediterranean region, a transitional zone between yearlong wet and dry climates, presents high soil moisture memory and high land-atmosphere coupling. This is mostly due to the high seasonality of precipitation, with a pronouncedly dry and warm summer and a wetter and colder winter. Focusing on the Iberian Peninsula, the question of how much memory can the long timescales of variation of the groundwater induce in soil moisture is one of the main objectives of research in this work.

Groundwater can be the main source for ecosystem evapotranspiration in water-limited environments [71], and observational evidences for the groundwater-soil link have been showed in recent years. *Vincke et al.* (2008) [114] found positive feedback between water table fluctuations and soil water content with measurements over a year in a shallow water table (0.8–2 m deep) Scots pine stand in Belgium. More recently, *Sutanudjaja et al.* [109] (2013) used spaceborne microwave based soil moisture products to predict groundwater heads in time and space over Germany with transfer function-noise models, and they reproduced groundwater head fluctuations reasonably well, especially in shallow water areas where soil moisture dynamics are tightly connected to groundwater head positions. In the Iberian Peninsula in particular, *David et al.* (2007) [25] found that during the summer drought in a plot in southern Portugal, daily soil moisture fluctuations in the top 1 m related to transpiration could be attributed to groundwater via isotopic analysis. These authors estimated that up to 70% of the evapotranspired water had its origin in groundwater in that area.

Other studies have explicitly included groundwater processes in land and atmosphere modeling during the last decade [9, 66, 67, 78, 82, 83, 88, 119]. *Maxwell &*

Miller (2005) [78] obtained results closer to observations in soil moisture fields when they coupled a groundwater model to the CLM (*Community Land Model*). *Miguez-Macho et al*. (2007) [83] performed a simulation over North America using an initial version of the coupled groundwater-land surface model LEAFHYDRO for the warm season of 1997, they found a strong spatial correlation between the distribution of shallow water table and wet soil and pointed out the double role of the groundwater reservoir, shifting from being primarily a sink during the wet spring to being primarily a source for the soil water above during the dry summer.

Following the latter (*Miguez-Macho et al*. (2007) [83]), a study was published by *Anyah et al.* (2008) [9] coupling LEAFHYDRO to the RCM RAMS (*Regional Atmospheric Modeling System*) where it was shown the link between the groundwater reservoir and the atmosphere (enhanced evapotranspiration and precipitation), mostly over the arid west of North America. *Yuan et al.* (2008) [119] ran a summer simulation over Asia with the regional climate model RegCM3 that included a groundwater dynamics implementation; in semiarid regions they found that the soil got wetter and enhanced evapotranspiration, and that the recycling rate and precipitation efficiency increased greatly. *Leung et al* (2010) [66] coupled the RCM MM5 (*Mesoscale Model 5*) to a version of the VIC (*Variable Infiltration Capacity*) LSM (*Land Surface Model*) that included groundwater dynamics in order to perform climatic simulations over the US, and discussed how the change in soil water partitioning between the land surface (0-0.5 m) and the subsurface (0.5-5 m) influence the partitioning of surface sensible and latent heat, provoking higher evaporative fraction in summer.

In a recent work by *Miguez-Macho & Fan* (2012) [82], they addressed the role of groundwater in the Amazon water cycle using a continental-scale groundwater and surface water coupled model (LEAF-Hydro-Flood) and found that the groundwater buffered the dry season soil moisture stress, explaining the well-known observation-model discrepancy in the Amazon dry season evapotranspiration over regions where the seasonality is strong and the presence of shallow water table made a difference.

1.3.3 The groundwater link to streamflow

Streams and lakes are connected through two-way water fluxes: the discharge from groundwater to the streams in gaining streams where the water table is above the river bed (typical of humid regions), and the water flux infiltrating into the groundwater from losing streams where the water table is below the river bed (typical of arid regions) [44]. In gaining streams, the groundwater reservoir may maintain the stream baseflow during dry seasons. Losing streams feed the groundwater reservoir during wet seasons, contributing to the groundwater memory during the following dry seasons. Hence, at a given location that presents a water table fluctuating around the river bed depth, the local rivers may act as gaining and losing streams,

depending on the season. A proper representation of such groundwater-streams connection makes a difference in hydrological and climate studies.

In order to consider this groundwater-streams connection and close continental hydrological cycles, river routing models are coupled with land surface models. *Decharme et al*. (2010) [31] pointed out the potential significance of the groundwater storage as an uncertainty in simulating continental hydrological systems. Performing global simulations at high (1/12 degrees) and low (1/2 degrees) resolutions with the global TRIP (*Total Runoff Integrated Pathways*) river routing model that includes a groundwater-streams exchanges scheme, *Vergnes et al.* (2012) [111] improved the caption of the spatio-temporal variability of the observed discharges and, particularly over the main rivers of France, the summer baseflow, as compared to TRIP performances with the groundwater scheme turned off.

More recently, as part of an ongoing collaborative work between the USC *Non-Linear Physics Group* and the *Rutgers University Department of Environmental Sciences*, *Miguez-Macho & Fan* (2012b) [81] explicitly evaluated groundwater's influence on the Amazon water dynamics using LEAF-Hydro-Flood at 2 km horizontal resolution. These authors found 4 important factors: 1) groundwater is the main source of streamflow in the headwater catchments, 2) in the floodplains and depending on water table depth, there are two-way exchanges between the floodwater and the groundwater through infiltration in the wet season and groundwater seepage in the dry season (as a result of lateral groundwater convergence), 3) groundwater supports wetlands in the Amazon lowlands and valley floors that present persistently shallow water table, and 4) groundwater buffers surface waters through seasonal climatic droughts due to its longer timescales.

1.3.4 The importance of a correct representation of groundwater interactions in the Iberian Peninsula

This work is a contribution to the cited efforts studying the influence of groundwater dynamics on the water cycle and the land-atmosphere fluxes over the Iberian Peninsula during a 10-year period. The Iberian Peninsula is a region of special interest for a groundwater-land-atmosphere interactions study provided its climatic variability detailed in Section 1.2. The groundwater's role is investigated in following chapters at 3 levels in the Iberian Peninsula:

1. Impact on soil moisture dynamics, spatial variability and long-term memory.
2. Effects on land-atmosphere fluxes through evapotranspiration to the atmosphere.
3. Direct impact on surface waters through the groundwater-streams connection.

To the USC *Non-Linear Physics Group* knowledge, there has not been a modeled study linking groundwater to soil moisture and land-atmosphere interactions in the Iberian Peninsula. However, the role of the Iberian Peninsula as a source itself for atmospheric moisture in the warmer periods (and all throughout the year in the eastern Mediterranean region) has been reported by *Gimeno et al.* (2010) [49].

Different efforts have addressed the importance of a proper representation of soil moisture in Iberian regional atmospheric and hydrological modeling. Performing climate simulations, *Jiménez et al.* (2011) [57] found up to 20% differences in regional wind speed in the Iberian Peninsula when changes in soil moisture availability are considered; in a case study of the 2003 drought, a drier soil (−50% of soil moisture availability), more concordant with real conditions, lead to higher wind speed, more in agreement with observations. *Sánchez et al.* (2010) [98] used in situ soil moisture measurements (0-1 m deep) to validate a water balance model in a region of shallow water table depth within the Duero river basin during 2002, finding that their model (which did not include groundwater interactions) underestimated soil moisture. The role of groundwater dynamics should be taking into account in this kind of studies, and may change the soil moisture behaviour at shallow water table regions.

The groundwater reservoir larger timescales with respect to the atmosphere fenomena connected to it has been observed in the Iberian Peninsula. Groundwater memory of long past surface episodes was pointed out in the *Doñana National Park* (southwestern Spain, by the Gulf of Cádiz) by *Serrano et al.* (2008) [106]; they found higher observed pond hydroperiod (wet phase duration) correlations with last two years rainfall than with last one year rainfall. Over the upper Guadiana basin, and according to the Spanish IGME (*Spanish Geological and Mining Institute*), *Mejías et al.* (2012) [80] pointed out how during the hydrological years 2009-2010 and 2010-2011 with rainfall about 50% above the average, the water table recovered 4 m and 8 m, respectively, and during the 2011-2012 hydrologically dry year, the water table still recovered 2.5 m up to the spring level. This water table level had not been observed since 1983 in the location [75]. In fact, the recovering of the several ponds in *La Mancha Húmeda* (Biosphere Reserve in the upper Guadiana basin) during last dry year 2012 has been reported in Spanish press. The evolution of the water table levels as a slow response to climatic conditions, keeping memory of wet periods even when the rainfall stops, shows the importance of groundwater memory in the Iberian Peninsula and the necessity of including it in modeled land-atmosphere interaction studies.

Furthermore, understanding the processes and the water cycle behaviour becomes of major importance for the integrated management of the hydric resources in the Iberian Peninsula provided the high irrigation withdrawal from wells or directly from rivers. There has been an spectacular increase over the last four decades in intensive groundwater use for irrigation in most arid and semiarid regions of Spain,

carried out mainly by modest individual farmers, often with little planning and control on the part of governmental water authorities [46]. According to the Spanish *Ministry of Natural Environment*, 7% of the national territory is irrigated, 67.7% of this irrigated land uses water that comes from surface runoff and 28.2% (942,244 ha) uses groundwater. Studies included in the report *Libro Blanco del Agua* (2010) [6] estimated that the fraction of natural flow that actually runs through the Iberian rivers after the anthropogenic extractions decreases from north to south, presenting significantly low values for the main southern rivers (52% for Guadiana river in Badajoz, 44% for Guadalquivir river in Alcalá del Río), as illustrated on Figure 1.5.

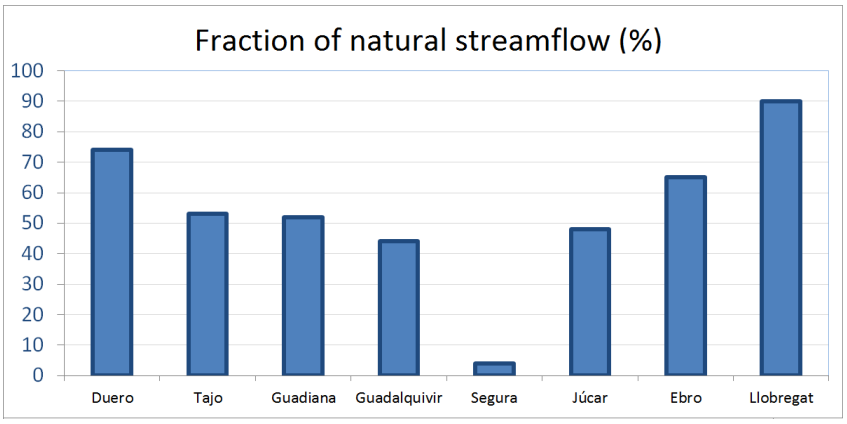

Figure 1.5: Percentage of natural flow that actually runs through the Iberian rivers after human influence; near the river mouth (Guadalquivir, Segura, Jucar, Ebro and Llobregat) and near the Portugal border (Duero, Tajo and Guadiana).

But the reduction of the natural streamflow is not the only consequence of an intensive groundwater withdrawal. The water table in the upper Guadalentín river basin aquifer (situated in southestern Spain; legally declared overexploited in 1987 [3]) has dropped by as much as 250 m since the 1960s as a result of the water extraction through ∼ 1000 wells [51]. Researching on the origin of the 2011 Lorca earthquake that took 9 lives and seriously damaged numerous buildings, *González et al.* (2012) [51] correlated the elastic response of the crust to removal of this amount of groundwater with a stress perturbation on the order of a few tens of kilopascals on the shallow fault patch where the earthquake initiated, inferring that the stress induced by the groundwater extraction helped trigger the earthquake and also controlled the final magnitude. The stress released by the earthquake of about 0.5 to 2 MPa cannot have been caused entirely by water extraction, but water extraction may have affected how this stress was released [13].

Chapter 2

LEAFHYDRO Land Surface and Groundwater Model description

The atmosphere-ecosystem-ocean system acting as a whole in numerical modeling is a concept that has grown over the decades in the atmospheric modeling community. Interactions and feedbacks between the atmosphere and underlying soil and vegetated surfaces were thought once to play a minor role in atmospheric circulations, but the SVAT (*Soil-Vegetation-Atmosphere Transfer*) schemes employed in atmospheric models (RCMs and GCMs) have become increasingly more sophisticated since the 1980s. Numerous field and modeling studies demonstrated their importance in atmospheric circulation for both climate simulations and weather forecasting in the 1990s [14, 23, 33, 91].

Similarly, in the last decade there has been a growing interest in the community to include groundwater exchanges with the land-atmosphere system as explained in Section 1.3. In this context, the LEAFHYDRO Land Surface and Groundwater Model is presented and described.

The original LEAFHYDRO model was the result of the implementation of a groundwater dynamics scheme, discussed by *Miguez-Macho et al.* (2007) [83], into the SVAT scheme LEAF-2 (*Land Ecosystem-Atmosphere Feedback 2*). LEAF-2 was presented by *Walko et al.* (2000) [115] as the land surface component of the RCM RAMS[1](*Regional Atmospheric Modeling System*), developed at Colorado State University. LEAF-2 was versioned from the original LEAF model described by *Lee* (1992) [63].

LEAFHYDRO is a modeled representation of energy and water storages and vertical exchanges in the land surface. It includes prognostic equations for soil temperature

[1] see http://rams.atmos.colostate.edu/

and moisture for multiple layers, vegetation temperature, surface water including dew and intercepted rainfall, snowcover mass and thermal energy for multiple temporary snow layers, temperature and water vapour mixing ratio of canopy air, water table depth and river streamflow. Exchange terms in these prognostic equations include turbulent exchange, heat conduction, water diffusion and percolation in the snowcover and soil, longwave and shortwave radiative transfer, transpiration, precipitation, runoff, groundwater recharge, groundwater-river exchange and groundwater lateral transport.

LEAFHYDRO can work as an offline land surface model forced by atmospheric forecasted, reanalysed or observed fields. However, its very conception as a SVAT scheme makes it a tool to work coupled with atmospheric models, such as RCM RAMS or RCM WRF – collaborative work between the NCAR and the USC *Non-Linear Physics Group* is ongoing to carry out fully coupled dynamical groundwater-land-atmosphere climate and weather simulations –. In this coupling with atmospheric models, LEAFHYDRO offers the ability to represent fine-scale variations in surface characteristics, since it is computationally inexpensive in comparison to the representation of processes in atmospheric models and can work at a higher spatial resolution [9, 115]. Characteristics such as vegetation type, terrain slope, land use, bodies of water, soil moisture or water table depth vary considerably over the typical horizontal scales used in RCMs and GCMs, hence the finer resolution in the SVAT scheme represent more realistically processes that occur at subgrid scale when using atmospheric models. Such processes are easily understood, like different vegetation responses to soil moisture or radiative fluxes, or accumulation of moisture in valleys leading to relative drying in neighbour higher zones due to a shallower water table in the valleys or a quick rainfall runoff from sloping areas.

The energy and water storages and exchanges that LEAFHYDRO resolves are represented schematically in Figure 2.1. The sketch shows two single model cells that represent the different reservoirs and fluxes. The reservoirs are atmosphere (A), canopy air (C), vegetation cover (V), river stream (R), snowcover layers (N), soil layers (S) and groundwater reservoir (G). In cell 1 there is no snowfall and cell 2 contains no river-groundwater exchange in order to better understand different possible situations in the model. The local importance of vegetated areas and its associated fluxes in each cell is determined in the model by the vegetation fractional coverage. Fluxes are denoted by terms of the form F_{123}, where F stands for flux, the first subscript indicates whether the flux is water transfer (w), heat transfer (h; by turbulent exchange, conduction or precipitation) or longwave radiative transfer (r), and the second and third subscripts denote the source and receptor, respectively, of the fluxed quantity (g for groundwater, s for soil, n for snow, v for vegetation, c for canopy air, and a for free atmosphere). The flux F_{wvc} is the sum of water flux by means of evaporation from surface vegetation moisture to the canopy air, such as dew or intercepted rain, and water flux actually coming from soil to canopy air via the vegetation in the form of transpiration. Fluxes are defined in the model as positive in the direction of the arrows. Possible negative values imply transport in

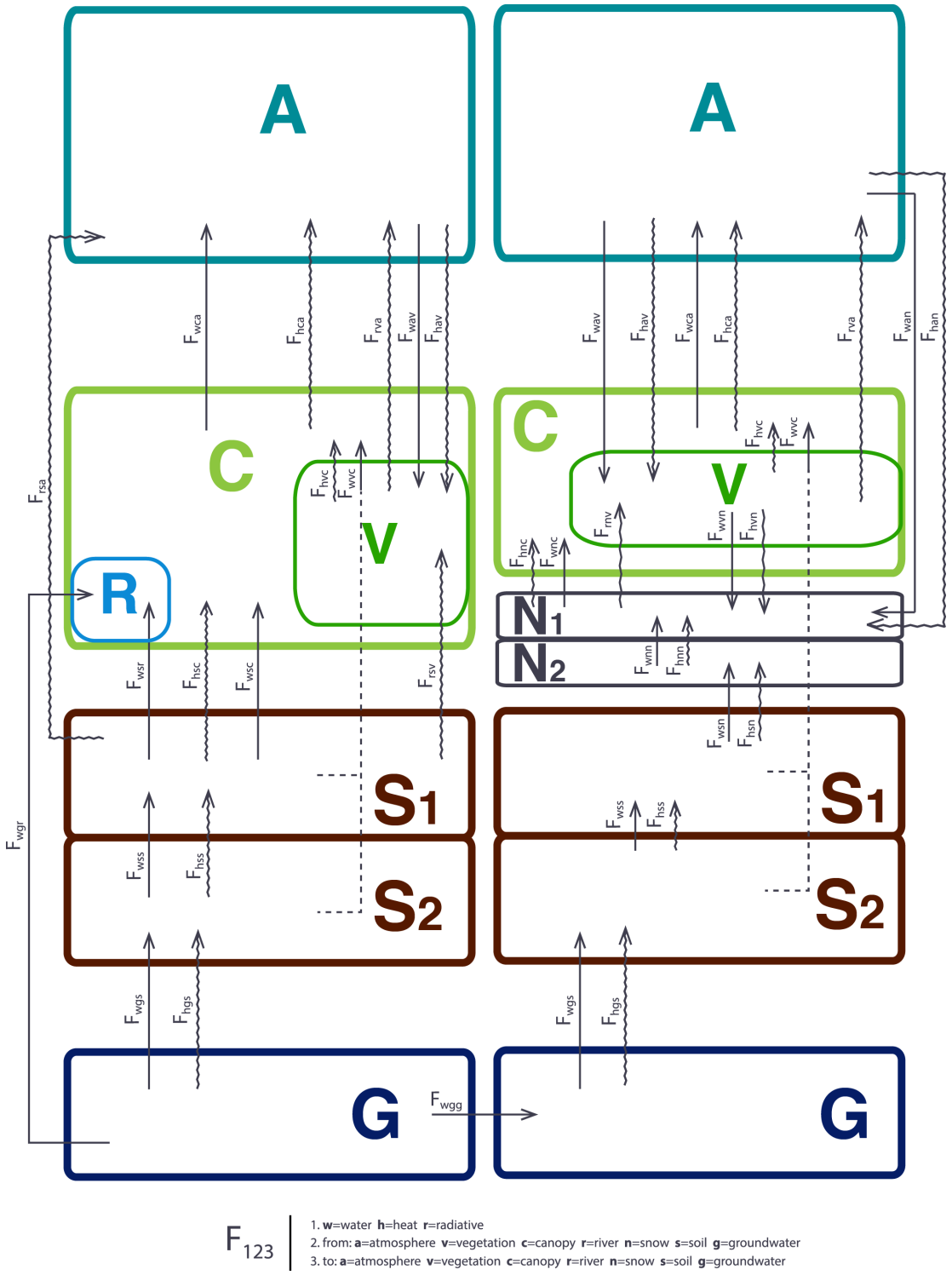

Figure 2.1: LEAFHYDRO storage reservoirs and water and energy fluxes sketch.

the opposite direction. Shortwave radiative transfer is represented as the net flux received by each component of the system under the combined influence of all others, rather than as fluxes exchanged between the components (not shown in Figure 2.1).

In the next sections the main LEAFHYDRO formulation is described. Firstly, Section 2.1 summarizes the main processes resolved by the model as a SVAT scheme (some calculations have changed since the original LEAF [63, 64] and LEAF-2 [115] formulations), and then Section 2.2 is focussed on the groundwater dynamics scheme implemented.

2.1 Land surface and soil layers formulation

In this section the methodology used in LEAFHYDRO for the resolved soil crust and the land surface is summarized, starting from the soil layers and following up through snow and temporary surface water, vegetation, bare ground, canopy air, incoming precipitation and radiation.

The methodology used by LEAFHYDRO is simple. First, incoming and outgoing water and heat fluxes in Figure 2.1 are calculated for each layer and surface represented by the model. Then, water mass and energy balances after such fluxes are performed in order to prognosticate temperature and moisture values for each layer and surface.

2.1.1 Soil formulation

LEAFHYDRO resolves the top 4 m of the soil. This 4 m column is divided into 14 layers and the layer thickness increases gradually from 5 cm for the top layer to 50 cm for the deepest layers. The layer configuration in a soil column is showed in Figure 2.2, where moisture fluxes are upward or downward capillary flux (C) and downward gravity drain (G).

The parameterization to calculate moisture fluxes within the soil is based on a multilayer soil model described by *Tremback & Kessler* (1985) [110], which was itself a modification of the scheme described by *Mahrer & Pileke* (1977) [73] and *McCumber & Pielke* (1981) [79]. Thus, the water vertical flux between adjacent unsaturated soil layers F_{wss} (kg m^{-2} s^{-1}) combines gravitational drain and capillary flux, and is given by the Richards' Equation,

$$F_{wss} = -\rho_w K_\eta \frac{\partial(\Psi + z)}{\partial z}, \tag{2.1}$$

where ρ_w (kg m^{-3}) is the density of liquid water, K_η (m s^{-1}) is the hydraulic conductivity at a given volumetric water content η, Ψ (m) is the soil capillary potential and z (m) is height.

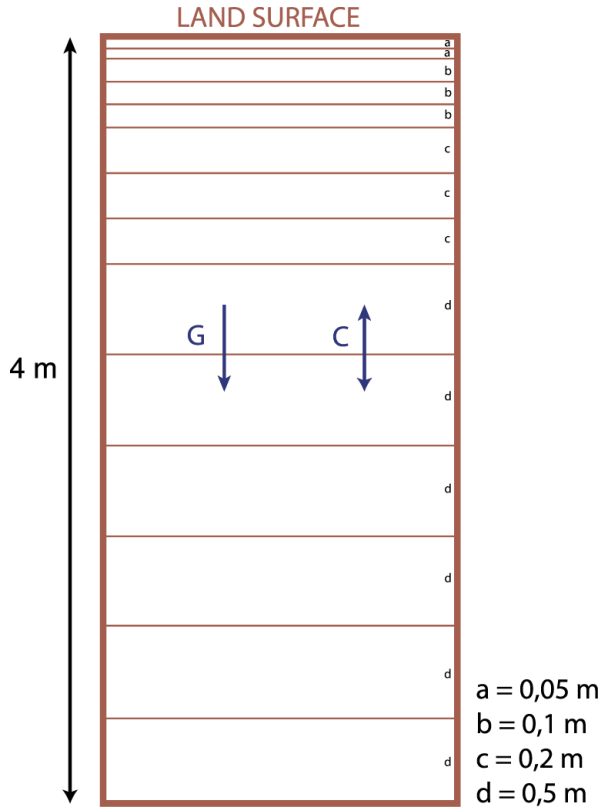

Figure 2.2: LEAFHYDRO soil column layers sketch.

Parameters K_η and Ψ depend on the water content and the pore-size index of the soil. To compute such parameters, the model follows the *Clapp & Hornberger* (1978) [24] formulation:

$$K_\eta = K_f \left(\frac{\eta}{\eta_f}\right)^{2b+3} \qquad \Psi = \Psi_f \left(\frac{\eta_f}{\eta}\right)^{b}, \tag{2.2}$$

where b is the soil pore-size index and subscript f denotes quantity at saturation.

From a simple water mass balance between incoming and outgoing water fluxes within each layer, LEAFHYDRO prognosticates the soil water content η of the given layer.

The soil heat flux between layers F_{hss} (J m^{-2} s^{-1}) is then due to the temperature gradient and the internal energy carried with the moisture flux, and it is given by

$$F_{hss} = -\lambda \frac{\partial T_s}{\partial z} + F_{wss}\,(C_l T_s + L_{il}), \tag{2.3}$$

where λ (J m^{-1} s^{-1} K^{-1}) is the thermal conductivity, T_s (K) is soil temperature, C_l (J kg^{-1} K^{-1}) is the specific heat of liquid water and L_{il} (J kg^{-1}) is the latent heat

of fusion. The soil thermal conductivity is calculated using the Johansen's method [58]:

$$\lambda = \left(\lambda_f - \lambda_d\right)\lambda_e - \lambda_d, \tag{2.4}$$

where λ_f is the thermal conductivity in saturated state, λ_d is the thermal conductivity in dry state (its value depends on the soil type) and λ_e is a function representing the influence of the degree of saturation on λ: $\lambda_e = 1 + 0.7log_{10}(\eta/\eta_f)$. For frozen and unfrozen soils, λ_f is calculated as:

$$(\lambda_f)_{frozen} = \lambda_d^{1-\eta_f}\lambda_i^{\eta_f - f_l\eta}\lambda_l^{f_l\eta} \qquad (\lambda_f)_{unfrozen} = \lambda_d^{1-\eta_f}\lambda_l^{f_l\eta}, \tag{2.5}$$

where f_l is the liquid water mass fraction, λ_l is the thermal conductivity of liquid water ($\lambda_l = 0.57$ J m^{-1} s^{-1} K^{-1}) and λ_i is the thermal conductivity of ice ($\lambda_i = 2.2$ J m^{-1} s^{-1} K^{-1}).

Once the heat fluxes between layers have been calculated, an energy balance prognosticates internal energy Q_s (J m^{-3}) of moist soil for each soil layer, relative to a reference state of soil and completely frozen moisture both at 0°C. It is defined by

$$Q_s = W_s f_i C_i T_s + W_s f_l \left(C_l T_{s_C} + L_{il}\right) + C_s m_s T_{s_C}, \tag{2.6}$$

where T_{s_C} (°C) is soil temperature, f_i and f_l are the ice and liquid water mass fractions relative to the total water mass in the soil, m_s and W_s are the mass of dry soil and water, respectively, in kilograms per cubic meter of total volume (including water, soil and air), C_i, C_l and C_s (J kg^{-1} K^{-1}) are the specific heats of ice, liquid, and dry soil particles, and L_{il} (J kg^{-1}) is the latent heat of fusion. The use of Q_s provides more information than temperature, as it represents the energy associated not only with temperature but also with latent heat of fusion. Temperature and liquid versus ice fraction are diagnosed from Q_s, with knowledge of W_s and m_s. An increase of the ice fraction reduces the water flux within the soil provided that the frozen soil has zero percolation.

2.1.2 Snow and temporary surface water formulation

Snowcover, snow melt, rainwater and temporary streams are included in the definition of temporary surface water. That is, water that had reached the ground surface as precipitation but has not yet percolated into the soil or run off to permanent water bodies, like oceans or rivers.

LEAFHYDRO divides the snowcover into vertical layers depending on the depth of snow present, up to 3 layers. For each snow layer, the mass W_n (kg m^{-2}) and internal energy Q_n (J kg^{-1}) are prognosticated via energy and mass balances.

In analogy with Equation 2.6, the internal energy of snowcover relative to a reference state of ice at 0°C is defined by

$$Q_n = f_i C_i T_{n_C} + f_l \left(C_l T_{n_C} + L_{il} \right), \tag{2.7}$$

where T_{n_C} (°C) is the snow layer temperature, f_i and f_l are the ice and liquid water mass fractions relative to the total mass of the layer, C_i and C_l (J kg^{-1} K^{-1}) are the specific heats of ice and liquid water and L_{il} (J kg^{-1}) is the latent heat of fusion.

Q_n values between zero and L_{il} do imply a mixture of ice and liquid at 0°C in the snowcover, hence f_l is diagnosed as Q_n/L_{il}. The snowcover layer temperature T_n is also diagnosed from Q_n.

The water fluxes between snowcover layers F_{wnn} (kg m^{-2} s^{-1}) and from the bottom snowcover layer to the soil F_{wsn} (kg m^{-2} s^{-1}), and their associated heat fluxes F_{hnn} (J m^{-2} s^{-1}) and F_{hsn} (J m^{-2} s^{-1}) are calculated in the model by percolation of liquid water, as an excess over the layer liquid water holding capacity, and heat diffusion:

- First, the incoming fluxes from the atmosphere to the top snowcover layer are added to the layer mass and internal energy, and hence the fractional liquid water content is diagnosed from the internal energy.
- Then, the liquid water exceeding 10% of the ice mass in the layer is percolated as F_{wnn} to the next snowcover layer.
- To calculate the heat flux to the next layer LEAFHYDRO uses a downgradient diffusion relation following *Adams & Brown* (1973) [7], combination of the sensible heat in the presence of a temperature gradient and the latent heat carried by the vapour flux from warmer to cooler layers – note that the vapour flux is neglected because it is typically weak [7] –. The combined diffusion coefficient K_n (J m^{-1} s^{-1} K^{-1}) is given by

  $$K_n = (1.093 \times 10^{-3}) \exp(0.028 T_n) f_{\rho_n}, \tag{2.8}$$

  where T_n (K) is the snow layer temperature, ρ_n (kg m^{-3}) is the density of the snowcover layer, and the last factor f_{ρ_n} is a ρ_n dependent function given by $f_{\rho_n} = 0.03 + 0.303(\rho_n \times 10^{-3}) - 0.177(\rho_n \times 10^{-3})^2 + 2.25(\rho_n \times 10^{-3})^3$. Additional heat flux carried by the percolating water must be taken into account, hence the net heat flux F_{hnn} is given by

  $$F_{hnn} = -K_n \frac{\partial T_n}{\partial z} - F_{wnn} Q_n, \tag{2.9}$$

  where Q_n is the internal energy of the upper snowcover layer carried with the moisture flux.
- The mass and energy values are then updated in the layer and the process is repeated for the layer below.

- For the lowest snowcover layer, the percolating liquid water into the soil F_{wsn} is limited by the top soil layer capacity to accept surface water before reaching saturation, and water exceeding this limit flows surface runoff. The net heat flux F_{hsn} is calculated as

$$F_{hsn} = -0.5(K_n + \lambda)\frac{\partial T}{\partial z} - F_{wsn}Q_n. \tag{2.10}$$

After the snowcover fluxes have been calculated and mass and energy layer values have been updated, the temporary surface water parameterization follows and adjustment procedure described by *Walko et al.* (2000) [115] to keep the total snowcover layers number and individual snowcover layer thickness within prescribed bounds. This adjustment assures that no snowcover layer is to become too thin for stable numerical computation and, in order to well resolve the snowcover, the total number of snowcover layers is to increase when mass is added to snowcover if allowed by numerical computation stability up to 3 snowcover layers. Only if the snowcover contains some ice, multiple snowcover layers will be used. If so little snowcover exists that prognosis of its internal energy by explicit time differencing may be computationally unstable (in which case snowcover resides in a single layer), an implicit computation is done instead in which the snowcover and top soil layer are brought into thermal equilibrium.

2.1.3 Surface vegetation formulation

When there is vegetation on the surface and it is not cover by snow, the water and heat exchanges between vegetation and the surrounding canopy air parameterization is based on *Avissar et al.* (1985) [11].

The specific humidity at the leaf-surface interface q_{vc} (kg kg^{-1}) is calculated as

$$q_{vc} = \frac{r_{vc}q_{vf} + r_{st}q_c}{r_{vc} + r_{st}}, \tag{2.11}$$

where q_{vf} (kg kg^{-1}) is the saturated specific humidity at the vegetation surface and q_c (kg kg^{-1}) is the specific humidity of the canopy air surrounding vegetation. The vegetation-canopy resistance r_{vc} (s m^{-1}) is calculated as a function of the vegetation leaf area index (LAI) and the friction velocity u_* by

$$r_{vc} = \frac{1 + 0.55LAI}{0.01\sqrt{116.6u_*}}, \tag{2.12}$$

whereas the stomatal resistance r_{st} (s m^{-1}) is defined as

$$r_{st} = \frac{r_{st_{min}}}{f_R f_T f_V f_C f_\Psi}, \tag{2.13}$$

where $r_{st_{min}}$ is the minimal stomatal resistance for a given vegetation type and occurs when the stomata are completely opened. Each f_i function quantifies the influence of a specific environmental factor upon the resistance (R stands for solar global radiation, T for leaf temperature, V for vapour pressure difference between leaf and the surrounding air, C for ambient atmospheric carbon dioxide concentration and Ψ for soil water potential in the root zone), and is given by

$$f_i = \frac{1}{1 + \exp[-S_i(X_i - X_{bi})]}, \tag{2.14}$$

where the subscript i refers to the environmental factor, X_i is the intensity of the factor i, X_{bi} is the value of X_i at $f_i = 0.5$, and S_i is the slope of the curve at this point [12]. This stomatal resistance r_{st} is limited by a variable lower threshold that corresponds to the maximum possible transpiration given the present atmospherical conditions.

The heat flux from vegetation to canopy air F_{hvc} (J m^{-2} s^{-1}) is calculated from the temperature difference and the resistance r_{vc}, as

$$F_{hvc} = -\frac{2.2LAIC_p\rho_a(T_c - T_v)}{r_{vc}}, \tag{2.15}$$

where LAI is again the dimensionless vegetation leaf area index, C_p (J kg^{-1}K^{-1}) is the specific heat capacity of air, ρ_a (kg m^{-3}) is the density of the air, and T_c and T_v (K) are the canopy air and vegetation temperatures, respectively.

Similarly, the water flux between vegetation and canopy air F_{wvc} (kg m^{-2} s^{-1}) is calculated from the humidity difference as

$$F_{wvc} = -\frac{2.2LAI\sigma\rho_a(q_c - q_{vf})}{r_{vc}}, \tag{2.16}$$

where q_c (kg kg^{-1}) is the canopy air specific humidity, q_{vf} (kg kg^{-1}) is the vegetation specific humidity at saturation. σ is a factor of the exchanged water that comes from the vegetated surface, depending on the available water at the leaf surface, as

$$\sigma = \left(\frac{w_v}{0.22LAI}\right)^{2/3}, \tag{2.17}$$

where w_v is the vegetated surface water content. w_v has an upper threshold of $0.22LAIf_v$ due to the shedding of moisture excess, and therefore σ is limited between 0 and $f_v^{2/3}$, where f_v is the vegetation fractional coverage.

The moisture exchange that transpirates through vegetation is given by

$$F_{wvc_{transp}} = -\frac{2.2LAI(1-\sigma)\rho_a(q_c - q_{vf})}{r_{vc} + r_{st}}. \tag{2.18}$$

The transpiration is taken from the moistest level in the root zone. Transpiration is limited between zero, when the canopy air is moister than the vegetation specific humidity at saturation, and the water available in the root zone.

2.1.4 Surface bare ground formulation

For the ground-canopy fluxes calculation, the formulation that LEAFHYDRO uses has been adopted from CLM (*Community Land Model*), which is the SVAT scheme developed by the NCAR Earth System Laboratory.

The formulation, similar to the described canopy-vegetation methodology, makes use of aerodynamic resistances to sensible heat transfer ,r_{ah}, and to water vapour transfer, r_{aw}, between the soil and the surrounding air, given by

$$r_{ah} = \frac{\theta_a - \theta_g}{\theta_* u_*} \qquad r_{aw} = \frac{q_a - q_g}{q_* u_*}, \tag{2.19}$$

where θ (K) is potential temperature, q (kg kg^{-1}) is specific humidity, the subscripts a and g stand for atmosphere and ground surface, respectively, u_* (m s^{-1}) is the friction velocity, θ_* (K) is temperature scale and q_* (kg kg^{-1}) is humidity scale. The profile terms $(\theta_a - \theta_g)/\theta_*$ and $(q_a - q_g)/q_*$ are calculated using the Monin-Obukov similarity theory [121].

The heat flux between the soil surface and the surrounding air F_{hsc} (J m^{-2} s^{-1}) is then calculated as

$$F_{hsc} = -\frac{\rho_a C_p (T_c - T_g)}{r_{ah}}, \tag{2.20}$$

where T_g (K) is the temperature at the soil/snow surface (taken as the top soil/snow layer temperature).

The water flux between the soil surface and the surrounding air F_{wsc} (kg m^{-2} s^{-1}) is given by

$$F_{wsc} = -\frac{\rho_a(q_c - q_{sfe})}{r_{aw} + r_{sc}}, \tag{2.21}$$

where q_{sfe} (kg kg^{-1}) is the effective saturation specific humidity of the soil surface and r_{sc} (m s^{-1}) is the soil-canopy water flux resistance.

Following *Lee & Pielke* (1992) [55], q_{sfe} is computed from the specific humidity of the soil surface at saturation q_{sf} (kg kg^{-1}) and the specific humidity of the canopy air q_c (kg kg^{-1}), as

$$q_{sfe} = \exp\left(\frac{g\Psi_g}{R_w T_g}\right)\beta q_{sf} + (1-\beta)q_c, \tag{2.22}$$

where g (m s^{-2}) is acceleration due to gravity, Ψ_g (m) is the soil water potential at the ground surface, R_w (J kg^{-1} K^{-1}) is the gas constant for water vapour and β is a surface wetness function, given by

$$\beta = \begin{cases} \frac{1}{4}\left[1 - cos\left(\frac{\eta_s}{\eta_{fc}}\pi\right)\right]^2 & \eta_s < \eta_{fc} \\ 1 & \eta_s \geq \eta_{fc} \end{cases}, \tag{2.23}$$

where η_s (m^3 m^{-3}) is the volumetric soil water content and η_{fc} (m^3 m^{-3}) is the volumetric soil water content at field capacity.

The soil-canopy resistance r_{sc} in Equation 2.21 calculation is based on *Sellers et al.* (1986) [102], as

$$r_{sc} = (1-f_n)\exp(8.206 - 4.255 w_s), \tag{2.24}$$

where f_n is the snow fraction in the cell and w_s is the dimensionless surface soil wetness defined as $w_s = (w_l/\rho_l + w_i/\rho_i)/(z_{s-top}\eta_{sf})$. Here, w (kg m^{-2}) is the water content, ρ (kg m^{-3}) is density, the subscripts l and i stand for liquid water and ice, respectively, z_{s-top} (m) is the depth of the top soil layer, and η_{sf} (m^3 m^{-3}) is the volumetric soil water content at saturation.

The ground dew/frost formation F_{dew} (kg m^{-2} s^{-1}) is based on the saturation value of specific humidity at the soil surface temperature q_{sf}, as

$$F_{dew} = -\frac{\rho_a(q_c - q_{sf})}{r_{aw} + r_{sc}}. \tag{2.25}$$

2.1.5 Canopy-atmosphere fluxes

LEAFHYDRO calculates the sensible heat H (J m^{-2} s^{-1}) and evapotranspiration ET (kg m^{-2} s^{-1}) to the atmosphere as:

$$H = -\rho_a C_p u_* \theta_* \qquad ET = -\rho_a u_* q_*. \tag{2.26}$$

Here, the temperature scale θ_*, humidity scale q_* and friction velocity u_* are computed from the surface layer similarity theory as *Louis et al.* (1981) [70, 115], using the canopy air values of humidity and temperature (calculated from surface balances as detailed further on in Section 2.1.8) and atmospheric values of humidity, temperature and wind. The atmospheric variables may come from an atmospheric model if LEAFHYDRO works as the land surface scheme coupled to an atmospheric model, or from the forcing data variables if LEAFHYDRO works offline (see Section 3.3 for a description of the atmospheric forcing).

Note that the H and E fluxes are referred to in Figure 2.1 as F_{hca} and F_{wca}, respectively.

2.1.6 Precipitation fluxes

LEAFHYDRO recieves moisture and energy fluxes from precipitation of hydrometeors, either produced by the physical parameterizations in the coupled atmospheric model or introduced as precipitation forcing when it works offline.

The precipitation fluxes are then partitioned between vegetation and surface water components with use of the vegetation fractional coverage. Vegetation intercepted precipitation may then exceed the maximum water content that the vegetation can hold, in this case the exceeded water is brought to thermal equilibrium with vegetation by heat transfer and then shed from vegetation to be treated as surface water.

The surface water then may form temporary surface snowcover layers, when the atmospheric conditions allow it, or percolate into the soil if the top soil layer water content has not reached the soil capacity. If after percolation there is still precipitated water on the surface, it flows as surface runoff.

2.1.7 Radiative fluxes

As explained for precipitation fluxes, longwave and shortwave radiation fluxes that reach the surface are introduced into the LEAFHYDRO system either from the atmospheric model coupled to it or as external forcing when working offline.

Longwave radiation is emitted to the atmosphere or to the next reaching surface, absorbed, and reflected by vegetation, snowcover, soil and permanent water bodies. Snowcover, even when shallow, acts nearly as a blackbody to longwave radiation. Hence, when snowcover is present, the top snow layer replaces the top soil layer as a radiating and absorbing surface. Soil and vegetation likewise have high emissivities and low reflectivities, and LEAFHYDRO hence makes the assumption that multiple longwave reflections do not occur; once-reflected radiation is assumed to be fully absorbed by the receiving surface. Then, defining $R_{L\downarrow}$ (J m^{-2} s^{-1})

as downward longwave radiation flux at the bottom of the atmosphere, the longwave radiation emitted by vegetation R_{L_v} and by the top soil layer R_{L_s} (J m^{-2} s^{-1}), and the absorbed radiation L (J m^{-2} s^{-1}) by vegetation, the top soil layer and the atmosphere are given, respectively, by

$$R_{L_v} = \epsilon_v \sigma T_v^4 \qquad R_{L_s} = \epsilon_s \sigma T_s^4 \tag{2.27}$$

$$L_{av} = R_{L\downarrow} \Gamma [a_v + (1 - \Gamma)(1 - a_s)] \tag{2.28}$$

$$L_{sv} = R_{L_s} \Gamma a_v \tag{2.29}$$

$$L_{as} = R_{L\downarrow} (1 - \Gamma) a_s \tag{2.30}$$

$$L_{vs} = R_{L_v} \Gamma a_s \tag{2.31}$$

$$L_{va} = R_{L_v} \Gamma (2 - a_s - \Gamma + \Gamma \epsilon_s) \tag{2.32}$$

$$L_{sa} = R_{L_s} (1 - \Gamma), \tag{2.33}$$

where ϵ is emissivity, σ (J m^{-2} K^{-4} s^{-1}) is the Stefan-Boltzmann constant, T (K) is temperature, Γ is the non-covered by snow vegetation fractional coverage, a is absorptivity and the subscripts v, s and a refer to vegetation, soil top layer and atmosphere, respectively. For the longwave absorbed radiation L, the first subscript indicates the emitting body and the second subscript indicates the receiving surface.

Shortwave solar radiation can penetrate to considerable depths into snowcover, and hence LEAFHYDRO considers the transmissivity of each snow layer. However, vegetation is assumed to be opaque. Defining $R_{S\downarrow}$ (J m^{-2} s^{-1}) as downward shortwave radiation flux at the bottom of the atmosphere, the net shortwave radiation S (J m^{-2} s^{-1}) received by vegetation v, snowcover layer n_i and the top soil layer s are given, respectively, by

$$S_v = R_{S\downarrow} \Gamma [1 - \alpha_v + \alpha_s (1 - \Gamma)], \tag{2.34}$$

$$S_{n_i} = R_{S\downarrow} (1 - \Gamma)(1 - \alpha_n)(1 - \tau_n + \tau_n \alpha_s) f_i, \tag{2.35}$$

$$S_s = R_{S\downarrow} (1 - \Gamma)(1 - \alpha_n) \tau_n (1 - \alpha_s), \tag{2.36}$$

where α_v, α_n and α_s are vegetation albedo, net albedo from all snow layers and soil albedo, respectively, Γ is again the non-covered by snow vegetation fractional coverage, τ_n is net transmissivity of all snow layers and f_i is the fraction of total radiation absorbed by snow that is absorbed by layer i.

The profile f_i is evaluated from the profile of transmissivities τ_{n_i} of each snowcover layer, which is a function of many factors including snow layer depth, density, snow grain size, and liquid water content. For simplicity, LEAFHYDRO parameterizes the snow layer i transmissivity as

$$\tau_{n_i} = \exp(-\epsilon D_{n_i}), \tag{2.37}$$

where D_{n_i} (m) is snowcover depth of layer i and ϵ (m^{-1}) is an extinction coefficient. ϵ is set to 20 m^{-1}, based on an average value given in *de Quervain* (1973) [28].

2.1.8 Surface balances

After all surface water and heat fluxes have been calculated as explained in previous sections, LEAFHYDRO prognosticates surface values of temperature and humidity from heat and water mass balances.

The vegetation temperature T_v is prognosticated from the heat balance at the vegetation surface between incoming and outgoing radiative, heat and moisture fluxes, given by

$$C_v \frac{\partial T_v}{\partial t} = S_v + L_{av} + L_{sv} - L_{vs} - L_{va} - F_{hvc} - (F_{wvc} + F_{wvc_{transp}})L_{lv}, \tag{2.38}$$

where C_v (J m^{-2} K^{-1}) is the effective heat capacity of vegetation, L_{lv} (J kg^{-1}) is the water latent heat of vaporization and the rest of terms are heat and water fluxes from Sections 2.1.3 and 2.1.7.

The prognosis of canopy air temperature T_c (K) is carried out through a heat balance in the canopy air between the outgoing sensible heat to the atmosphere and the incoming fluxes from the ground surface and vegetation, as

$$C_c \frac{\partial T_c}{\partial t} = F_{hsc} + F_{hvc} - H, \tag{2.39}$$

where C_c (J m^{-2} K^{-1}) is the effective heat capacity of canopy air and the rest of terms are heat fluxes from Sections 2.1.3, 2.1.4 and 2.1.5.

And similarly, the water mass balance in the canopy air that LEAFHYDRO carries out to prognosticate the canopy air specific humidity q_c (kg kg^{-1}), is given by

$$W_c \frac{\partial q_c}{\partial t} = F_{wgc} - F_{dew} + F_{wvc} + F_{wvc_{transp}} - ET, \tag{2.40}$$

where W_c (kg m^{-2}) is the moisture capacity of canopy air and the rest of terms are water fluxes from Sections 2.1.3, 2.1.4 and 2.1.5.

2.2 Dynamic groundwater scheme

The LEAFHYDRO dynamic groundwater scheme was first presented by *Miguez-Macho et al.* (2007) [83]. The concepts that the scheme is based on are the dynamical behaviour of the groundwater reservoir and its interactions with the land-atmosphere system. There are three main interactions represented by the model:

1. Groundwater recharge: Water flux between the groundwater reservoir and the soil. Depending on the soil wetness and the atmosphere demands, the recharge can be downwards, causing the water table to rise, or upwards, causing the water table to deepen.
2. Lateral groundwater flow: Water flux to or from neighbour cells within the saturated groundwater reservoir. This flux is governed by topography and the water table head elevation in the cells.
3. Groundwater-streams exchange: It can occur as groundwater discharge (subsurface runoff) into the streams when the water table head is above the river bed, maintaining the streams baseflow, or as river infiltration to the groundwater reservoir when the water table head is below the river bed, leaving the streams baseflow to be maintained by surface runoff and upstream inflow.

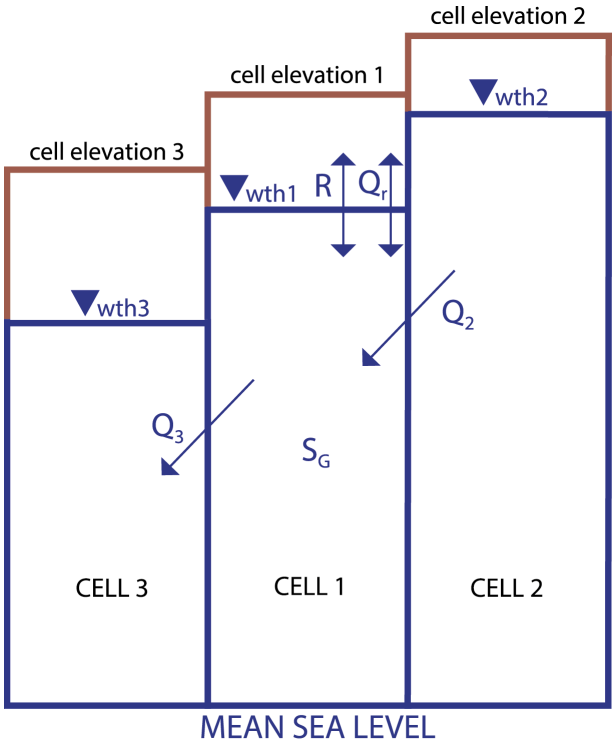

Figure 2.3: LEAFHYDRO groundwater balance in a model cell (cell 1).

Hence, the mass balance of the dynamic groundwater reservoir in a LEAFHYDRO cell is given by

$$\frac{dS_G}{dt} = \Delta x \Delta y R + \sum_{n=1}^{8} Q_n - Q_r, \tag{2.41}$$

where S_G (m^3) is the groundwater storage in a model column, $\Delta x \Delta y$ (m^2) is the horizontal resolution of the model, R (m s^{-1}) is the groundwater recharge, Q_n (m^3 s^{-1}) is the lateral flow from or to the nth neighbour model cell, and Q_r (m^3 s^{-1}) is the groundwater-streams exchange. Fluxes in Equation 2.41 are assumed to be positive when incoming the groundwater reservoir and negative when outgoing.

Figure 2.3 represent the groundwater balance in a model cell (cell 1). All water fluxes represented by arrows in Figure 2.3 are referred to cell 1, the flux Q_2 is an incoming flux from the neighbour cell 2 with a higher water table head ($wth2$), and the flux Q_3 is an outgoing flux towards the neighbour cell 3, which presents a lower water table head ($wth3$).

2.2.1 Groundwater recharge formulation

The range of water table depths in extended regions with significant topographic and climatic variabilities (as in the case of the Iberian Peninsula) is very wide. Hence, a numerical column soil-groundwater model has to find a balance between the need to resolve the upper most dynamic portion of the soil column and the convenience of resolving the column down as deep as the water table marks for the calculation of the groundwater recharge. Since resolving Equation 2.1 to calculate the moisture flux within the soil over as many layers as the water table may require could be computationally unfeasible, LEAFHYDRO calculates the groundwater recharge in two different ways, depending on whether the water table is within the top-4 metres of the soil column (scenario *A* in Figure 2.4) or below the resolved top-4 metres (scenario *B* in Figure 2.4), as discussed in *Miguez-Macho et al.* (2007) [83].

Under scenario *A* conditions (left graph in Figure 2.4), the model first diagnoses the water table position, assuming that it is contained within the same soil layer where it was in the previous timestep. To do so, the soil water content in the unsaturated portion of the layer containing the water table (layer 1) is obtained assuming that there is equilibrium (no vertical water flux) between two saturated layers. Hence, the flux between layer 1 and the layer below (layer 2) is zero, and then setting F_{wss} to 0 in Equation 2.1 leads to

$$\frac{\partial(\Psi + z)}{\partial z} = 0, \qquad \text{or} \qquad \Psi_1 - \Psi_2 = z_2 - z_1, \tag{2.42}$$

where Ψ (m) is soil capillary potential and z (m) is height, evaluated in the layers referred to by subscripts 1 and 2. Applying the relationship between Ψ and η in

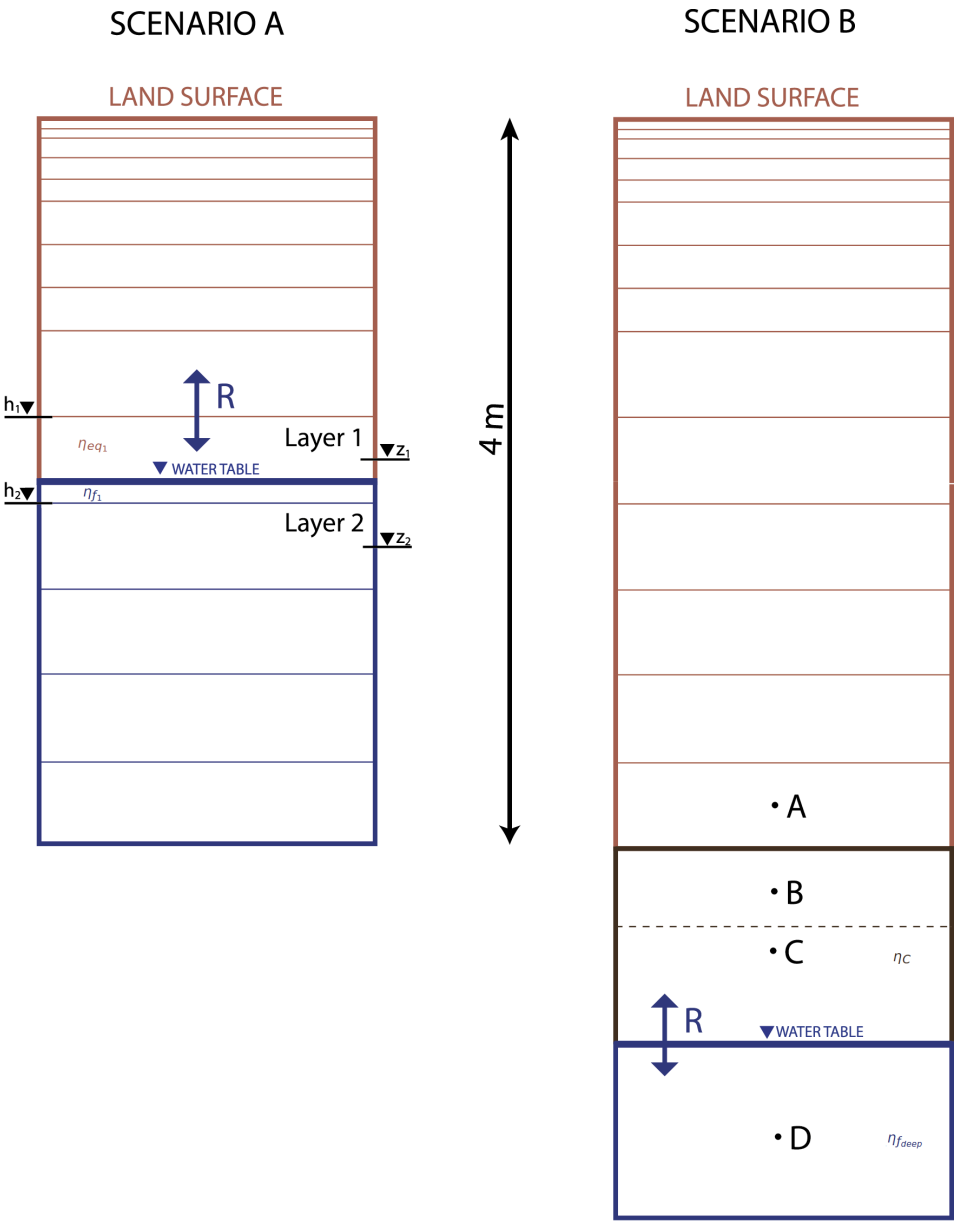

Figure 2.4: LEAFHYDRO double scenario to calculate groundwater recharge.

Equation 2.2 to Equation 2.42, and provided that layer 2 is saturated, the equilibrium water content in the unsaturated portion of layer 1 η_{eq_1} (m^3 m^{-3}) is obtained as

$$\eta_{eq_1} = \eta_{f_1} \left(\frac{\Psi_{f_1}}{\Psi_{f_2} + z_2 - z_1} \right)^{1/b_1} . \tag{2.43}$$

Then, assuming even distribution of total soil water in the layer, the layer 1 soil water content η_1 that the model calculated in the soil fluxes routine as described in Section 2.1.1, can be expressed as

$$\eta_1 = \eta_{eq_1}\left(\frac{h_1 - wtd}{h_1 - h_2}\right) + \eta_{f_1}\left(\frac{wtd - h_2}{h_1 - h_2}\right), \tag{2.44}$$

where wtd (m) is the water table depth, h_1 (m) is the head of layer 1 height and h_2 (m) is the head of layer 2 height. Now, from Equation 2.44, the water table depth is diagnosed as

$$wtd = \frac{\eta_{f_1} h_2 - \eta_{eq_1} h_1 + \eta_1 (h_1 - h_2)}{\eta_{f_1} - \eta_{eq_1}} \tag{2.45}$$

And finally, knowing the water table fall or rise Δwt (m s^{-1}) as the difference between the new wtd calculated in Equation 2.45 and the previous depth, the model calculates the groundwater recharge R (m s^{-1}) as the water amount necessary to fill or drain the pore space between saturation and present equilibrium water content in the unsaturated portion of the layer after the water table movement, as

$$R = \Delta wt(\eta_{f_1} - \eta_{eq_1}). \tag{2.46}$$

This approach to diagnose the water table depth allows a smooth evolution, since the water table may appear in between the model soil layers. If the soil water content η_1 from the soil fluxes routine is the saturation value η_{f_1}, layer 1 is already saturated, hence the water table is taken up to the layer above, where the calculations just described for the diagnosis of its depth wtd and the groundwater recharge R are carried out. On the other hand, if η_1 is lower than the equilibrium value η_{eq_1}, the water table is taken down to layer 2, where the water table depth and recharge calculations are done.

Under scenario B conditions (right graph in Figure 2.4), the water table depth appears below the 4 metres soil crust resolved by the model. A bottom layer (darker brown layer in Figure 2.4) is added that extends from 4 m deep to the water table position, centred in point C. This is a virtual layer, of variable thickness in space and time. Since it can be much thicker than the layer above (problematic for finite difference schemes), an auxiliary layer is added which contains point B (defined by a dashed line in Figure 2.4). This auxiliary layer has equal thickness as the layer above which contains point A (deepest layer resolved by the model).

The water content of point B is initially obtained by linear interpolation between A and C (water content in the virtual layer containing C is part of the model initialization). Given water content at A and B, the flux between the two can be calculated. In the same manner, an auxiliary layer is added below the water table, containing point D and with equal thickness as the layer containing C. The water content gradient between C and D (layer containing D is saturated) determines the flux between the two, which is the groundwater recharge R. Knowing the fluxes above and below, the new water content η_C of the layer containing C can be determined by mass

balance. The change in water content in the virtual layer is added to or taken away from the groundwater reservoir as Δwt, calculated similarly to Equation 2.46 from the groundwater recharge as

$$\Delta wt = \frac{R}{\eta_{f_{deep}} - \eta_C}, \tag{2.47}$$

where $\eta_{f_{deep}}$ ($m^3\ m^{-3}$) is the saturation soil water content for the soil at the water table position depth.

2.2.2 Groundwater lateral flow formulation

The methodology for the calculation of the lateral flow within the saturated groundwater reservoir carried out in LEAFHYDRO was discussed by *Fan et al.* (2007) [42]. Applying Darcy's Law, the water flux from the nth neighbour into a model cell (positive), or from a model cell into the nth neighbour (negative), is given by

$$Q_n = cT\left(\frac{wtd_n - wtd}{l}\right), \tag{2.48}$$

where c (m) is the flow cross-section connecting the cells, T ($m^2\ s^{-1}$) is the flow transmissivity between the cells, wtd and wtd_n (m) are the water table depths or positions for the centre cell and the nth neighbour cell, respectively, and l (m) is the distance between cells, which is taken as $l = \Delta x$ along x and y directions or as $l = \sqrt{2}\Delta x$ along the diagonal (note that $\Delta x = \Delta y$).

Under the assumption of equal width of flow for all 8 directions, and provided that $\Delta x = \Delta y$ in the model, the flow cross-section c is taken as $c = \Delta x\sqrt{0.5\tan(\pi/8)}$, which is the length of the sides of a regular octagon of the same area of a model cell (see Figure 6b-c in *Fan et al.* (2007) [42]).

The flow transmisivity T is calculated as

$$T = \int_{-wtd}^{\infty} K_{L_f} \mathrm{d}z', \tag{2.49}$$

where K_{L_f} ($m\ s^{-1}$) is the lateral hydraulic conductivity at saturation and z' (m) is vertical downwards direction.

Given the lack of observations for this lateral hydraulic conductivity at saturation, the model uses the anisotropy ratio α, that relates K_{L_f} with the hydraulic vertical conductivity at saturation K_{V_f} as $\alpha = K_{L_f}/K_{V_f}$. The values taken for the anisotropy ratio α are well within the range observed in nature and based on the clay content of the soil [42]. But available data for vertical hydraulic conductivity only covers the

top soil metres, hence continental and regional scale groundwater modeling needs to make assumptions on the vertical distribution of hydraulic conductivity. Exponential decrease with depth is commonly assumed for hydrological model over the scales of metres, *Decharme et al.* (2006) [32] found K_{V_f} to improve its performance using an exponential profile for discharge simulations over the Rhône Basin with the LSM ISBA (*Interaction Soil-Biosphere-Atmosphere*). LEAFHYDRO uses available data for K_{V_f} up to 1.5 m deep and assumes exponential decrease downwards, in the form

$$K_{V_f} = K_0 \exp\left(-\frac{z'}{f}\right), \tag{2.50}$$

where K_0 (m s^{-1}) is the known value at 1.5 m deep, z' (m) is the depht below 1.5 m and f (m) is the e-folding depth, discussed later.

Hence, using the anisotropy ratio and the vertical profile for hydraulic conductivity, the flow transmissivity T has to be calculated from Equation 2.49 under the two possible scenarios showed in Figure 2.5.

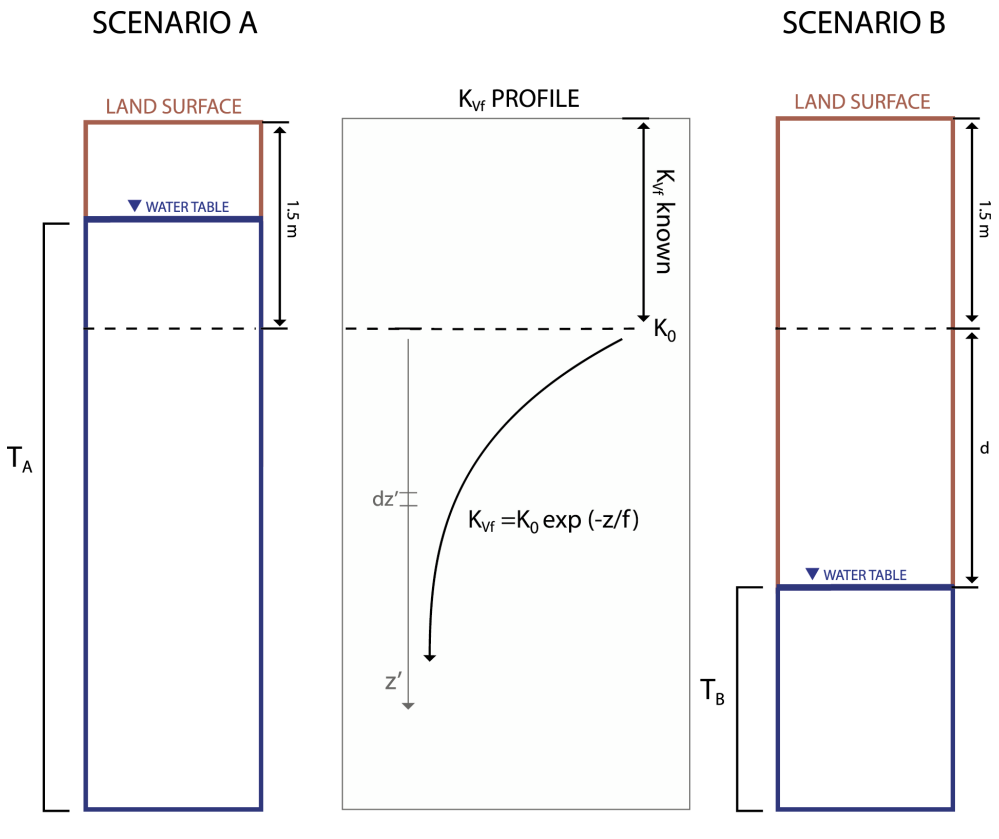

Figure 2.5: LEAFHYDRO double scenario to calculate groundwater lateral flow.

Under scenario *A*, the water table appears above 1.5 deep, and the flow transmissivity is calculated from Equation 2.49 as

$$T_A = \alpha K_0 \Delta z + \int_0^{\infty} \alpha K_0 \exp\left(-\frac{z'}{f}\right) \mathrm{d}z' = \alpha K_0 \Delta z + \alpha K_0 f, \tag{2.51}$$

where Δz (m) is the distance between the water table and 1.5 m deep, and the origin of coordinates for the z' direction is situated at 1.5 m deep.

Under scenario B, the water table appears below 1.5 m deep, thus T is given by

$$T_B = \int_d^{\infty} \alpha K_0 \exp\left(-\frac{z'}{f}\right) \mathrm{d}z' = \alpha K_0 f \exp\left(-\frac{d}{f}\right), \tag{2.52}$$

where d (m) is the positive distance between the water table position and 1.5 m deep, as $d = -wtd - 1.5$.

The e-folding depth f (m) reflects the sediment-bedrock profile at a location. It is a complex function of climate, geology and biota, but the balance depends strongly on terrain slope. As a first order approximation to capture features of the water table depth distribution along an area as large as the Iberian Peninsula, LEAFHYDRO calculates f as a function of the terrain slope. Thorough calibration of f was carried out by *Fan et al.* (2007) [42] to best reproduce more than 567,000 water table depth observations across North America. For this work, LEAFHYDRO uses a function for f that depends on terrain slope β as

$$f = \frac{75}{1 + 150\beta}. \tag{2.53}$$

The f depth value is limited to 4 m when $\beta \geq 0.118$.

In order to ensure that flow from the considered cell to the neighbour is the same as from the neighbour to the considered cell under the same hydraulic potential, LEAFHYDRO calculates T for both cells involved and uses the average of the two.

2.2.3 Groundwater-streams exchange formulation: Gaining and losing streams

For the calculation of the groundwater-streams flux, LEAFHYDRO distinguishes between gaining streams, when the water table is above the riverbed elevation and feeds the streams, and losing streams, when the water table is below the river elevation and the streams drain water towards the groundwater reservoir. The sketch in Figure 2.6 shows the two possible modes in nature (left) and its modeled representation in LEAFHYDRO (right). Given the dynamic nature of the water table, the same cell can work as a losing or as a gaining stream under different climatic conditions, depending on the water table position.

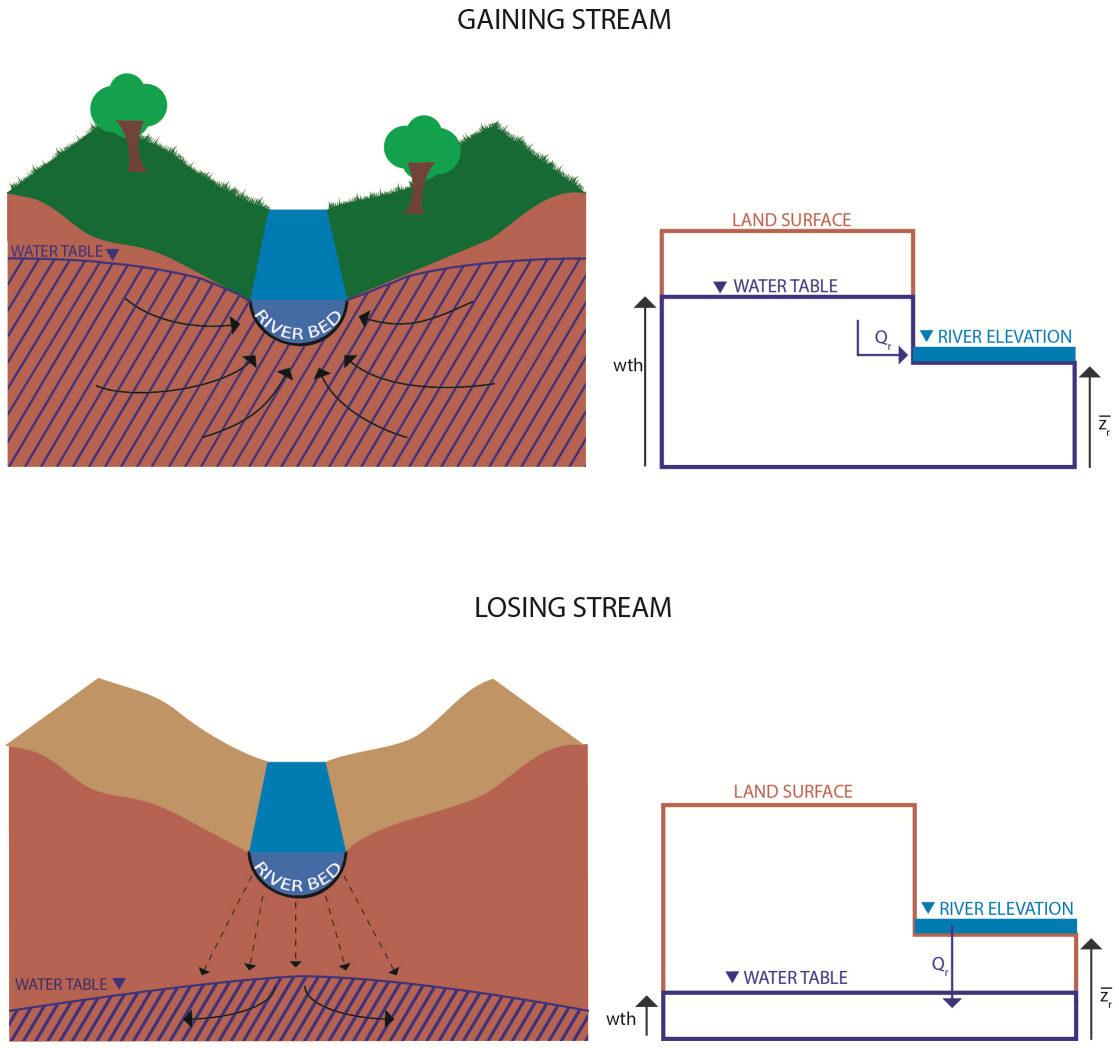

Figure 2.6: Gaining and losing streams sketch. Representation of the cases in nature (left) and in LEAFHYDRO (right).

For gaining streams, the groundwater flux into the stream in a given area depends on the positive elevation difference between the water table and the river stage, the hydraulic connection between the river and the groundwater reservoir through the river bed, and the contact area. Since the LEAFHYDRO resolution is too coarse for explicitly represent the individual channels in the domain (as is typically the resolution atmospheric models hydraulic schemes), the channels in a cell are treated as an individual stream of averaged parameters. Hence, applying Darcy's Law for each cell, the groundwater-streams flow Q_r ($m^3\ s^{-1}$) is given by

$$Q_r = \left(\frac{\bar{K_{rb}}}{\bar{b_{rb}}}\right)\left(\bar{w}_r \sum L_r\right)(wth - \bar{z}_r), \tag{2.54}$$

where $\bar{K_{rb}}$ ($m\ s^{-1}$) is the mean river bed hydraulic conductivity in the cell, $\bar{b_{rb}}$ (m) is the mean thickness of river bed sediments in the cell, $\bar{w}_r$ (m) is the mean river

width within the cell, L_r (m) is the length of individual channels in the cell (the river depth is neglected for the calculation of contact area), wth (m) is the water table head in the cell (as $wth = z + wtd$, where z (m) is the cell elevation and wtd (m) is the water table depth), and $\bar{z_r}$ (m) is the mean river elevation in the cell.

Combining the first to parenthesis in the right side of Equation 2.54, the river conductance RC (m^2 s^{-1}) is obtained. RC is a parameter commonly referred to in groundwater modeling literature, defined as

$$RC = \frac{\bar{K_{rb}} \bar{w_r} \sum L_r}{\bar{b_{rb}}}. \tag{2.55}$$

However, given the lack of observations in the Iberian Peninsula for detailed river bed sediments data, RC needs to be parameterized. Such parameterization consists in a two parts representation of RC; an equilibrium part, and a dynamic part that depends on the water table deviation from equilibrium at the time, as

$$RC = ERC \cdot F(wtd - ewtd), \tag{2.56}$$

where ERC (m^2 s^{-1}) is the equilibrium river conductance, F is a function discussed later, wtd (m) is again water table depth and $ewtd$ (m) is equilibrium water table depth (wtd initialization). The use of a dynamic river conductance was proposed in *Miguez-Macho et al.* (2007) [83] and is justified by the dynamics of the groundwater-streams contact area [29, 30].

The equilibrium part of the river conductance, ERC, represents the hydraulic connection between the streams in a cell and the groundwater reservoir in the long-term river channel evolution. Hence, ERC is linked to the equilibrium water table, calculated for the Iberian Peninsula, following *Fan et al.*(2007) [42] methodology, by *Gestal-Souto et al.* (2010) [47], and the long-term recharge. Both these long-term fields are discussed in more detail in following Chapter 3 (Section 3.2.2). Setting an equilibrium long-term hydraulic situation, the left side of Equation 2.41 vanishes, leaving the groundwater-streams exchange to balance recharge and lateral groundwater convergence, as

$$Q_r = \Delta x \Delta y R + \sum_{n=1}^{8} Q_n. \tag{2.57}$$

Applying Equations 2.54 and 2.55, and replacing RC, wtd and R with the long-term equilibrium values in Equation 2.57, ERC (m^2 s^{-1}) is calculated as

$$ERC = \frac{\Delta x \Delta y R_{lt} + \sum_{n=1}^{8} Q_n}{ewtd - \bar{z_r}}, \tag{2.58}$$

where R_{lt} (m s^{-1}) is the climatic long-term groundwater recharge, $ewtd$ (m) is the equilibrium water table depth, and the lateral flow to or from the neighbours Q_n (m^3 s^{-1}) is calculated from $ewtd$ as discussed in previous Section 2.2.2.

The dynamic par of the river conductance, $F(wtd - ewtd)$, represents the RC deviation from equilibrium as a response to the channels expansions and contractions caused by seasonal hydrological changes. Based on an observational study in Illinois (USA) on the connection between the different water cycle factors, such as groundwater reservoir and river flow, by *Eltahir & Yeh* (1999) [37], and on the need to include a function of the river valley morphology given the river channel dynamics dependence on valley profiles [29, 30], *Miguez-Macho et al.* (2007) [83] hypothesized an exponential function dependant on terrain slope for the RC response to water table deviations from equilibrium. These authors found that it reproduced reasonably well observed river flow over North America. Hence, the dynamic part of the river conductance is given by

$$F(wtd - ewtd) = \exp[\alpha(wtd - ewtd)], \tag{2.59}$$

where $\alpha = 0$ in steep terrain, since the channels have little room to grow and the dynamic part of RC vanishes, and $\alpha = 1$ where the terrain slope β satisfies $\beta < 0.2$.

For losing streams, the groundwater-streams flow Q_r (m^3 s^{-1}) is downwards, feeding the groundwater storage. Applying Darcy's Law, the distance of flow (river bed thickness for the case of gaining streams in Equation 2.54) is the same as the water table - riverbed elevation difference (third parenthesis in Equation 2.54, only for losing streams such difference have negative sign provided that $wth < \bar{z}_r$), and hence these factors cancel out one another, leaving the flux calculation to be given by

$$Q_r = -K_{rb}\bar{w}_r \sum L_r. \tag{2.60}$$

Therefore, the losing stream flux Q_r in the model is not dependant on the water table position, but on the groundwater-streams hydraulic connection. Again river bed sediments data are not available. However, K_{rb} is approximated by the hydraulic conductivity for the loamy sand soil class: $K_{rb} \approx 1.563 \times 10^{-4}$ ms^{-1}, and the river stream parameters $\bar{w}_r$ and $\sum L_r$ used here, as well as the mean riverbed elevation in the cell $\bar{z}_r$ in Equations 2.54 and 2.58, are calculated in the domain cells for initialization as detailed in following Chapter 3 (Section 3.2.4).

2.3 River flow scheme

LEAFHYDRO closes the water cycle resolving the streamflow discharging through the river channels in the model domain and ultimately to the ocean. The streamflow q

(m^3 s^{-1}) is calculated as

$$q = \frac{S_s}{K_s}, \tag{2.61}$$

where S_s (m^3) is the surface water storage and K_s (s) is the residence time for the surface water in the cell.

The surface water storage is calculated from a mass balance every river scheme timestep, as

$$\frac{dS_s}{dt} = Q_h + Q_r + Q_s + \sum_{n=1}^{m} Q_n - Q_0, \tag{2.62}$$

where Q_h (m^3 s^{-1}) is the hillslope overland runoff given from the temporary surface water routine, Q_r (m^3 s^{-1}) is the groundwater-streams exchange flux, Q_s (m^3 s^{-1}) is water springing out when the water table reaches the surface, Q_n (m^3 s^{-1}) is the river inflow from the nth neighbour cell, m is the number of neighbour cells sloping down to the given cell, and Q_0 (m^3 s^{-1}) is the river outflow from the given cell to the neighbour cell where it flows to.

Figure 2.7 shows a typical river or stream in nature (left) and the schematic representation in the model (right). In the model representation, all water fluxes represented by arrows are referred to cell 1, which has two neighbour cells, one to the right driving the streamflow Q_n towards it, and the other to the left receiving the streamflow Q_0 from it once the surface water have been updated by the rest of fluxes in Equation 2.62.

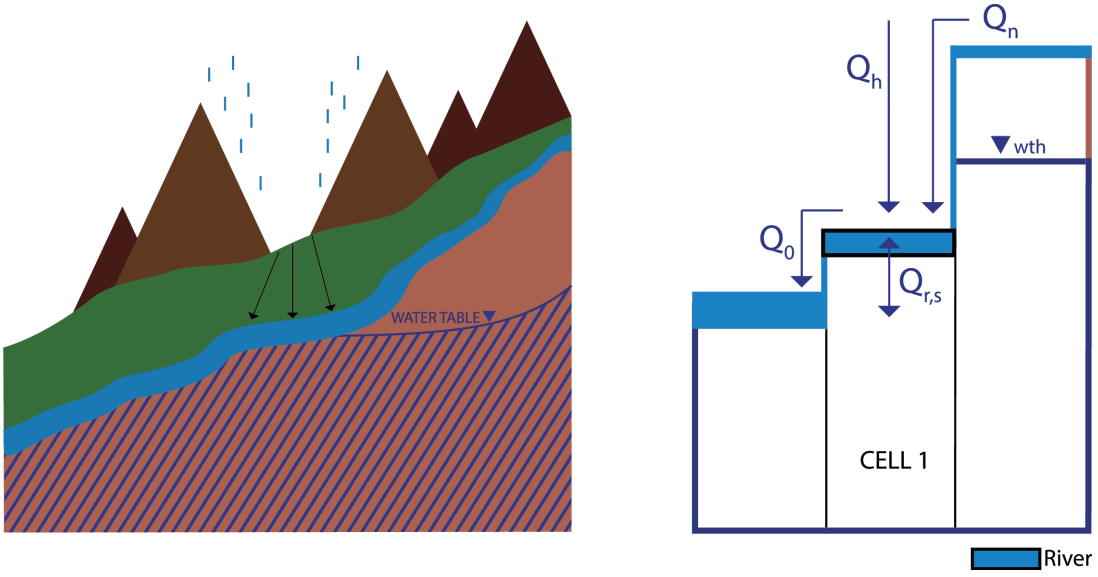

Figure 2.7: Typical river in nature (left) and its representation with the surface water balance fluxes in LEAFHYDRO (right).

The residence time K_s (s) for the surface water is calculated as

$$K_s = \frac{L}{V}, \tag{2.63}$$

where L (m) is the stream length in the cell and V (m s^{-1}) is the velocity of flow in the cell. LEAFHYDRO calculates V using the Gauckler-Manning formula [22]:

$$V = \frac{1}{n} \bar{R_h}^{2/3} \sqrt{\bar{s_r}}, \tag{2.64}$$

where n is the dimensionless roughness Gauckler-Manning coefficient (set to the typical value $n = 0.03$), $\bar{R_h}$ (m) is the mean hydraulic radius of the cell, and $\bar{s_r}$ (dimensionless) is the mean river channel slope in the cell. The mean hydraulic radius $\bar{R_h}$ is a measure of the channel flow efficiency, defined as $\bar{R_h} = \bar{A_h}/\bar{P_h}$, where $\bar{A_h}$ (m^2) is the mean cross sectional area of flow and $\bar{P_h}$ (m) is the mean wetted perimeter of the cross sectional area of flow.

LEAFHYDRO assumes rectangular channel cross section, therefore $\bar{A_h}$ is given by $\bar{A_h} = \bar{w_h}\bar{d_h}$ and $\bar{P_h}$ is given by $\bar{P_h} = 2\bar{d_h} + \bar{w_h}$, where $\bar{w_h}$ (m) is the mean river channel width in the cell and $\bar{d_h}$ (m) is the mean river channel depth in the cell.

Geometry stream parameters at the model resolution, such as stream length, mean river channel width, mean river channel slope and flow direction, necessary to determine the neighbour cell the stream is flowing to, are determined from a public higher resolution database as detailed in Section 3.2.4. The mean river depth $\bar{d_h}$ is dynamically calculated as

$$\bar{d_h} = \frac{S_r}{\bar{w_h} L}. \tag{2.65}$$

Chapter 3

LEAFHYDRO simulation settings. Initial conditions and forcings

3.1 10-year simulations

LEAFHYDRO is used to investigate the role of groundwater dynamics in the Iberian Peninsula soil moisture fields and land-atmosphere fluxes over a 10-year period simulation. The simulation will be referred to hereafter as WT (Water-Table) simulation. In addition, to help isolate the role of the groundwater, another simulation is performed with the groundwater scheme switched off. This second simulation will be referred to hereafter as FD (Free-Drain) simulation.

The FD simulation uses the commonly adopted free-drain approach, where soil water is allowed to drain out of the soil column at a rate set by the hydraulic conductivity at the water content of the bottom soil layer. The potential drawback of this approach is that the escaped water is no longer available for subsequent dry period evapotranspiration. It should work very well where the water table is deep and the soil is sandy, but where the water table is shallow and the soil is clay-rich, it may underestimate the soil water storage and overlook water persistence. This may be one of the reasons that recent climate reanalysis must rely on significant soil water nudging where water is added to or removed from the soil column to meet atmospheric demands [94].

The work domain is a polar-stereographic grid centred in the Iberian Peninsula. It extends 1500 km in south-north and west-east directions, covering the entire Iberian Peninsula, as well as some regions in the north of Africa and the south of France. The horizontal spatial resolution is 2.5 km. The spatial resolution needs to be consistent with typical climatic studies horizontal resolutions, since the final objective

in this line of research is to run fully coupled land-atmosphere simulations, where the land grid can be tiled into the atmospheric grid.

The simulated time is a 10-year period from January 1989 to December 1998. The period was chosen long enough to include wet and dry years in order to study the soil moisture and water table memory. It includes the 1991-1995 drought, reported as the most severe drought in the Iberian Peninsula during the last 60 years [6], as well as other dry and wet spells over different pluviometric Iberian regions that allow a study of the groundwater effects under different climatic conditions.

The time resolution for resolving heat and water fluxes in the soil and at the land surface is 60 s, with the exception of the heat and water fluxes associated with the canopy, calculated every 15 s. The timestep for groundwater-streams exchange, groundwater mass balance and water table adjustment is 900 s.

3.2 Initial conditions

3.2.1 Land, vegetation and soil parameters

3.2.1.1 Topography

The topography used by the LEAFHYDRO simulations and by other preprocessing algorithms in this work is the NASA (*National Aeronautics and Space Administration, USA*) SRTM (*Shuttle Radar Topography Mission*) digital elevation data.

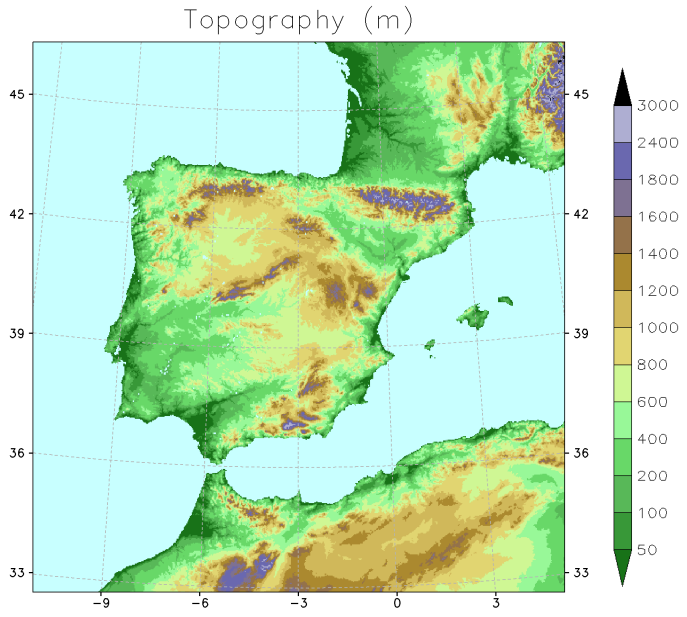

Figure 3.1: Topography (m) used in the LEAFHYDRO simulations.

The original data was obtained with a DEM (*Digital Elevation Model*) at 3 arc second resolution (approximately 90 m), processed for void filling by the CGIAR-CSI (*Consultative Group for International Agricultural Research - Consortium for Spatial Information*) by *Jarvis et al.* (2008) [56], and made publicly available. For the LEAFHYDRO 2.5 km horizontal resolution, the elevation data is aggregated. Figure 3.1 shows the resultant model domain topography used in the LEAFHYDRO simulations.

3.2.1.2 Vegetation parameters

The vegetation type or land cover field for the work domain is shown in Figure 3.2 (left). The categories in the Figure 3.2 coloured table (right) are the 30 categories used in the original LEAF model [63]. The data was originally extracted from the CORINE (*COoRdination of INformation on the Environment*) Land Cover project [1] database, developed by the EEA (*European Environment Agency*). For this work, the vegetation data is adapted from the 44 CORINE land use categories to the 30 categories used in LEAFHYDRO and aggregated from the original 125 m horizontal resolution to the 2.5 km grid used here.

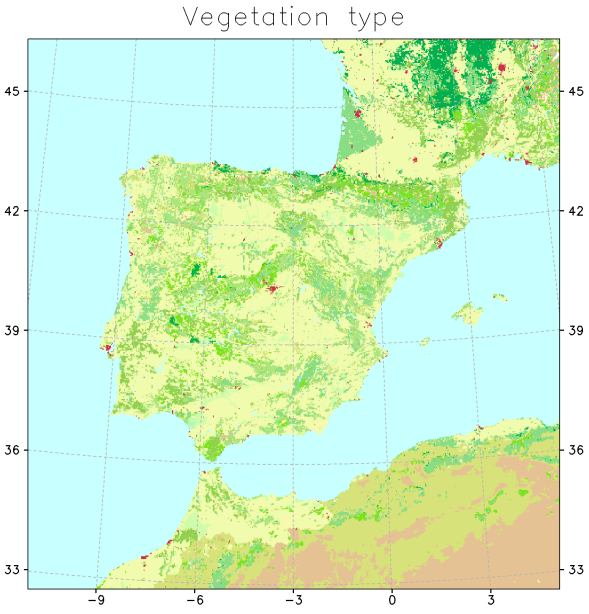

Category	Vegetation type
0	Ocean
1	Inland water (lakes, rivers, streams)
2	Ice cap/glacier
3	Evergreen needleleaf tree
4	Decidious needleleaf tree
5	Decidious Broadleaf tree
6	Evergreen broadleaf tree
7	Short grass
8	Tall grass
9	Dessert
10	Semi-dessert
11	Tundra
12	Evergreen shrub
13	Decidious shrub
14	Mixed woodland
15	Crop/mixed farming
16	Irrigated crop
17	Bog or marsh
18	Evergreen needleleaf forest
19	Evergreen broadleaf forest
20	Decidious needleleaf forest
21	Decidious broadleaf forest
22	Mixed cover
23	Woodland
24	Wooded grassland
25	Closed shrubland
26	Open shrubland
27	Grassland
28	Cropland
29	Bare ground
30	Urban and built up

Figure 3.2: Vegetation type. Left: Vegetation type field for the simulation domain. Right: Coloured table listing the vegetation categories and their mapping colour, in black the most common in the Iberian Peninsula.

As an improvement from the original LEAF model, a climatological 0.15° resolution monthly satellite-derived green vegetation fraction dataset [52] is used dynamically. The *LAI* (*Leaf Area Index*) is then derived from the vegetation fraction. Other vegetation type dependent parameters required by the model, such as roughness

length, albedo or longwave vegetation emissivity, are extracted from the original LEAF initialization tables.

3.2.1.3 Soil parameters

The soil textural classes used in LEAFHYDRO are defined by the USDA (*United States Department of Agriculture*) as fractions of silt, clay and sand[1]. LEAFHYDRO uses two soil classes for each column, one for the top layers (from surface to 0.30 m deep) and another one for the bottom layers (from 0.30 m to 4 m deep). The data for both top and bottom layers comes originally from the FAO (*Food and Agricultural Organization of the United Nations*) 30 arc second world soil database[2].

Table 3.1 lists the soil classes and the soil dependent parameters in Equation 2.2 used in LEAFHYDRO (from original LEAF initialization tables).

Soil class	η_f ($m^3\ m^{-3}$)	Ψ_f (m)	K_f ($m\ m^{-1}$)	b	C_d ($J\ m^{-3}\ K^{-1}$)
Sand	0.395	-0.121	1.760×10^4	4.05	1.465×10^6
Loamy sand	0.410	-0.090	1.563×10^4	4.38	1.407×10^6
Sandy loam	0.435	-0.218	0.347×10^4	4.90	1.344×10^6
Silt loam	0.485	-0.786	0.072×10^4	5.30	1.273×10^6
Loam	0.395	-0.451	0.070×10^4	5.39	1.214×10^6
Sandy clay loam	0.420	-0.299	0.063×10^4	7.12	1.177×10^6
Silty clay loam	0.477	-0.356	0.017×10^4	7.75	1.319×10^6
Clay loam	0.476	-0.630	0.025×10^4	8.52	1.227×10^6
Sandy clay	0.426	-0.153	0.022×10^4	10.40	1.177×10^6
Silty clay	0.492	-0.490	0.010×10^4	10.40	1.151×10^6
Clay	0.482	-0.405	0.013×10^4	11.40	1.088×10^6
Peat	0.863	-0.356	0.080×10^4	7.75	0.874×10^6

Table 3.1: Soil parameter for the USDA textural classes used in LEAFHYDRO. Parameters are, from left to right: volumetric soil water content at saturation η_f, soil capillarity potential at saturation Ψ_f, conductivity at saturation K_f, pore-size index b and volumetric specific heat of dry soil C_d.

3.2.2 Equilibrium Water Table Depth

The climatic equilibrium water table position is a balance between the atmospheric influence in the form of climatic groundwater recharge ($R = P - ET - Q_h$, recharge R equals precipitation P minus evapotranspiration ET minus surface runoff Q_h) and the topographic influence in the form of gravity-driven lateral convergence [42]. A recent effort by *Fan et al.* (2013) [40] produced a world water table depth map, setting global water table depth patterns. These authors compiled observations available from government agencies or published in literature, and filled in the gaps

[1] http://nrcs.usda.gov/wps/portal/nrcs/main/soils/edu/
[2] http://fao.org/soils-portal/soil-survey/

with a simple two-dimensional groundwater model presented by *Fan et al.* (2007) [42].

As initial condition for this work, the climatic EWTD (*Equilibrium Water Table Depth*) for the Iberian Peninsula in Figure 3.3 is used. This field is a first guess to introduce and understand patterns in the peninsula water table depth distribution.

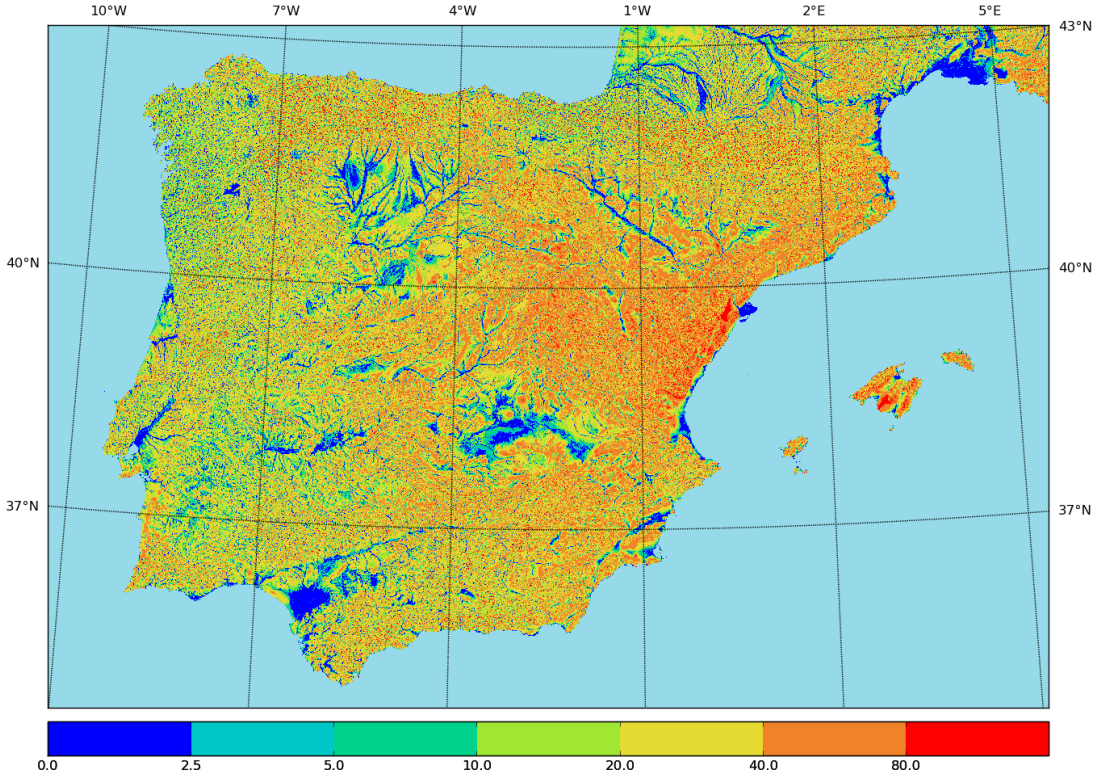

Figure 3.3: Initial Iberian Peninsula Equilibrium Water Table Depth (m) at 9 arc second spatial resolution.

The initial Iberian Peninsula EWTD was calculated using the aforementioned groundwater model [42] at 9 arc second spatial resolution (213x278 m cells at 40° N) and validated with 2,601 observation points along the Iberian Peninsula by *Gestal-Souto et al.* (2010) [47]. The groundwater model assumes equilibrium, therefore balances the recharge R with lateral divergence (as the sum of the 8 neighbours contributions Q_i) to the lower neighbours at hillslope cells, as

$$R = \sum_{i=1}^{8} Q_i. \tag{3.1}$$

And at valley cells balances the lateral convergence (as the sum of the 8 neighbours contributions Q_i) with runoff Q_h into rivers and wetlands, as

$$\sum_{i=1}^{8} Q_i = Q_h. \tag{3.2}$$

The lateral flux Q_i is calculated as explained in Section 2.2.2. The climatic recharge R used for this Iberian Peninsula EWTD calculation was obtained at 1° spatial resolution from the Mosaic LSM, participant in NASA's GLDAS (*Global Land Data Assimilation System*) [96], and is shown in Figure 3.4 (left).

The result in Figure 3.3 is an equilibrium between the atmospheric recharge input and the topography characteristics of the Iberian Peninsula. The water table is suggested to be shallow under large areas. In the Inner Plateau (northern and southern subregions) the lateral groundwater flow from surrounding mountains results in very shallow water table depth (*wtd*) zones in spite of the semiarid climate. Low elevation coastal plains and river valleys also present shallow *wtd*. The west-east pattern, with shallower *wtd* in the west and deeper *wtd* in the east, result from the atmospheric recharge pattern.

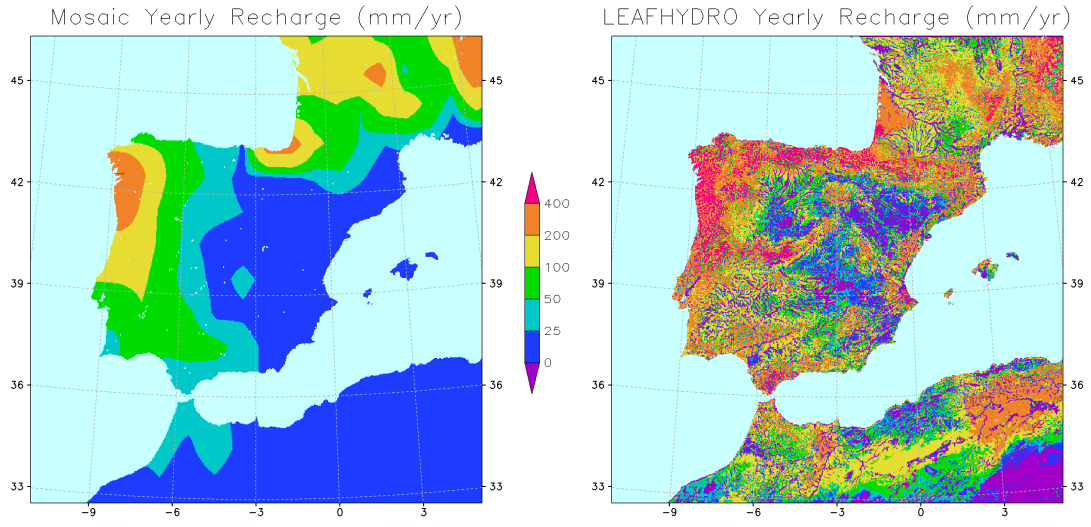

Figure 3.4: Iberian Peninsula groundwater recharge (mm yr^{-1}). Left: calculated with a LEAFHYDRO 10-year run at 2.5 km spatial resolution. Right: from the Mosaic LSM (GLDAS) at 1° spatial resolution.

The high spatial resolution in the EWTD calculation is necessary to catch the topography variability. However, the 1° spatial resolution of the climatic recharge (left plot in Figure 3.4) cannot represent the spatial variability in the LEAFHYDRO domain used in the WT simulation (2.5 km horizontal resolution). In order to overcome this limitation, a 10-year test LEAFHYDRO run (1989-1998) was carried out, using the high resolution EWTD aggregated to the model resolution as initial water table position condition and 0.2° spatial resolution analysis precipitation forcing (see next Section 3.3). The yearly water table flux or groundwater recharge (see Section

2.2.1) obtained with the test run responds to the spatial resolution of the water cycle processes in the model domain and to the climatic conditions during the 10-year period. This yearly water table flux is shown in Figure 3.4 (right), and was used as recharge R to recalculate the Iberian Peninsula EWTD with the groundwater model, obtaining a more realistic initial water table.

The result is the Iberian Peninsula EWTD in Figure 3.5, used as initial condition in the WT simulation. Comparing this EWTD to the initial EWTD (Figure 3.3) calculated with the Mosaic 1° recharge, the shallow water table regions (blue and turquoise colours) are equally captured, but overall the water table is not as deep since the test run recharge is higher (Figure 3.4). Over the western half of the Peninsula the higher recharge produces a less deep water table, as a result of higher water availability in the groundwater model from the Pyrenees, the Iberian System and the western coast by the Gulf of Valencia, where the Mosaic recharge is very low.

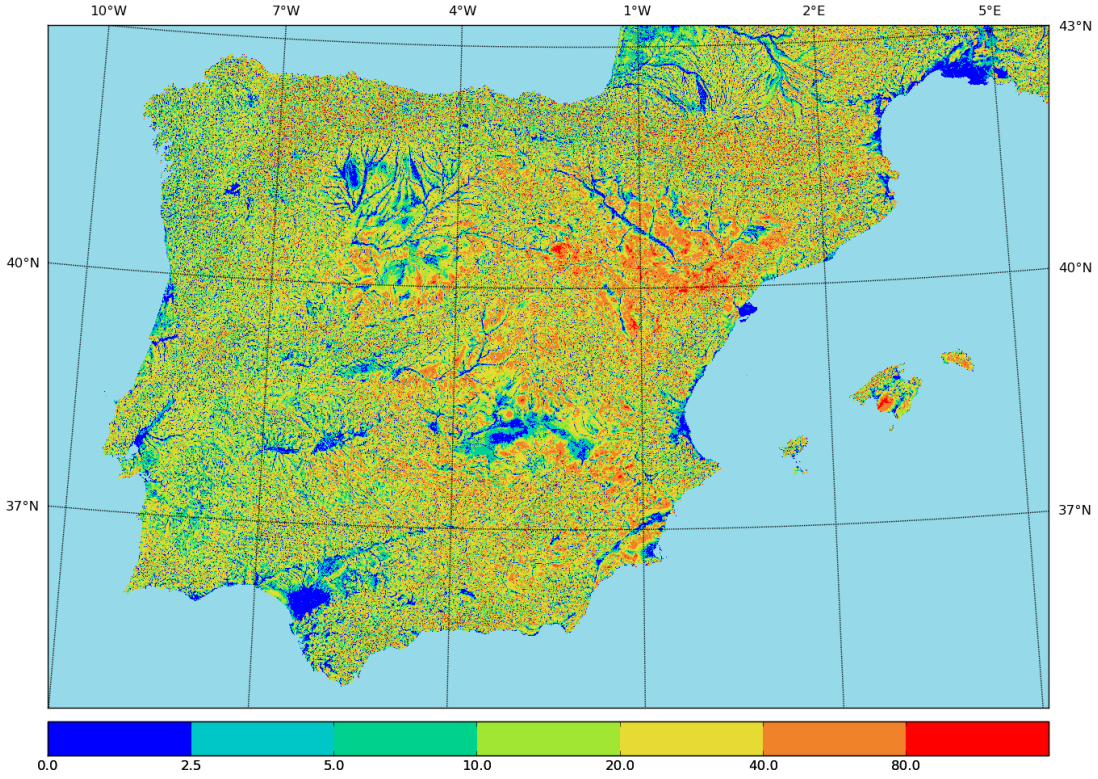

Figure 3.5: Iberian Peninsula Equilibrium Water Table Depth (m) at 9 arc second spatial resolution, calculated with a LEAFHYDRO 10-year test run recharge.

3.2.3 Soil moisture initialization

For the soil moisture LEAFHYDRO initialization, the soil water content is calculated in preprocessing from bottom to top, parting from the knowledge of the equilibrium water table position;

- Firstly, knowing the initial water table position (EWTD), the equilibrium soil water content at the virtual layer between the water table and the last layer resolved by the model (η_{eq_1} or η_C in Figure 2.4, depending on the water table appearing in the soil crust resolved or below) is calculated resolving Richards' Equation (Equation 2.1) at the water table position, where the flux F_{wss} is taken to be the groundwater recharge R used in the initial EWTD calculation and the soil water content in the layer below the water table is known since the layer is saturated (Table 3.1).
- Then, the soil water content for the rest of layers from bottom to top is calculated similarly, resolving Richards' Equation at every surface between layers.

3.2.4 River parameters

The model requires an estimation of the riverbed mean elevation in the cell $\bar{z}_r$ in order to calculate the equilibrium river conductance and the groundwater-streams flux in gaining streams (Section 2.2.3, Equations 2.54 and 2.58). However, $\bar{z}_r$ is a scale-dependent quantity and requires detailed data on mean river stage for all orders of streams in the domain. Such data are yet to be compiled, and hence the elevation of the river cells that naturally appeared in the calculation of the initial high resolution EWTD is taken as the riverbed elevation estimation. When no river cells are found within a 2.5 km cell, the minimum high resolution land elevation in the cell is used.

The river flow scheme included in LEAFHYDRO (see Section 2.3) needs a series of initial parameters: flow direction, river width, river length and river slope. Also, the calculation of the groundwater-streams flux in losing streams (Section 2.2.3, Equation 2.60) requires the mean river width in the cell $\bar{w}_r$ and the length of individual channels $\sum L_r$. For the calculation of such parameters in the domain grid, the USGS (*United States Geological Survey*) HydroSHEDS (*Hydrological data and maps based on SHuttle Elevation Derivatives at multiple Scales*) 15 arc second resolution data [65] are used. The variables extracted from the HydroSHEDS database are: fd (flow direction), acc (accumulated drainage area) and dem (void filled elevation).

Using the HydroSHEDS variables and the Mosaic LSM recharge, the following methodology is applied in preprocessing for the calculation of river parameters in the model 2.5 km grid domain (see Figure 3.6):

- First, the high resolution (15 arc second) cell with the largest acc within a low resolution cell (2.5 km grid) is spotted.
- The fd of this cell (black arrows in Figure 3.6), together with the location of the low resolution cell containing the high resolution cell where it flows to, determines the flow direction of the low resolution cell (blue arrows in Figure 3.6).

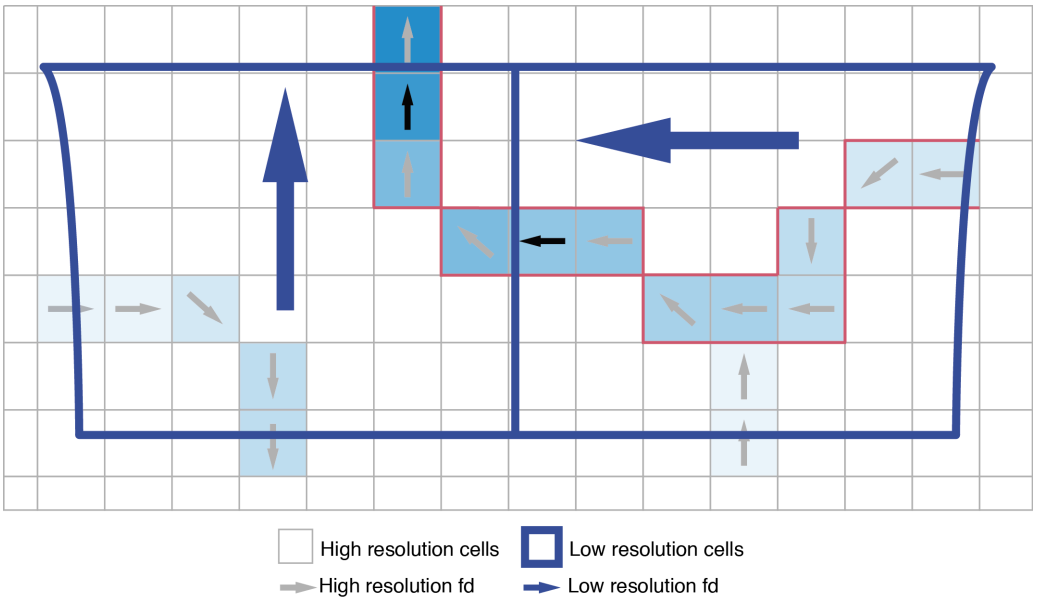

Figure 3.6: Sketch for the methodology to calculate river parameters from the HydroSHEDS high resolution database to the 2.5 km grid domain in LEAFHYDRO.

- The flow of the main high resolution stream within every low resolution cell is then followed, highlighting the stream (red streams in Figure 3.6).
- The distance made by this high resolution main stream is taken as the low resolution river length L.
- The low resolution river slope s_r is taken as the average slope for all high resolution cells that take part in the main high resolution stream, where the high resolution slopes have been previously calculated from the flow direction fd and the elevation dem.
- The low resolution drainage area A_d is calculated aggregating the area of all high resolution cells within a low resolution cell, and then accumulating it from all cells addressed to a given cell with the use of the low resolution fd.
- Finally, the width w_r is calculated using the recharge R and the drainage area A_d in each low resolution cell, as discussed by *Lucas-Picher et al.* (2003) [72],

$$w_r = (0.00013Q_m + 6.0)Q_m^{1/2}, \tag{3.3}$$

where Q_m is the annual mean discharge passing through a river section, approximated for this calculation by the accumulation of flow $Q = RA_d$ for the cells along the low resolution stream.

3.3 Atmospheric forcings

The atmospheric forcing data fields at the surface, needed for the LEAFHYDRO simulations, were extracted from the ECMWF ERA-Interim[3] reanalysis database [2, 4, 5]. A processing scheme has been introduced into the LEAFHYDRO forcing routines that transfer the ERA-Interim fields from the original GRIB (*GRIdded Binary*) format and then bilinearly interpolates them from the original N128 gaussian grid (approximately 0.7° latitude resolution and varying in longitude resolution from 0.75° at the bottom of the domain to 1.58° at the top) to the model 2.5 km resolution polar-stereographic grid.

Surface pressure, 2 m temperature and surface wind speed data are reanalysis fields and are input in LEAFHYDRO every 6 hours of simulation time. The incoming surface radiation (shortwave and longwave) and precipitation (convective and large-scale) data are forecasted fields from reanalysis datasets and are input in LEAFHYDRO every 3 hours of simulation time. Once these forcings are read, they are interpolated in time for the 60 s model timestep.

However, given the importance for the water cycle of the incoming water in the system through precipitation, the regional higher resolution analysis of daily precipitation dataset over Spain and Portugal (IB02) introduced in Section 1.2.1 is also used. Such dataset was presented by *Herrera et al.* (2010) [54] and *Belo-Pereira et al.* (2011) [16]. It was built using all stations from the climatic monitoring network of both Iberian meteorological public agencies; the AEMET in Spain and the IPMA in Portugal. This gridded dataset has a horizontal resolution of 0.2°, much higher than the ERA-Interim precipitation data resolution, and therefore represent the Iberian precipitation variability at a higher degree.

Once this daily precipitation analysis is read and bilinearly interpolated to the 2.5 km resolution model grid, the model redistribute the data in time along the day using the time distribution of the 3-hourly ERA-Interim precipitation data. Hence, the model uses the daily IB02 data for the precipitation quantity and the 3-hourly ERA-Interim data for the precipitation distribution along the day. However, the daily precipitation only covers Spanish and Portuguese territory, and for the regions of the model domain not covered (France and Africa) the ERA-Interim 3-hourly precipitation is used.

[3] http://ecmwf.int/research/era/do/get/era-interim

Chapter 4

LEAFHYDRO 10-year simulation validation

A realistic water table depth estimation is essential to couple groundwater with soil moisture. Moreover, a modeled dynamic water table is expected to oscillate around its equilibrium position (EWTD) at different timescales in response to rainfall events, soil hydrology demands and multi-year dry or wet spells, as it does in nature [25, 42, 114]. Hence, a validation of the WT simulation water table depth and its evolution in time across the studied region is necessary to support the findings of this work. Only with a realistic water table the importance of the groundwater-soil interactions for climate can be reliably assessed in the large scale.

One of the strengths of the otherwise simple model LEAFHYDRO presented in Chapter 2 is the representation of the lateral gravitational groundwater flow, which is precisely the main driver of the water table distribution across the landscape (*Fan & Miguez-Macho*, 2010 [41]).

Lateral groundwater flow depends on the slope of the water table surface, and occurs at local and regional scales. Only regional lateral flow can be resolved with the grid spacing of the order of several kilometres typical of current large scale modeling studies, but this is for the most part slow comparing to the duration of the simulations, ranging from several months to a few years. On the other hand, local groundwater flow is much faster, occurring at smaller scales from hilltops to valleys. For a grid cell of larger size in a land surface model like the 2.5 km cells in this work, local groundwater flow results in its internal drainage or baseflow and needs to be parameterized.

The net lateral groundwater flow and the net recharge balance determine the water table depth, and hence, the same water table depth value can correspond to a high or low baseflow depending on what the net recharge of the area and the converging lateral flow are. For example there can be shallow water tables in a region of dry climate with poor drainage and converging groundwater flow, and on the other

hand the same shallow water tables can be found in a wet climate with a much higher drainage. And there can be deep water tables with high drainage rate when the river network is well carved in, like for example in a mountainous area with humid climate, and the same deep water tables can exist in a desert with gentler slopes and scarce rivers. Therefore, the relationship between water table depth and baseflow is not equal for all settings, which should be considered when the baseflow is parameterized.

LEAFHYDRO considers the lateral groundwater flow explicitly (as described in Section 2.2.2) and implicitly. The local groundwater flow intended to represent is parameterized by being implicitly considered. The high resolution EWTD, calculated first with climatology recharge (as described in Section 3.2.2), resolves explicitly the local drainage, and then it is used to initialize the water table in the low resolution runs and to calculate the river conductance *RC* that parameterizes the internal drainage (as described in Section 2.2.3). The result is a baseflow consistent with the topography and climate of the given cell and that keeps the water table balancing around its equilibrium value as it does in nature.

Treating the evolution of the water table in land surface models as a process mainly dependent on vertical fluxes, as is done with soil moisture, and ignoring or misrepresenting the lateral gravitational groundwater flow, might explain why most modeling schemes that do explicitly include groundwater processes in recent studies [66, 67, 88, 119] fail to produce a realistic water table spatial distribution, compromising the generality of their results (see section 1.3.2).

Some of these models consider the baseflow in a manner largely uncorrelated to the process it is intended to quantify, like for example making it solely dependent on the moisture content of the lowest soil layer [119] or the water table depth [88, 117]. Even when in the model, through calibration or any other strategy, the baseflow amount is accurate and the water table does not have a spurious interannual temporal trend, it can still be either too shallow or too deep, depending on the initial condition imposed, and hence the interaction between groundwater and the top soil moisture be exaggerated or neglected entirely. Long spin-up times will not help if the parameterized baseflow of the cell is inconsistent with its internal drainage to the river network driven by local lateral groundwater flow, and the ending result will be a water table pattern that reflects mostly climate, which is the ultimate responsible for vertical fluxes, instead of topography, with deeper water table under hilltops and shallower in valleys, and that dynamically does not respond as in nature.

The water table pattern and baseflow representation in this work come from the high resolution EWTD, where local drainage is resolved, reflecting topography and internal drainage of the cells realistically. And therefore, the validation with actual water table depth and streamflow observational data in this chapter is intended to support the results in next chapters, based on water table position and evolution in time.

4.1 Water table depth and time evolution: validation with observations

Actual water table depth (*wtd*) observational data is used in this section to validate the model performance in terms of capturing the water table position and its time evolution.

Time series graphs in Figure 4.1 represent the *wtd* (m) time evolution at 16 selected observation sites, corresponding to the 16 numbered points on the map (top left corner of Figure 4.1). On each graph are plotted; the observed *wtd* at the available times (red dots connected with red line), the simulated *wtd* in the model cell containing the observation site at the same times (blue dots connected with blue line), and the simulated *wtd* daily series (dashed blue line).

4.1.1 Observational *wtd* data

The observational *wtd* data were provided by the IGME (*Institute of Geology and Mining of Spain*), several *Confederaciones Hidrológicas* (Spanish agencies managing the main watersheds within the country) and the SNIRH (*National Information System for Hydrological Resources of Portugal*).

The time and space resolutions of these datasets are very irregular. For validation, stations with a water table deeper than 100 m were eliminated in order to rule out measurements in confined aquifers as much as possible, since confined aquifers are not hydrologically connected to land surface and the atmosphere. Stations with a slope steeper than 0.05 m month^{-1} (very likely caused by pumping) were also ruled out. After these eliminations, only observation stations with at least 3 years of data within the 10-year simulation period (1989-1998) are used, leaving 623 stations suitable for *wtd* time evolution validation.

The map in Figure 4.1 highlights the 623 water table stations analysed, using a colour code in function of validation results (detailed below the map).

The spatial resolution of LEAFHYDRO needs to be consistent with the resolution of climatic and meteorological models for fully coupled studies, hence the water table behaviour of one grid cell in the model must be understood as an approximation of the different possible behaviours of the natural water table within the cell. This situation is a handicap for the *wtd* validation, since the 2.5 km resolution of the simulation is very low compared to the scale of the topography and *wtd* variabilities. Out of the 623 observation sites analysed, 136 do not correspond uniquely to one model cell and are contained in only 60 cells (2 or 3 stations per cell, orange points on the map). These different observation sites belonging to one model cell do not always present the same depth or evolution in time, as it can be seen in the orange points graphs in Figure 4.1:

- Inside the *Point 15* grid cell in the Duero river basin there are 3 different observation stations that present very different (up to 20 m difference) depth values along the simulation period (red, green and purple series), making it very difficult for the model to reach the right depth. However, in this case the 3 observation sites *wtd* series average (orange) is clearly the closest to the simulation series (blue).
- Inside the *Point 16* grid cell in the southeast there are 2 observation sites, the model underestimate the depth of both but reflect accurately the annual cycle and the long-term trends, deepening from 1992 to 1996 and reaching shallow positions from 1996 to 1998.

4.1.2 Model performance

Some studies incorporating explicitly groundwater dynamics in land surface modeling find the water table effects to be negligible at depths below 5 m [66, 77], but the potential contribution by upward capillary flux to evapotranspiration of water table depths below 5 m have been found considerably important at localized sites over the Amazonia by *Fan & Miguez-Macho* (2010) [41], covering large fractions of the observed evapotranspiration at depths around 10 m. In a compromise to work close to these studies, water table depths below 8 m are considered to be shallow in this Iberian Peninsula study. A total of 31.4% of the Iberian Peninsula territory is found in the model WT simulation to have shallow mean water table (light blue shaded on the map in Figure 4.1), giving an estimation of the potential influence of the groundwater dynamics in the peninsula that will be addressed in following chapters.

The main validation results found are (see Figure 4.1):

1. 203 of the studied stations present a shallow mean water table ($wtd \leq 8$ m) along the simulation period, and the model performs well at capturing them, finding 66.0% of the grid cells containing those shallow observational points to be also shallow in the simulation.
2. In terms of the error in the mean *wtd*:
   - 14.0% of the stations present less than 2 m difference between the mean *wtd* simulated and observed for the times available at the observational datasets (red points on the map).
   - The ratio increases up to 33.0% when analysing only shallow *wtd* points ($wtd \leq 8$ m).
   - *Points 1* to *12* graphs correspond to red stations (all shallow *wtd* stations except *point 2*), as some examples of the model performance at capturing the mean water table position.

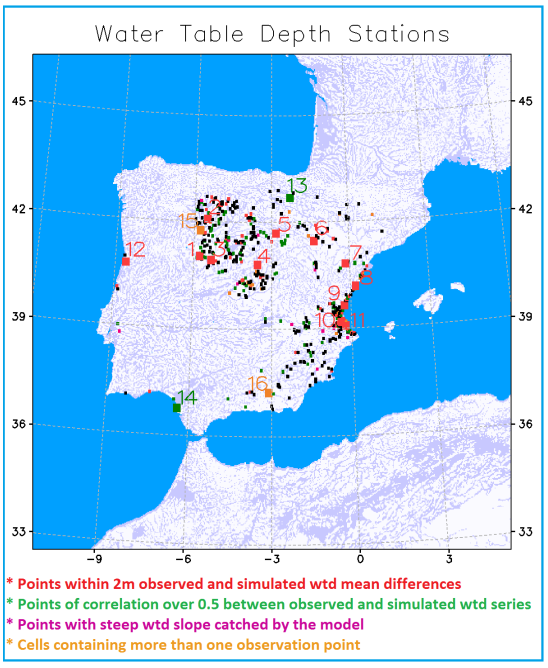

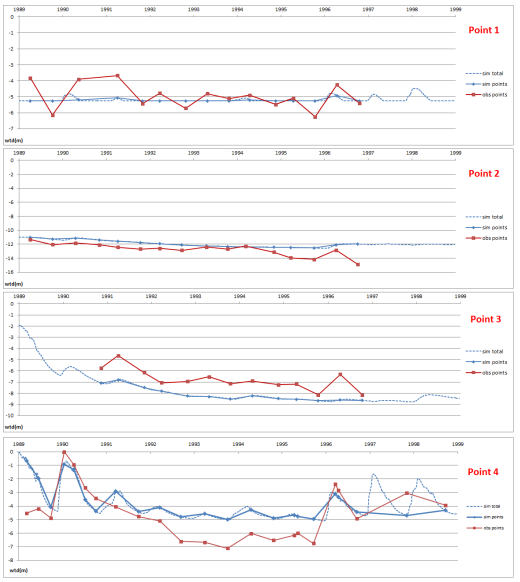

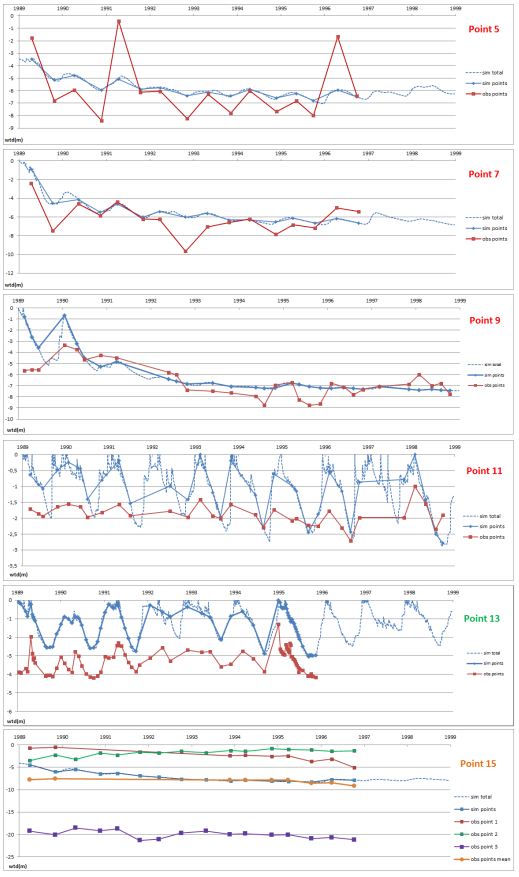

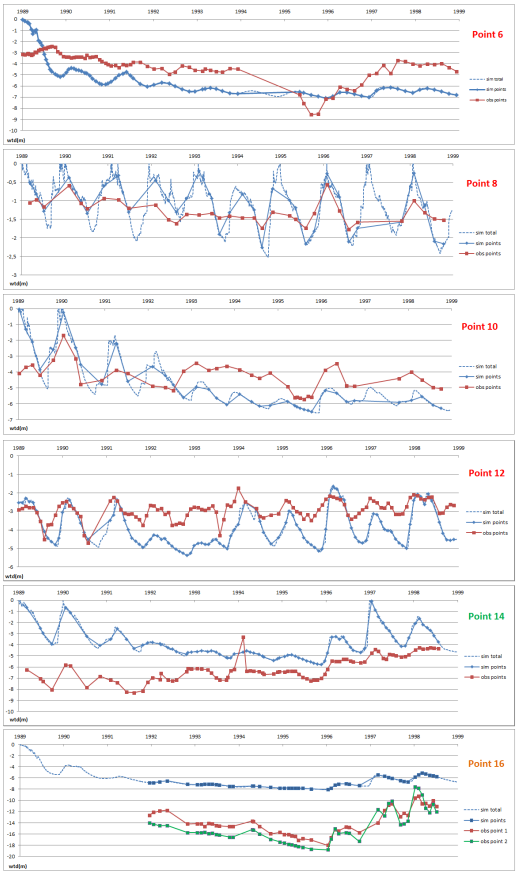

Figure 4.1: Top left map: Shallow water table zones (light blue shade) and Iberian Peninsula water table depth stations highlighted using the detailed colour code (under the map). Top right and bottom graphs: Water table depth (m) time series at the stations numbered (*1* to *16*); observed values in red and simulated values in blue.

3. Focusing not on the mean *wtd* values but on their time evolution:
    - 32.3% of the observation sites time series present a correlation coefficient over 0.5 with the simulated series (green points in the map).
    - All the red points graphs plus *Points 13* and *14* graphs correspond to green stations, selected at different shallow water table zones over the peninsula, and show how the model is accurate in representing the seasonal fluctuations and the long-term deepening and rising trends.
    - *Point 12* near the Duero river mouth in Portugal is an example on catching the seasonal cycle and a slightly upward trend of the *wtd* through the simulation.
4. A total of 94 stations present a steep *wtd* long-term trend ($slope \geq 0.035$ m month^{-1}) within the prescribed limits to avoid artificial trends ($slope \leq 0.05$ m month^{-1}), and 26.6% of them are captured in the simulation (purple points in the map, mean slope difference between the observation and simulation series lower than 0.02 m month^{-1}).

For the purpose of this work, and provided the increase of the groundwater hydrological linkage to the land surface as the water table appears closer to the shallow soil layers, the accuracy of LEAFHYDRO at representing the shallow water table regions is an encouraging factor. Also, the model performs well at capturing the mean water table positions, the seasonal cycle and the long-term trends, resulting in a realistic water table.

4.2 Modeled streamflow: validation with streamflow observations

In this section the LEAFHYDRO streamflow that results from the simulated water cycle in the WT and FD simulations is analysed and the model is validated over the Iberian Peninsula using observational streamflow data.

Streamflow is a suitable parameter to validate land surface-hydrology models, since streamflow time cycles result from the models interactions between the different reservoirs represented, and there is access to observational data. However, it is important to mention that the goal of LEAFHYDRO is not to simulate the surface water flow and use these results for hydrological purposes, but to carry out simulations of the complete water cycle inland and the land-atmosphere interactions.

The initial version of LEAFHYDRO that first included the dynamic water table implementation was validated over North America by *Miguez-Macho et al.* (2007) [83]. They found that the groundwater-rivers linking scheme did not perform equally well in all river basins, and used daily streamflow data at five stream gauges in the Mississippi drainage to adjust the model aerodynamic resistance parameters, linking

the evaporative flux with the observed streamflow. For this work the model evaporative flux formulation has not been adjusted using streamflow observations from any Iberian basin. No model calibration has been carried out, all calculations and parameterizations are physically-based as described in Chapter 2, as the intention is to work with a model capable of capturing the water cycle balance as accurately as possible, independently of the region studied.

The simulated river network obtained with LEAFHYDRO compares well with the observed river network in *Libro Blanco del Agua* (2010) [6], published by the Spanish *Ministry of Natural Environment*. This is expected since the river parameters that determine the river network and streamflow in the model (flow direction, river width, river length, river slope) were derived from the high resolution HydroSHEDS database as detailed in Section 3.2.4.

The natural water cycle is intensely affected by anthropogenic actions in the Iberian Peninsula. Such actions modify the real measurable streamflow through regulation reservoirs, wells, power generation plants or irrigation withdrawals. As pointed out in Section 1.3.4, and according to *Libro Blanco del Agua* (2010) [6], the fraction of natural streamflow that actually flows under this affected regime is high in northern rivers (Duero, Miño, Llobregat), but lower in southern rivers: 52% in Guadiana (Badajoz station, near the Portuguese border), 44% in Guadalquivir (Alcalá del Río station) or 4% in Segura (Guardamar station, by the river mouth). Hence, it is necessary to be fully aware of the limitations introduced in a model validation with observed streamflow by these anthropogenic actions.

4.2.1 River flow scheme in the FD simulation

The river flow scheme used by LEAFHYDRO was described in Section 2.3. The surface water storage is calculated every timestep by means of the mass balance in Equation 2.62. In order to highlight the groundwater influence on the streamflow results, for the FD simulation the surface water storage $(S_s)_{FD}$ (m^3) is calculated substituting the water table fluxes Q_r and Q_s in Equation 2.62 for the free-drain recharge R_{FD}, as

$$\frac{d(S_s)_{FD}}{dt} = Q_h + R_{FD} + \sum_{n=1}^{m} Q_n - Q_0, \tag{4.1}$$

where Q_h ($m^3\ s^{-1}$) is the hillslope overland runoff given from the temporary surface water routine, R_{FD} ($m^3\ s^{-1}$) is the free-drain recharge, understood as the water drained downwards at the bottom of the layers resolved by the model, Q_n ($m^3\ s^{-1}$) is the river inflow from the nth neighbour cell, m is the number of neighbour cells sloping down to the given cell, and Q_0 ($m^3\ s^{-1}$) is the river outflow from the given cell to neighbour cell where it flows to.

With this approach the water budget in the FD simulation is closed as it is in the WT simulation, but the water draining through the bottom model soil layer goes directly to the rivers, and therefore it is no longer available for the soil or land-atmosphere interactions.

4.2.2 Observational streamflow data

A monthly streamflow observation dataset has been compiled for validation. The original data were provided by the CEH (*Hydrographic Studies Center*, Spanish *Ministry of Natural Environment*). However, the data availability and time resolution for the studied period is variable, and 20 discharge stations were selected covering the main river basins in the Iberian Peninsula where monthly streamflow data was available.

The next Figure 4.2 shows a map of the simulated river network in the model domain and the main Iberian basins colour shaded, highlighting with numbered points the stations used to validate the model streamflow. The table on the right (Figure 4.2) refers to the numbered stations and lists the name of the stations, the main Iberian river basin the stations belong to, the drainage area at the station and the number of months with available data within the validation period. The validation period considered goes from October 1989, in order to leave the model a 9 months spin-up period, to the end of the simulation, hence 111 is the maximum possible number of months available for validation.

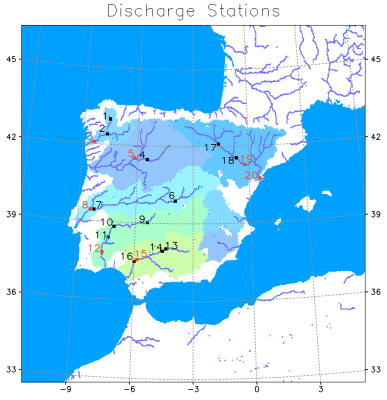

Station no.	Station - Basin	Drainage Area (km^2)	Number of Months
1	Lugo - MIÑO	2,303	104
2	Sil - MIÑO	7,899	48
3	Foz de Mouro - MIÑO	15,407	111
4	Carrascal - DUERO	46,700	92
5	Puentepino - DUERO	63,160	72
6	Toledo - TAJO	24,788	111
7	Tramagal - TAJO	62,148	111
8	Almourol - TAJO	67,482	109
9	Don Benito - GUADIANA	26,125	109
10	Monte de Vinha - GUADIANA	49,865	111
11	Ponte Mourao -GUADIANA	52,294	66
12	Pulo do Lobo - GUADIANA	61,885	102
13	El Carpio - GUADALQUIVIR	23,372	99
14	Córdoba - GUADALQUIVIR	25,450	84
15	Cantillana - GUADALQUIVIR	44,871	60
16	Alcalá del Río - GUADALQUIVIR	47,000	59
17	Castejón - EBRO	25,194	72
18	Zaragoza - EBRO	40,434	72
19	Sástago - EBRO	48,974	111
20	Tortosa - EBRO	84,230	111

Figure 4.2: River Streamflow Stations. Left: Station locations on simulated river network; main Iberian river basins shaded on light colours. Right: Table listing the stations number, name, main basin they belong to, drainage area at the station (km^2) and number of months with available data.

The southern Guadalquivir basin has the lesser streamflow data availability for validation, with the number of available months decreasing towards the Atlantic Ocean and with the added handicap that the non available data refers to the last and wettest years of simulation, leaving only dry year data available. Moreover, previous analysis of the observed data revealed the difficulty of this southern basin for

validation, since the observed streamflow hardly reflects the precipitation regime. Under such difficulties, a different set of streamflow data is used as *true* data for the Guadalquivir basin validation: the natural streamflow. The natural streamflow dataset used here was calculated using the hydrological SIMPA (*Simulation Precipitation-Discharge*) model [97] forced with precipitation observations, and provided by the Spanish *Ministry of Natural Environment*.

The next plots on Figure 4.3 show how the observed streamflow (light green lines) and the natural streamflow (dark green lines) behave very differently for both the monthly time series (left) and the monthly mean time series (right) at the Alcalá del Río station (*point 16* on Figure 4.2). The natural streamflow resembles the precipitation regime (blue columns) from the model forcing data, whereas the observed streamflow is very low or null along the whole available period with the only exception of the wet seasons 1989/1990 and 1990/1991, when the streamflow is still very low in comparison to the natural streamflow. The correlation values between the precipitation and the streamflow in both time series point out the disconnection between the hydrology annual and interannual cycles and the observed streamflow data.

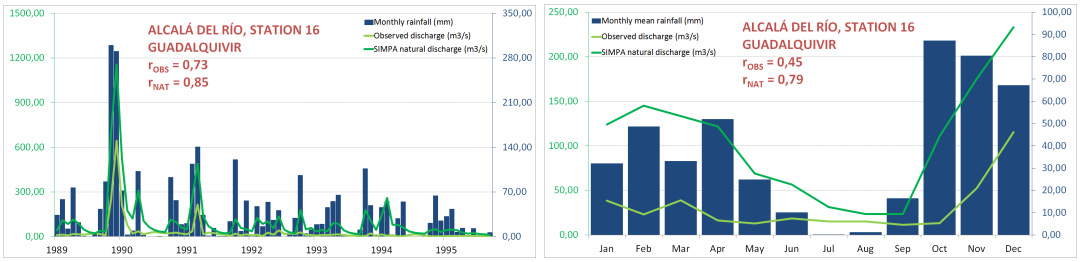

Figure 4.3: Forcing precipitation (mm) (blue columns), observed streamflow (m^3 s^{-1}) (light green lines) and natural streamflow (m^3 s^{-1}) (dark green lines) at the Alcalá del Río Station for the period with observed data availability (Jan/1989-Sep/1995). Left: Monthly time series. Right: Monthly mean time series. Inside the graphs: Correlation indexes between streamflow and precipitation time series (red).

The disconnection of the observed streamflow with the natural streamflow in the Guadalquivir basin responds to anthropogenic influence.

4.2.3 Validation and WT-FD streamflow comparison

To illustrate the behaviour of both the WT and FD simulated streamflow in comparison to observations, one station was selected from each Atlantic basin and two from the Ebro river basin discharging to the Mediterranean Sea. The selected stations were those closer to the river mouth (with the exception of the Cantillana station) and are highlighted in red on Figure 4.2. The next set of plots on Figure 4.4 shows two graphs for each one of the 7 selected stations. The graphs on the left show monthly mean streamflow (m^3 s^{-1}; blue for the WT simulation, red for

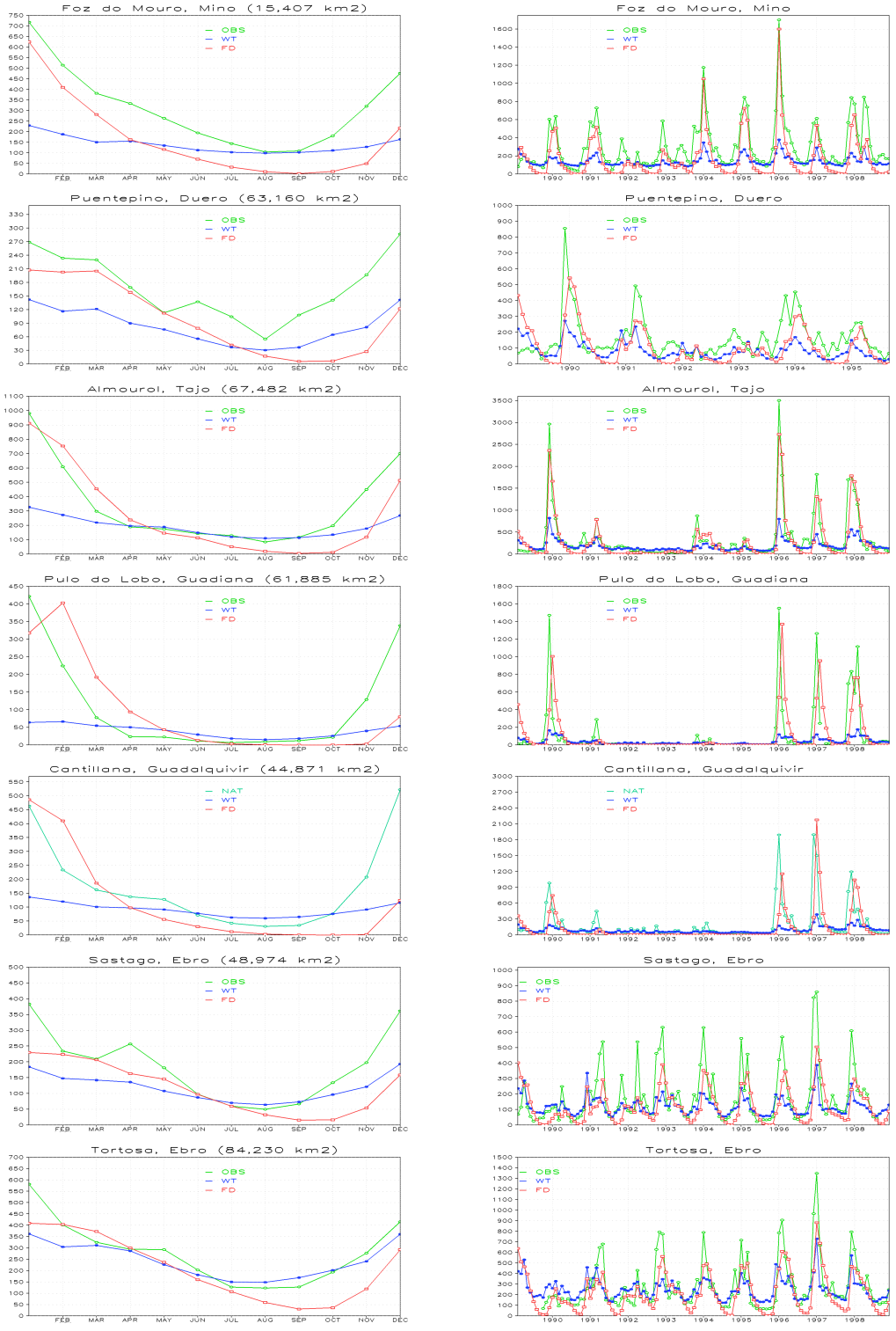

Figure 4.4: River streamflow plots at the 7 stations highlighted in red on Figure 4.2. Left: Monthly mean streamflow ($m^3\ s^{-1}$) (blue for the WT simulation, red for the FD simulation and green for observations) along the simulation period. Right: Monthly streamflow ($m^3\ s^{-1}$). The drainage area at the station (km^2) is indicated on top of the left graphs. Persian green series in the Cantillana Station plots represent natural modeled streamflow.

the FD simulation and green for the observations) for the validation period. The graphs on the right show monthly streamflow (m^3 s^{-1}) for the whole simulation period (Puentepino station data availability ends in September 1995). The drainage area (km^2) at the station is indicated on the top of each graph on the left.

Three main facts are observed from Figure 4.4:

1. There is a clear underestimation of the winter streamflow in the WT simulation, due in part to the lack of precipitation in the forcing data and in part to model deficiencies in the representation of the soil-groundwater linkage when the water table is deep, as it will be discussed in the next section.
2. The summer baseflow representation in the WT simulation (blue) improves in comparison to the FD simulation (red):
    - From the graphs on the left; the WT streamflow during the dry season is closer to observations (green) for all basins, even though it results overestimated in the southern Guadiana and Guadalquivir basins.
    - From the graphs on the right; the rivers dry out in summer practically every year in the FD run, whereas in the WT run the groundwater reservoir feeds the rivers during the dry season using accumulated wet season recharge, and keeping the summer baseflow higher and closer to observations. This is clearly observed in the Miño, Tajo and Ebro stations.
3. The seasonal cycle is differently represented by the WT and FD simulations:
    - The FD simulation reaches higher and closer to observations streamflow values in the winter months.
    - As the dry season starts, the rivers get drier below the observed values in the FD run, while the WT run maintains higher summer baseflow.
    - After summer, the WT simulation follows the observation trends, recovering streamflow with the autumn precipitation from September/October. However, in the FD simulation it takes longer to recover from the dry summer, since there is no former wet periods recharge accumulated and the precipitated water needs flow through the whole soil column before flowing to the streams.

The Tortosa station near the Ebro river mouth, with the highest drainage area of the available stations (84,230 km^2), shows the best model performance by the WT simulation. On the other hand, the Miño station in the North Atlantic coast and the southern Tajo, Guadiana and Guadalquivir stations performances are very much constrained by the wet season streamflow underestimation. The Duero basin model performance is the most difficult to evaluate since the streamflow data available do not complete the last particularly wet 3 years of simulation and belong to stations very far from the Duero river mouth in Portugal.

The correlation coefficients for both monthly and monthly mean streamflow time series and the Nash-Sutcliffe coefficient are used as skill scores to evaluate the LEAFHYDRO accuracy at simulating streamflow. It is recognized that correlation coefficients between forecasts and observations suffer from deficiencies as model validation measures and may give misleading high values due to seasonal variations while being insensitive to any bias or scale error [18]. Here, correlation coefficients are used not to point out the model accuracy at simulating the streamflow values, but to show the model representation of seasonal and interannual variability and to compare this representation between the WT and the FD simulations. The Nash-Sutcliffe model efficiency coefficient E [87] is used to assess the predictive power of hydrological models, E can range from $-\infty$ to 1, whereas $E = 1$ corresponds to a perfect match of modeled streamflow to the observed data and $E = 0$ indicates that the model predictions are not useful, as accurate as the mean of the observed data. E is defined as

$$E = 1 - \frac{\sum_{t=1}^{T}(Q_{obs}^{t} - Q_{mod}^{t})^2}{\sum_{t=1}^{T}(Q_{obs}^{t} - \bar{Q}_{obs})^2}, \tag{4.2}$$

where T is the number of times in the time series, Q_{obs} is the observed streamflow and Q_{mod} is the modeled streamflow. In general hydrology model simulation, E values between 0.0 and 1.0 are generally viewed as acceptable levels of performance. For basin scale models, *Moriasi et al.* (2007) [85] estimated that $E > 0.50$ values in streamflow simulation can be judged as satisfactory.

Figure 4.5 shows, at the 20 stations from Figure 4.2, column graphs with the skill scores for the WT and FD simulations (top) and the annual mean streamflow (Hm^3 yr^{-1}) for both simulations and observations (bottom). The stations are placed in order from upriver to downriver and from northern to southern basins in the Atlantic watershed, ending with the Mediterraean Ebro basin. This way the model performance can be visually evaluated for different drainage areas and climatic conditions.

From Figure 4.5, a series of features are outlined:

- The overall underestimation of the winter flow pointed out in Figure 4.4 results in annual streamflow underestimation all over the peninsula, as can be seen from the larger green columns in the bottom graph.
- Looking at the skill scores colour columns (upper graph), the correlation indexes show numerical evidence of a better representation of the seasonal cycle and interannual variability by the WT simulation (blue and light blue), in comparison to the FD simulation (red and orange), as it was visually inferred from the time series plotted on Figure 4.4.
- The E coefficients (green columns for WT and yellow columns for FD) are very conditioned by the aforementioned winter underestimation, resulting in only

stations 6 (Toledo in the Tajo basin) and 20 (Tortosa station in the Ebro basin) close to 0.50 in the WT simulation.

- The FD simulation gets better *E* scores than the WT simulation at the Atlantic Miño, Tajo and Guadiana basins, where the winter WT underestimation contrasts with a good performance at reaching the winter peaks by the FD simulation, but still the correlation scores are improved by the WT simulation.
- At the Atlantic southern Guadalquivir basin and the Mediterranean Ebro basin the WT *E* scores improve the FD *E* scores, due to the better simulation of the dry season baseflow and the better timing at both dry and wet seasons.

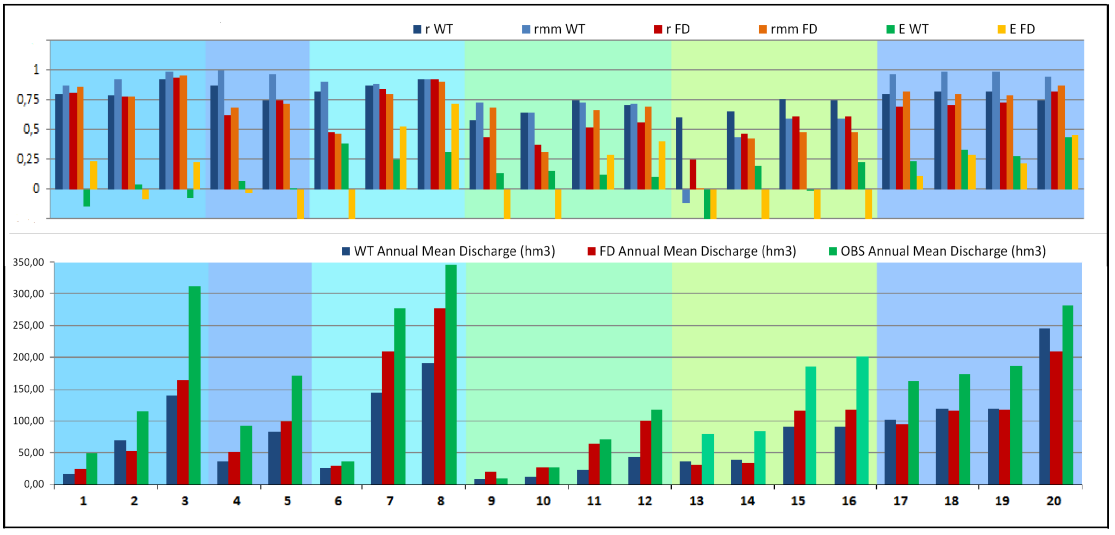

Figure 4.5: LEAFHYDRO streamflow simulation skill scores for the 20 stations higlighted on Figure 4.2. Top: Correlation coefficient *r* for the WT simulation monthly streamflow (dark blue), correlation coefficient *rmm* for the WT simulation monthly mean streamflow (light blue), correlation coefficient *r* for the FD simulation monthly streamflow (red), correlation coefficient *rmm* for the FD simulation monthly mean streamflow (orange), Nash-Sutcliffe coefficient *E* for the WT simulation monthly streamflow (green) and Nash-Sutcliffe coefficient *E* for the FD simulation monthly streamflow (yellow). Bottom: Annual mean streamflow ($Hm^3\ yr^{-1}$) in the WT simulation (blue), FD simulation (red) and observed (green).

4.2.4 Winter streamflow underestimation

The clear underestimation of the flow during the wet season in the WT simulation observed in Figure 4.4 is attributed to two different factors: the precipitation input and the model itself.

1. The first factor is a low input precipitation in high mountainous areas. The density of observations used to build the analysis precipitation dataset, IB02 [16, 54], that forces the LEAFHYDRO simulations correspond to that of the AEMET and IPMA monitoring network, and after the quality selection criteria

the mean distance between pairs of stations was 7 km in Spain and 11.7 km in Portugal, with 28 km and 41.6 km as maximum distance, respectively. Such density might not be enough to capture the high winter precipitation peaks over elevated zones or very wet areas, where heavy rainstorms trigger surface runoff.

Figure 4.6 shows the differences between daily precipitation observed at 4 stations in northwestern Spain from the *MeteoGalicia* observation network (green lines) and the IB02 daily precipitation analysis for the model grid containing each station (blue lines). *MeteoGalicia* is a regional meteorological service, its observation network spreads over the Galicia region (Spanish territory in the northwestern corner of the Iberian Peninsula) and is independent to the AEMET network used to build the IB02 dataset. The stations precipitation data are always much higher than the analysis, sometimes 2-3 times higher in the most rainy episodes. Hence, the streamflow representation in a model forced with analysis data is expected to be underestimated in the rainy season, where the analysis precipitation over elevated and wet areas is underestimated.

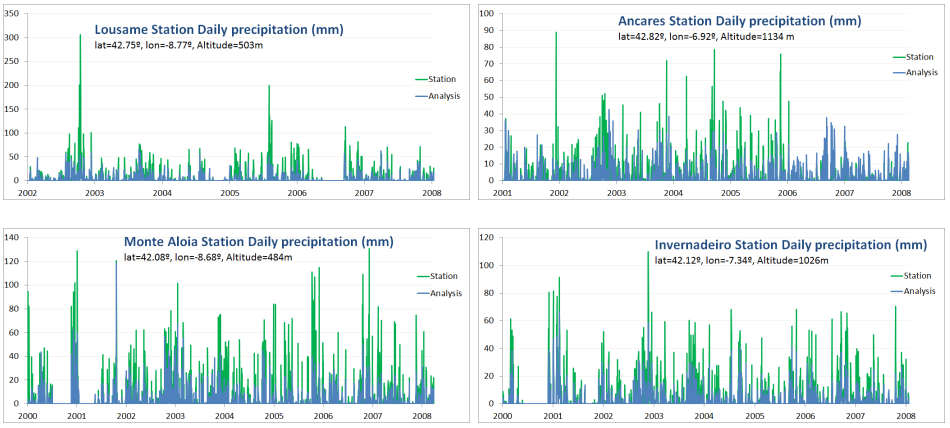

Figure 4.6: Observed daily precipitation (mm, blue lines) at 4 stations from the MeteoGalicia observation network (independent to the AEMET network used in the IB02 analysis) and IB02 analysis precipitation (mm, green lines) used to force the model at the grid cell containing each station. The two stations to the left are wet stations at about 500 m altitude near the Atlantic coast and the two right stations are elevated inland stations, at over 1000 m altitude.

2. The second factor affecting the winter streamflow underestimation by the WT simulation (in comparison to the FD simulation) is related to the simplicity of the model in representing the groundwater-soil connection when the water table appears very deep below the resolved soil layers. Given the lack of data for deep soil, the soil properties used to calculate drainage in the deeper soil before reaching the water table are those of the bottom resolved layers (0.30-4 m deep), and this brings to an excess of soil water accumulation in the deeper soil in winter that is used to drive up the water table at a slow velocity.

   This situation is not what occurs in nature when the water table is deep. The soil properties (porosity, conductivity, capillary potential) change with depth.

At some locations the soil changes to less permeable rocks or even the groundwater might be trapped in confined aquifers, in which case the infiltrated water does not reach as deep as the water table and is available for the soil quicker. At other locations, the porosity might increase due to rock crevices in the deeper soil, in which case the connection between the groundwater and the land surface is quicker than the model representation.

The deeper soil-groundwater linking representation needs to be improved in LEAFHYDRO, but it is out of the scope of this work. In any case, the results in following chapters based on the groundwater-land surface connection might be conservative, since a better representation of the deeper soil hydraulic properties is expected to increase the groundwater linkage to the land surface as suggested by the winter streamflow underestimation.

Subgrid scale surface geological features, like rocks less permeable than the grid cell soil type representation, also may strengthen these problems. A better representation of subgrid scale surface runoff processes and deep soil properties is considered for future work in this line of research.

4.3 Discussion

This chapter objective is to validate the 10-year LEAFHYDRO WT simulation with water table depth and streamflow observational data, and hence support the thesis findings in following chapters. The water table pattern and baseflow representation in the WT simulation both come from a high resolution EWTD (see Section 3.2.2), where local drainage at subgrid model scale is resolved. Hence, *wtd* and streamflow reflect topography and internal drainage, and their time evolution reflect climate through vertical fluxes, regional lateral groundwater flow and surface runoff.

A realistic water table spatial distribution and time evolution is essential to assess the groundwater-land surface link. Validation with observational *wtd* data (623 stations) shows a good model performance at capturing shallow water table positions ($wtd \leq 8$ m); 66.0% of the observational shallow points are also shallow in the model. This is an important result on the potential groundwater influence assessment because 31.4% of the Iberian Peninsula territory presents shallow water table in the simulation and the groundwater-soil connection is stronger at shallow water table regions [41, 48, 77]. The model captures the mean water table position (less than 2 m difference between simulated and observed *wtd* means) at 33.0% of the shallow water table stations (14.0% when all stations are considered) . The seasonal cycle and long-term trends are also realistically represented in the model (Figure 4.1); 32.3% of the observed time series present a correlation coefficient greater than 0.5 with the simulated time series.

The observational streamflow dataset compiled for validation is not ideal, since the simulation period is not completely covered at all stations, the stations are located far from the river mouth (particularly Duero stations), and the observed streamflow is affected by anthropogenic influence (especially Guadalquivir stations). However, from validation and WT-FD comparison, three main conclusion are drawn:

1. Winter streamflow is clearly understimated. In the FD run this is due to lack of precipitation in the forcing data. On top of the lack of precipitation, deficiencies in the model representation of soil-groundwater linkage when the water table is deep strengthen the WT winter streamflow, since the deep soil accumulates too much water from the wet season.
2. The dry season baseflow is better represented in the WT run, since the groundwater reservoir feeds gaining streams where the water table is above the riverbed elevation, whereas the FD simulation dries out the streams when there is no precipitation.
3. The seasonal cycle is differently represented by the WT and FD runs; winter higher and closer to observations streamflow in the FD run, better representation of summer baseflow in the WT run, faster recovery of streamflow when the autumn precipitation begins (September-October) following observations in the WT run. Correlation coefficients between observed and simulated streamflow time series indicate the better simulation of the seasonal cycle and interannual variability by the WT run.

The validation results encourage the work in this thesis. The findings in following chapters regarding water table influence on soil moisture and land-atmosphere fluxes in the Iberian Peninsula are based on a realistic water table. Also, the streamflow in the WT run that closes the water cycle presents realistic seasonal and interannual variability that improves the FD run representation, even though the wet season streamflow is understimated.

A better modeled streamflow will strengthen the line of research of this thesis. Hence, future work in the development of LEAFHYDRO should be addressed towards *a*) improvement of the deeper soil-groundwater linkage, since deep soil (4 m-*wtd*) properties (porosity, conductivity, capillary potential) might be misrepresented by the bottom soil layer (0.30-4 m) properties, leading to slow drainage and accumulation of water in the deep soil, *b*) improvement of surface runoff representation, triggered by heavy rainstorms or snowcover depletion from high mountainous areas, and *c*) improvement of subgrid scale geological features representation, since rocks less permeable than the cell soil type in localized zones also trigger surface runoff.

Chapter 5

Water table effects on the land-atmosphere system. Spatial and seasonal variability

The water table presence, due to its longer timescale of variation in comparison to the atmospheric forcings, induces changes in soil wetness via capillary upward fluxes and drainage control, and those changes translate to the surface through evapotranspiration fluxes. A study of such effects and their seasonal and spatial variability in the Iberian Peninsula is carried out in this chapter.

5.1 Water table control on soil moisture

The experiment in this work consists of long-term simulations using the LEAFHYDRO LSM to assess the role of groundwater dynamics in the Iberian Peninsula soil moisture and land-atmosphere fluxes (WT simulation with dynamic water table interactions switched on, and FD simulation with dynamic water table interactions switched off, see Section 3.1). Because of the 2-way fluxes linking soil moisture to the water table, the long-term soil moisture spatial structures are expected to respond somehow to the groundwater reservoir presence below.

As a first result in the simulations, the water table induces a new pattern in soil moisture fields. In order to highlight this pattern, the plots in Figure 5.1 show the difference between the mean top-2 m (root zone) soil moisture fields that result in the WT and FD simulations (left) and the water table depth (*wtd*) along the WT

simulation (right). The soil moisture differences show the new pattern induced by groundwater interactions.

The soil moisture differences in Figure 5.1 reach higher values (green and bluish colours in the left plot) where the water table is shallower (turquoise and bluish colours in the right plot), and are minimum or null in the regions with deeper *wtd* values (yellow and orange colours in both plots). The similarity between the patterns on both plots illustrates the controlling role of the water table position on the soil moisture spatial variability, mostly over river valleys and different regions of shallow water table:

a) Coastal plains and vast regions like the low Guadalquivir basin, due to low elevation.
b) The Inner Plateau (northern and southern subregions) and northern areas between the Pyrenees and the Iberian System, due to lateral groundwater flow convergence from the surrounding mountain ranges.
c) Zones in the north-west of the peninsula (Galicia and northern Portugal), due to high recharge rates.

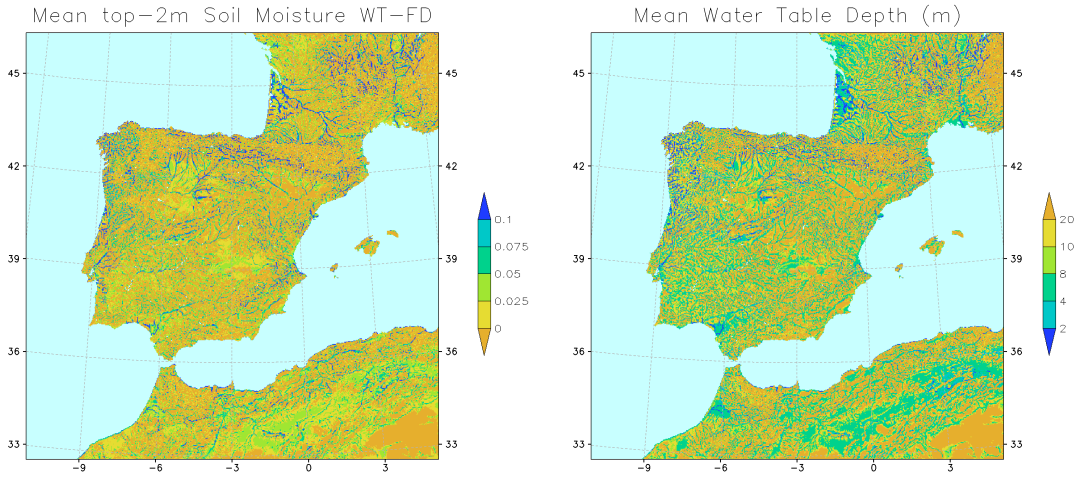

Figure 5.1: Soil soisture difference (WT-FD) and water table depth patterns. Left: Mean top-2 m soil moisture difference (m^3 m^{-3}) between the 2 simulations (WT-FD) along the 10-years simulation period. Right: Mean *wtd* (m) in the WT simulation along the 10-year simulation period.

However, given the Iberian Peninsula climatic variability analysed in Section 1.2, a deeper look into the water table controlling role on the soil moisture fields is required. The influence of groundwater dynamics on soil moisture is not equally strong in all regions or seasons.

The groundwater influence on soil moisture under different climatic situations is evaluated here using seasonal means. Figure 5.2 shows a series of plots for the four seasons in order to help in such evaluation. From top to bottom; the top row

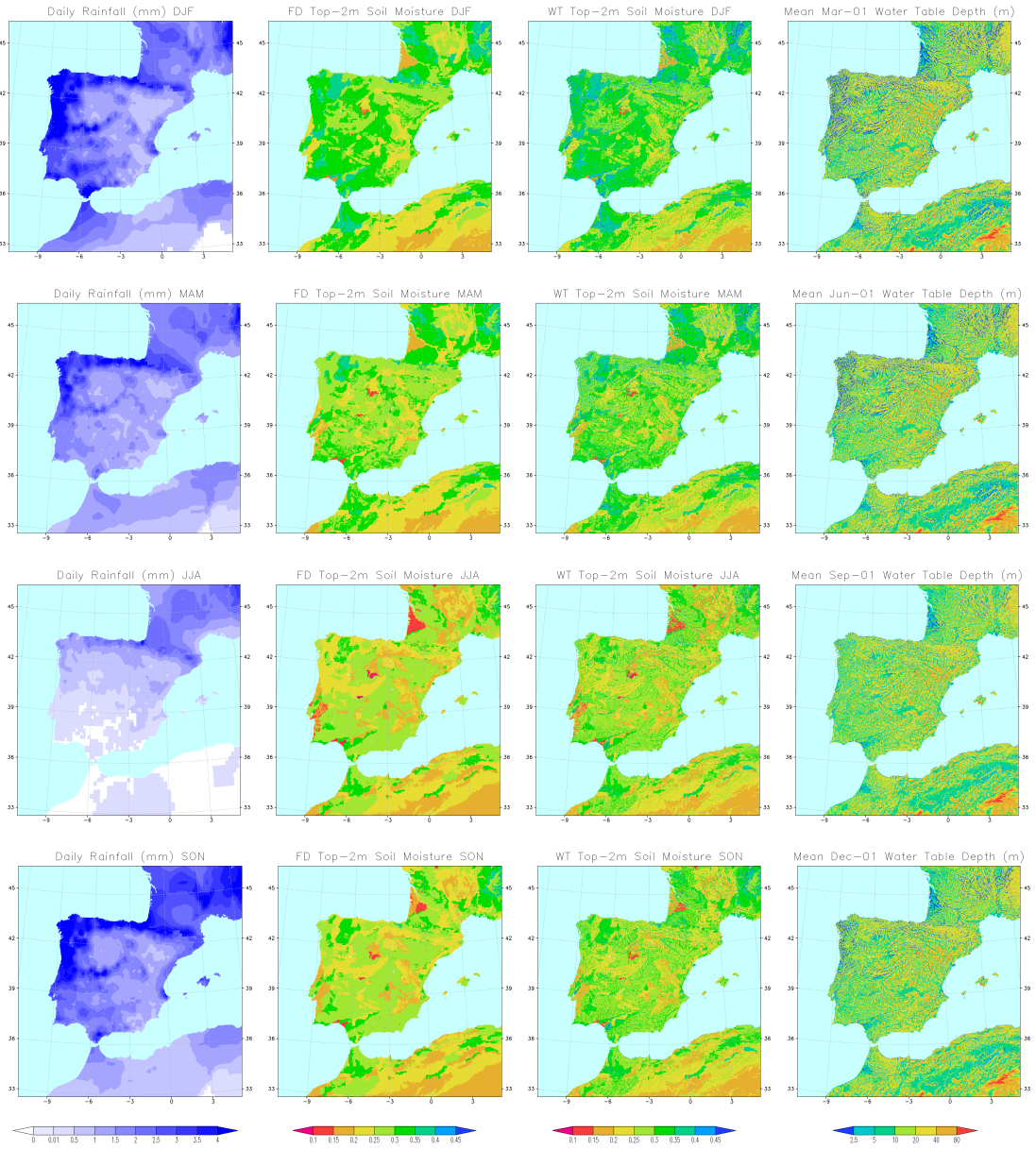

Figure 5.2: Seasonal means along the simulation. Left to right: Mean daily precipitation (mm) input, mean top-2 m soil moisture (m^3 m^{-3}) in the FD simulation, mean top-2 m soil moisture (m^3 m^{-3}) in the WT simulation and mean *wtd* (m) after each season. From top to bottom: winter, spring, summer and autumn.

plots are for winter (December-January-February), which is the wettest season in the peninsula overall; the second row from the top plots are for spring (March-April-May); the third row from the top plots are for summmer (June-July-August), the drier season; and the bottom row plots are for autumn (September-October-November). These seasonal plots are averaged for the 10 years simulated and represent, from left to right; mean daily precipitation forcing, mean top-2 m soil moisture in the FD simulation, mean top-2 m soil moisture in the WT simulation and mean water table depth that results immediately after each season.

From Figure 5.2, three different patterns are observed in soil moisture fields:

1. **Soil texture pattern.** The different soil textures in the domain impose a first non season-dependent pattern in soil moisture fields that can be spotted in all 8 seasonal soil moisture plots. It is a response to disparate water-holding capacities, making drier conditions at localized sandy regions of low water-holding capacities and high hydraulic conductivity due to the larger size of the sand particles, like the *Doñana National Park* by the Gulf of Cádiz between the Guadiana and Guadalquivir river mouths, the *Tierra de Pinares* inland sand dunes in the Northern Sub-Plateau [45], or the *Les Landes* coastal region in south-western France. On the other hand, conditions invariably wetter appear at clay regions of lower hydraulic conductivity and higher water holding capacity due to the smaller size of the clay particles, like the southern coast of Portugal, some parts of the Guadalquivir downriver basin or the Sebou river valley in the north of Morocco.

2. **Climatic pattern.** The seasonal differences in the FD simulation soil moisture plots (second column) follow the different climatic conditions, represented by the seasonal precipitation plots (first column). Starting from wet conditions in winter, the soil wetness decreases gradually through spring and summer due to the weakening of the precipitation patterns and the rising of the evapotranspiration season, then in autumn the decreasing trend stop and the soil recovers some wetness because the precipitation increases, and finally in winter the maximum soil wetness is reached again after the two high precipitation seasons of autumn and winter and the end of the evapotranspiration season in autumn.

3. **Water table pattern.** In addition to the patterns of soil texture and climatic conditions, the WT simulation soil moisture plots (third column) present an overall wetter soil and a more defined soil moisture spatial structure, that responds to the shallow water table depth patterns (fourth column). The seasonal variability in the *wtd* plots is not as strong as the seasonal differences in the precipitation and FD soil moisture plots, and hence the water table presents significant seasonal persistence that is translated to the WT soil moisture plots.

The seasonal soil moisture differences between the WT and FD simulations account for the influence of the water table over the different seasons. Averaged for the Iberian Peninsula, the soil moisture differences ($\Delta\eta = \eta_{WT} - \eta_{FD}$) are; 1.85×10^{-2} m^3 m^{-3} in winter, 2.14×10^{-2} m^3 m^{-3} in spring, 1.82×10^{-2} m^3 m^{-3} in autumn and 1.66×10^{-2} m^3 m^{-3} in summer. Therefore, the water table makes the soil wetter and the influence in absolute terms is stronger in spring, then similarly strong in winter and summer, and finally weaker in autumn.

However, in relative terms (as the percentage change $100\Delta\eta/\eta_{FD}$), the influence becomes a bigger issue at water scarcity times, as the surface balance $P - ET$ (precipitation minus evapotranspiration) is lower:

- 7.7% wetness increase in spring, when the evapotranspiration demands are the highest ($P - ET = -0.55$ mm day^{-1})
- 7.4% wetness increase in summer, when the precipitation rates are the lowest ($P - ET = -0.80$ mm day^{-1})
- 6.5% wetness increase in autumn, when the evapotranspiration season finishes and the precipitation rates are high ($P - ET = 1.24$ mm day^{-1})
- 6.2% wetness increase in winter, when the precipitation rates are the highest ($P - ET = 1.50$ mm day^{-1})

The Iberian Peninsula shallow water table zones, defined in Chapter 4 as regions with a mean *wtd* above 8 m deep, represent the 31.4% of the territory and account for all the soil moisture difference figures detailed above (the rest of the domain present negligible differences). Figure 5.3 shows the seasonal soil moisture differences between the WT and FD runs for the shallow water table cells, in both absolute and relative terms.

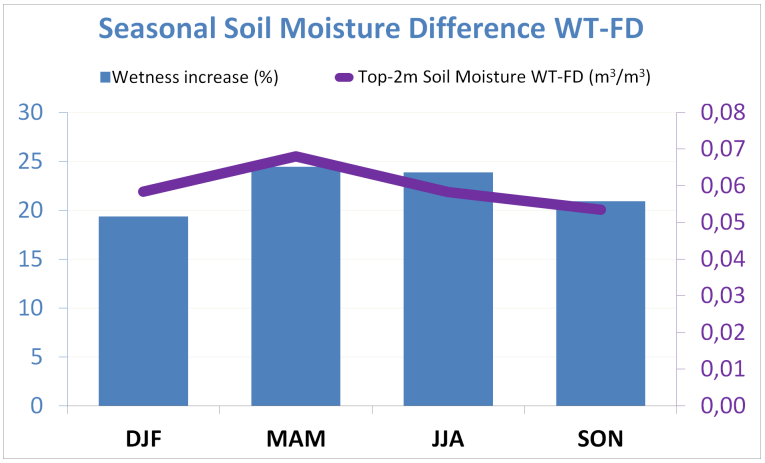

Figure 5.3: Seasonal soil moisture difference between the WT and FD runs, averaged over the shallow water table zones (*wtd* $\leq$ 8 m) in the Iberian Peninsula. Soil wetness increase (%, blue columns) and top-2 m soil moisture WT-FD difference (m^3 m^{-3}, purple line).

In relative terms (blue columns), the water table greater influence on soil moisture at water scarcity seasons (24.4% wetness increase in spring and 23.9% in summer) is appreciated, reducing partly soil moisture seasonality. Note that the data represented in Figure 5.3 are $\sim$ 3.2 times the given data averaged for the whole Iberian Peninsula.

To summarize, the soil moisture fields are not only a direct response to the soil water holding capacity and the seasonal climatic different conditions; the water table induces a new pattern in soil moisture that keeps the soil wetter in all seasons, mainly over shallow water table regions. Due to the water table persistence, the influence is greater at water scarcity seasons; in spring, when evapotranspiration

reaches the maximum rates, and summer, when the soil moisture is at a minimum due to the lack of precipitation and high evapotranspiration rates.

5.2 Water flux across the water table: Recharge

The introduction of the groundwater interactions with the unsaturated soil as the model lower boundary condition changes the nature of the water flux across the water table or *recharge*. The study of this variable gives an understanding of the connection between the groundwater reservoir and the soil.

The recharge is the water flux directly responsible for the soil moisture differences between the WT and FD simulations analysed in Section 5.1. The connection between the unsaturaded soil and the groundwater reservoir through the recharge flux is bimodal, depending on the soil wetness conditions:

- Negative recharge appears when the groundwater reservoir acts as a sink to infiltrated water that comes from precipitation and exceeds evapotranspiration to the atmosphere at the surface.
- Positive recharge appears when the groundwater reservoir takes the role of water source to soil moisture via upward capillary flux as atmosphere evapotranspiration demands exceed the water input from precipitation.

In this section, the *Long-Term Recharge* obtained as the yearly mean water table flux along the WT simulation is presented and analysed first, and the recharge seasonal variability is studied later.

5.2.1 Long-Term Recharge

In methods commonly used, groundwater recharge is inferred by tracer studies from streams flow (limited to river basins spatial scale) [10] or indirectly diagnosed from other variables, as $R = P - ET - Q_h$, where the evapotranspiration ET and surface runoff Q_h are calculated using LSMs without groundwater dynamics, and precipitation P usually comes from analysis datasets [47].

In this work, the methodology is different, the water table flux for a large region as the Iberian Peninsula is explicitly calculated every timestep (900 s) in the WT simulation. Hence, the Long-Term Recharge, understood as the yearly mean water table flux along the WT 10-year simulation, has been obtained considering explicitly long-term feedbacks between the groundwater reservoir, soil moisture, evapotranspiration and stream baseflow, as the result of a long-term land surface and hydrology model simulation that incorporates groundwater dynamics. The Long-Term

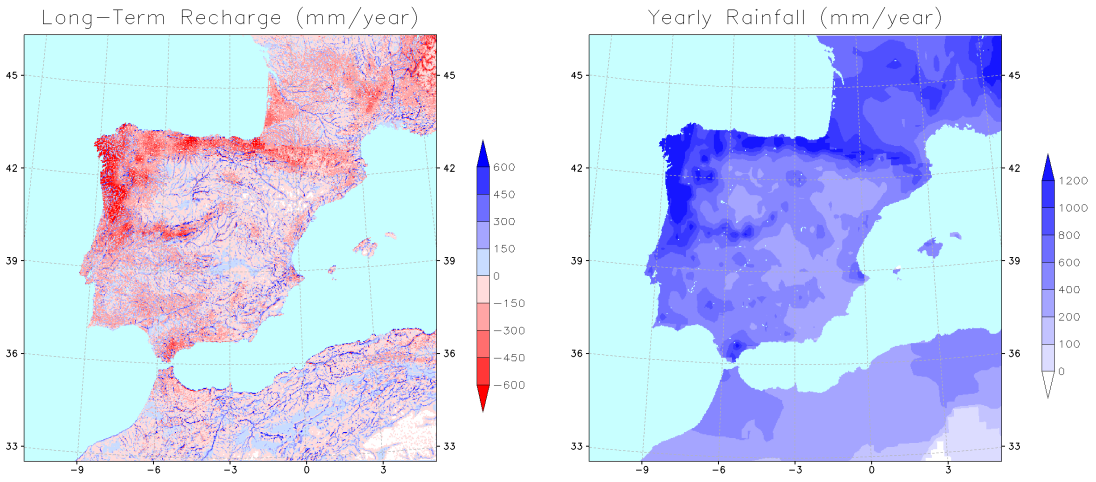

Figure 5.4: Left: Long-Term Recharge (mm yr^{-1}). Right: Mean precipitation forcing (mm yr^{-1}) along the WT simulation.

Recharge is presented in Figure 5.4 (left), together with the mean yearly precipitation forcing (right).

In Figure 5.4 (left), red colours mean negative (downwards) recharge and blue colours mean positive recharge (upward flux). Precipitation and evapotranspiration in Mediterranean climates are typically in opposite phases, and hence the long-term recharge red negative patterns respond to high precipitation patterns – dark blue shadows in Figure 5.4 (right) –, although the amount is diminished by surface runoff and evapotranspiration.

The upward flux appears as a result of groundwater lateral flow from surrounding higher water table cells and river infiltration when the water table is below the river bed (see Section 2.2). These fluxes represent a water source to the groundwater reservoir from surrounding areas, different to the vertical drainage through the water table, allowing upward capillary flux to meet evapotranspiration demands. The long-term blue (upward) recharge presents two different patterns:

1. Light blue shadows over extended shallow water table regions affected by insufficient rainfall input to meet evapotranspiration demands, like in the Inner Plateau (northern and southern subregions).
2. Marked blue streams following the main river valleys all over the domain, since the river valleys are zones of strong lateral groundwater flow convergence.

A proper estimation of the recharge is of major importance for water management systems, mainly in high irrigation areas such as the arid and semiarid regions of the Iberian Peninsula, helping understand where unconfined aquifers are at risk of being overexploited. Furthermore, a long-term recharge estimation that results from a long-term LSM simulation with a fully dynamic water table, where the net yearly upward flux is allowed, can be of great value for research purposes.

5.2.2 Seasonal variability

The groundwater recharge presents a strong seasonal variability. Figure 5.5 shows the mean daily recharge plots obtained in the WT simulation for spring (top left), winter (top right), summer (bottom left) and autumn (bottom right). Again as in Figure 5.4, red colours mean downward recharge and blue colours mean upward flux.

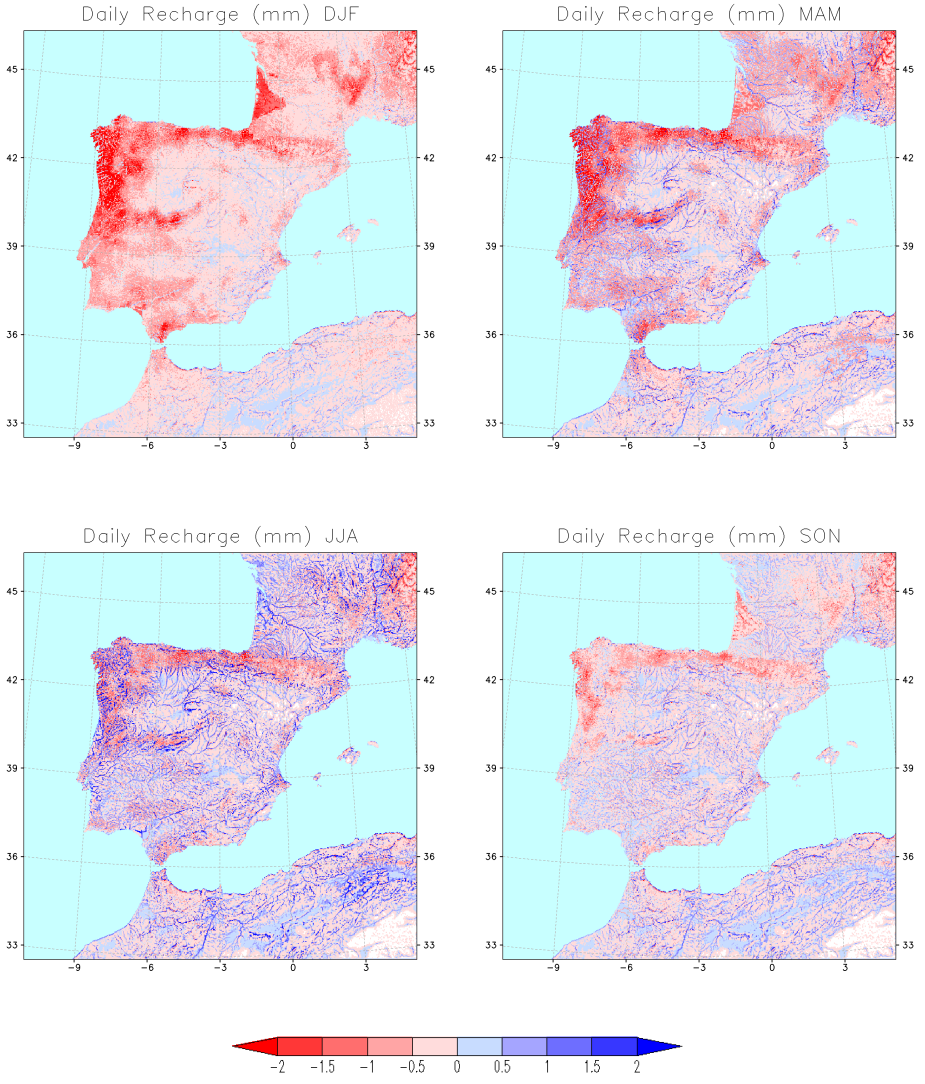

Figure 5.5: Mean seasonal recharge (mm day^{-1}) along the 10-year simulation period. From top left to bottom right: winter (DJF), spring (MAM), summer (JJA) and autumn (SON).

A clear seasonal evolution in the recharge can be appreciated from Figure 5.5 plots:

- The winter plot is mostly red and resembles the structure of the autumn and winter precipitation plots in Figure 5.2, therefore the groundwater reservoir is

a sink to the wet season precipitation water that infiltrates through the soil layers.

- In spring the winter rainfall keeps flowing down through the soil layers and to the groundwater reservoir, maintaining the negative recharge pattern as strong as it was in winter, but spring precipitation is not as high and the evapotranspiration demands start to rise, so there begin to appear important blue upward flux patterns over valleys and shallow water table regions.
- The summer plot shows a maximum in recharge all over the peninsula. The precipitation input is minimal during summer, weakening the red negative pattern, and the evapotranspiration demands from the atmosphere keep forcing the groundwater reservoir to act as a water source, strengthening the blue upward patterns that already appeared in spring.
- In the autumn plot the role of the groundwater reservoir as a water source starts to weaken since autumn precipitation is enough to cover autumn evapotranspitation demands, and drainage through the water table is not as strong as it was in spring, even though the precipitation input is similar or even stronger for the wetter regions in autumn (Figure 5.2), since the infiltrated water takes time to reach deeper water tables.

In conclusion, the groundwater recharge presents a clear seasonal cycle following the precipitation and evapotranspiration cycles. Downward recharge is strong during winter and spring, responding to drainage of infiltrated precipitation from the wet season, and weaker during summer and autumn after the dry season. Upward flux is appreciated over shallow water table regions; it presents significant values in spring, when the evapotranspiration season starts, and reach the maximum in summer when the surface balance is minimal ($P - ET = -0.80$ mm day^{-1}), then during autumn it decreases significantly due to the decrease of evapotranspiration demands, and finally it reaches the minimum in winter when precipitation presents the highest rates and evapotranspiration the lowest.

5.3 Enhanced Evapotranspiration (ET)

The fluxes across the water table result in water table depth fluctuations (see Section 4.1) and changes in soil moisture as seen in Section 5.1. But the effects on land-atmosphere fluxes are also significant.

Fan & Miguez-Macho (2010) [41] calculated the potential groundwater contribution to the atmosphere via upward capillary flux and found that it reaches high values of 50.86 mm day^{-1} for clay loam soil type and 14.95 mm day^{-1} for clay, when the water table position is very shallow (1 m deep), and decrease rapidly as the water table position deepens. These authors used a simple method resolving the

Richards equation (Equation 2.1) numerically through the unsaturated soil (divided into 0.05 m thick layers) for different water table positions, under imposed boundary conditions of wilting point in the top layer (constant maximum water demand) and saturation in the layer containing the water table.

More recently, *Gestal-Souto et al.* (submitted) [48] applied the same method to the Iberian Peninsula using the EWTD applied here as initial condition (Section 3.2.2), and they found upward capillary flux patterns with maximum values in the main river valleys and the main shallow water table regions. With a coupled dynamic groundwater-land surface simulation such as the WT simulation in this work, such patterns of upward capillary flux translate into upward groundwater recharge during dry periods (summer upward flux patterns in Figure 5.5), and the potential groundwater contribution to the land surface ET can be ascertained.

The Iberian Peninsula seasonal ET fields obtained with LEAFHYDRO are shown in Figure 5.6. The plots represent the mean daily ET in the FD simulation for, from left to right; winter, spring, summer and autumn. The seasonal character of the ET induced by the water availability and the incoming radiation is clear, showing maximum values and higher spatial variability in spring and summer and then minimum values and variability in autumn and winter, when the incoming radiation is lower and the leaf area index decreases. The higher values are reached over the more vegetated areas of the north and west of the peninsula, where the surface temperatures are lower. These ET patterns are in agreement with ET seasonal patterns obtained by *Sobrino et al.* (2007) [108] using NOAA satellite images for the Iberian Peninsula.

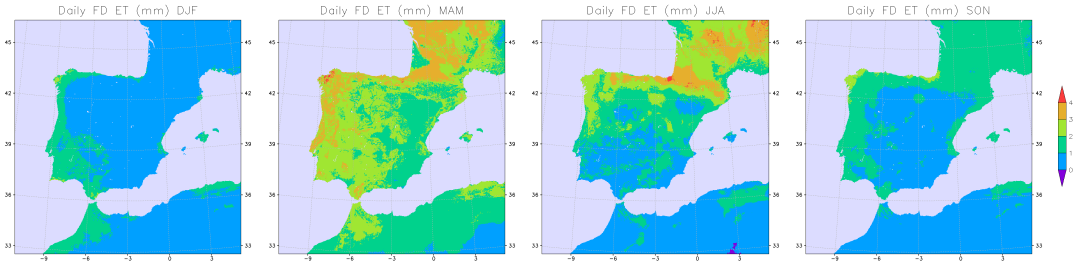

Figure 5.6: Mean seasonal evapotranspiration (ET, mm day^{-1}) along the 10-year simulation period (FD run). From left to right: winter (DJF), spring (MAM), summer (JJA) and autumn (SON).

The WT simulation reveals an enhancement of the ET towards the atmosphere, mainly in dry seasons and shallow water table regions. In comparison to the FD run, the ET flux is higher in the WT run over the most part of the peninsula. The averaged Iberian Peninsula ET in the WT run results 17.4% higher (0.24 mm day^{-1} difference).

The Iberian Peninsula averaged enhanced ET presents strong seasonal variability, reaching its maximum in summer (34.9%, 0.54 mm day^{-1}), with WT-FD ET values

over 2 mm day^{-1} at some shallow water table points. In spring and autumn the difference is similarly important in relative terms (10.8% and 13.4% respectively), but considerably higher in absolute terms in spring (0.24 mm day^{-1} and 0.14 day^{-1}, respectively), since it is in spring when ET fields reach maximum values as shown in Figure 5.6. The low ET values in winter lead to very small and practically insignificant ET differences between the WT and FD simulations (6.8%, 0.05 mm day^{-1}).

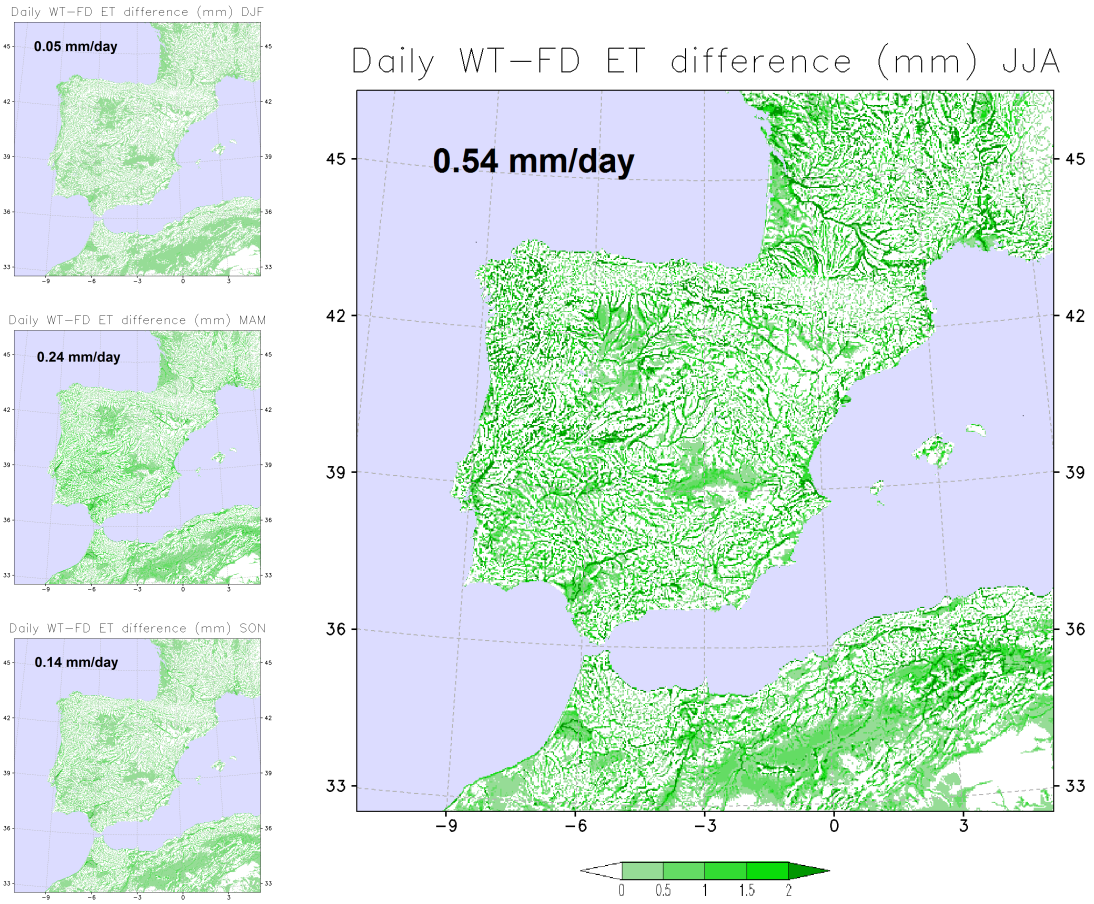

Figure 5.7: Mean seasonal evapotranspiration (ET) difference (mm day^{-1}) between the WT and FD runs (WT-FD) along the 10-year simulation period, and mean daily difference averaged over the Iberian Peninsula (black text). Left, from top to bottom: winter (DJF), spring (MAM) and autumn (SON). Right: summer (JJA).

From Figure 5.7, that shows the enhanced ET fields for the four seasons as the mean daily ET differences between the WT and the FD simulations, a series of features are outlined:

- The spatial pattern is the same in all seasons, but considerably stronger in the summer season (larger plot), when the incoming precipitation is the lowest, the atmosphere demands are high (see Figure 5.6), and in the WT simulation there is more soil water availability due to the presence of the water table

and the soil moisture memory from previous wetter periods that it induces (following Chapter 6 will focus on the water table persistence and the seasonal and long-term soil moisture memory induced by it).

- The ET differences pattern clearly resembles the mean water table position (Figure 5.1, right plot), and reaches the highest values over the main river valleys, where groundwater flow convergence leads to strong upward flux.
- The main vast shallow water table regions in the Northern Sub-Plateau, the upper Guadiana basin (Southern Sub-Plateau) or the *Doñana National Park* region by the Guadalquivir river mouth, are spotted as enhanced ET zones all year.
- Over high regions like the Pyrenees or the Cantabrian Mountains, the deep position of the water table translates into less or none enhanced ET.

The *extra* water that flows to the atmosphere as enhanced ET is not available in the soil in the FD simulation. This is an important result that confirms the potential groundwater contribution to land ET over the Iberian Peninsula anticipated by *Gestal-Souto et al.* (submitted) [48] – work also carried out in the USC *Non-Linear Physics Group*.

5.4 Discussion

The objective of this chapter is to study the seasonal and spatial variability of the water table effects on the land-atmosphere system. To do so, the long-term results (soil moisture, groundwater recharge and evapotranspiration fluxes) of two 10-year simulations with the coupled groundwater-land surface model LEAFHYDRO over the Iberian Peninsula are studied. The simulations are referred to as WT (Water-Table), in which the water table interactions are switched on, and FD (Free-Drain), in which the water table interactions are switched off.

Results on long-term soil moisture show that the water table makes the soil wetter over shallow water table regions, introducing a new pattern in soil moisture fields different to the climatic conditions and soil texture patterns. Analysing seasonal means, the water table influence on soil moisture is found to reduce partly seasonality, since the soil wetness increase over the shallow water table regions is greater at water scarcity seasons (24.4% in spring, when evapotranspiration reaches the maximum rates, and 23.8% in summer, when the soil moisture is at a minimum due to the lack of precipitation and high evapotranspiration rates), and lower in autumn and winter ($\sim 20\%$), when the surface water balance $P - ET$ is higher.

The soil moisture effects are induced by the groundwater recharge or water flux across the water table, that can be positive (upwards via capillary flux) in the WT simulation due to lateral groundwater convergence and river infiltration, acting as a source to soil moisture to meet evapotranspiration demands. The Long-Term

Recharge is presented, showing an upward flux pattern over extended shallow water table regions and river valleys. The seasonal variability of groundwater recharge responds to the surface precipitation and evapotranspiration cycles:

- The negative recharge is stronger during winter and spring, responding to drainage of infiltrated precipitation from the wet season, and weaker during summer and autumn after the dry season.
- The upward flux is strong in spring, due to the beginning of the evapotranspiration season, and maximal in summer, when the surface balance is minimal. Then, during autumn the upward flux decreases significantly due to the decrease of evapotranspiration demands, and finally it reaches the minimum in winter, when precipitation presents the highest rates and evapotranspiration the lowest.

The water table effects on soil moisture translate to the atmosphere via evapotranspiration enhancement. The evapotranspiration differences between the simulations with and without groundwater dynamics present again the spatial pattern induced by the water table (reaching significant differences over river valleys and shallow water table regions in the Inner Plateau and coastal plains). The enhanced evapotranspiration averaged over the Iberian Peninsula is 0.54 mm day^{-1} in summer, when the precipitation is the lowest and evapotranspiration demands are high, 0.24 mm day^{-1} in spring, when evapotranspiration demands are the highest, 0.14 mm day^{-1} in autumn and 0.05 mm day^{-1} in winter, when the evapotranspiration demands are very low.

These results of wetter soil and enhanced evapotranspiration over shallow water table regions lead to hypothesise that the introduction of the groundwater dynamics in fully coupled land surface and climate simulations over the Iberian Peninsula will result in:

- **Convective precipitation enhancement** through recycling of local water vapour over the semiarid interior regions, that present a peak of precipitation in early spring and shallow topographically-driven water table zones in spite of low rainfall [9, 93].
- **Summer temperature decrease** due to lower sensible fluxes and higher cloudiness. This is an interesting line of research, since the Iberian Peninsula is a region of high land-atmosphere coupling (mainly over interior regions insulated from the maritime moisture source by the Iberian mountains ranges), and the summer temperature increase and interannual variability are hot topics in climate change studies.

Chapter 6

Soil moisture memory induced by the water table

The soil moisture link to the atmosphere is of major importance for weather and climate forecasting as discussed in Section 1.3.1. Soil moisture memory refers to dry or wet anomalies of longer persistence in time, as compared to the atmosphere. The soil can "remember" atypically dry or wet conditions long after such conditions have been "forgotten" by the atmosphere (*Koster & Suarez*, 2001 [61]).

The influence of soil moisture memory on seasonal forecasting has been an important research issue for the scientific community in recent years [60, 68, 101, 120]. Different authors have worked on the identification of strong land-atmosphere coupling regions (e.g. *Koster et al.*, 2004 [59], *Seneviratne et al.*, 2006 [105]), and on setting a framework to assess soil moisture memory from climate data (e.g. *Koster & Suarez*, 2001 [61], *Seneviratne & Koster*, 2012 [103]). Using ten different modeling systems experiments, participant in GLACE-2 (*Global Land-Atmosphere Coupling Experiment*) project[1], *Koster et al.* (2010) [60] related temperature and precipitation predictabilities to higher soil moisture initial anomalies, hence the importance of soil moisture memory in forecasting.

The integrative nature of soil moisture memory as water storage has been pointed out by *Orth et al.* (2013) [89] by inferring soil moisture memory from streamflow observations at small catchment scales. Here, LEAFHYDRO introduces water table dynamics as a new player into the soil-atmosphere system. Therefore, the timescales of water table dynamics, which can range form days to years in the Iberian Peninsula [80, 106], are accounted for by the soil and expected to enhance soil moisture memory. In this chapter, such water table longer timescale and its influence on the soil moisture memory over the Iberian Peninsula and over a localized shallow water table region are studied.

[1] http://gmao.gsfc.nasa.gov/research/GLACE-2/

6.1 Water table seasonal and interannual persistence

An important water table seasonal persistence, as compared to that of precipitation, was observed in the previous chapter while analysing the seasonal mean water table depth plots (Figure 5.2, Section 5.1). The choice of a 10-year simulation period allows a deeper look into this water table persistence. In this section, the 9 complete hydrological years (September 1989 - August 1998) simulated are used in order to extract information about the seasonal and interannual water table behaviour.

The Iberian Peninsula presents, as noted from the precipitation plots in Figure 5.2, an overall maximum of precipitation in winter months (2.3 mm day^{-1} for the simulation period) and a minimum in summer months (0.7 mm day^{-1}). A collection of anomaly plots for both extreme seasons and for the 9 hydrological years simulated is presented in Figure 6.1. Each column corresponds to each hydrological year, chronologically from left to right (hy1 to hy9). The four rows represent, from top to bottom; winter precipitation anomalies, end of winter (March 1st) *wtd* anomalies, summer precipitation anomalies, and end of summer (September 1st) *wtd* anomalies. The colour bars below each row average the anomaly values of each plot for the Iberian Peninsula, in order to give a quick idea of the anomaly evolution along the simulation.

The precipitation plots show high interannual variability in summer (first row) and also in winter (third row). However, the peaks and lows in precipitation anomalies are independent for both seasons; the main winter drought starting in hy2 over the south and centre of the peninsula that lasts until hy7 is not reproduced in summer, since hy3 summer anomalies are positive all over the domain and other years present very different patterns (hy4 and hy6).

Looking at the end of season *wtd* plots (second and bottom row), the interannual variability is not as marked; the changes are slow along the simulation, showing a longer timescale of evolution in comparison to the precipitation plots. Hence the water table position persists, in spite of different precipitation regimes at the surface every year. This water table persistence is not only interannual but also seasonal, as can be concluded from the similarity between *wtd* end of winter anomaly plots (second row) and *wtd* end of summer anomaly plots (bottom row).

From Figure 6.1 it is concluded that the water table evolution responds mostly to long-term climatic conditions and not so much to seasonal or annual peaks and lows.

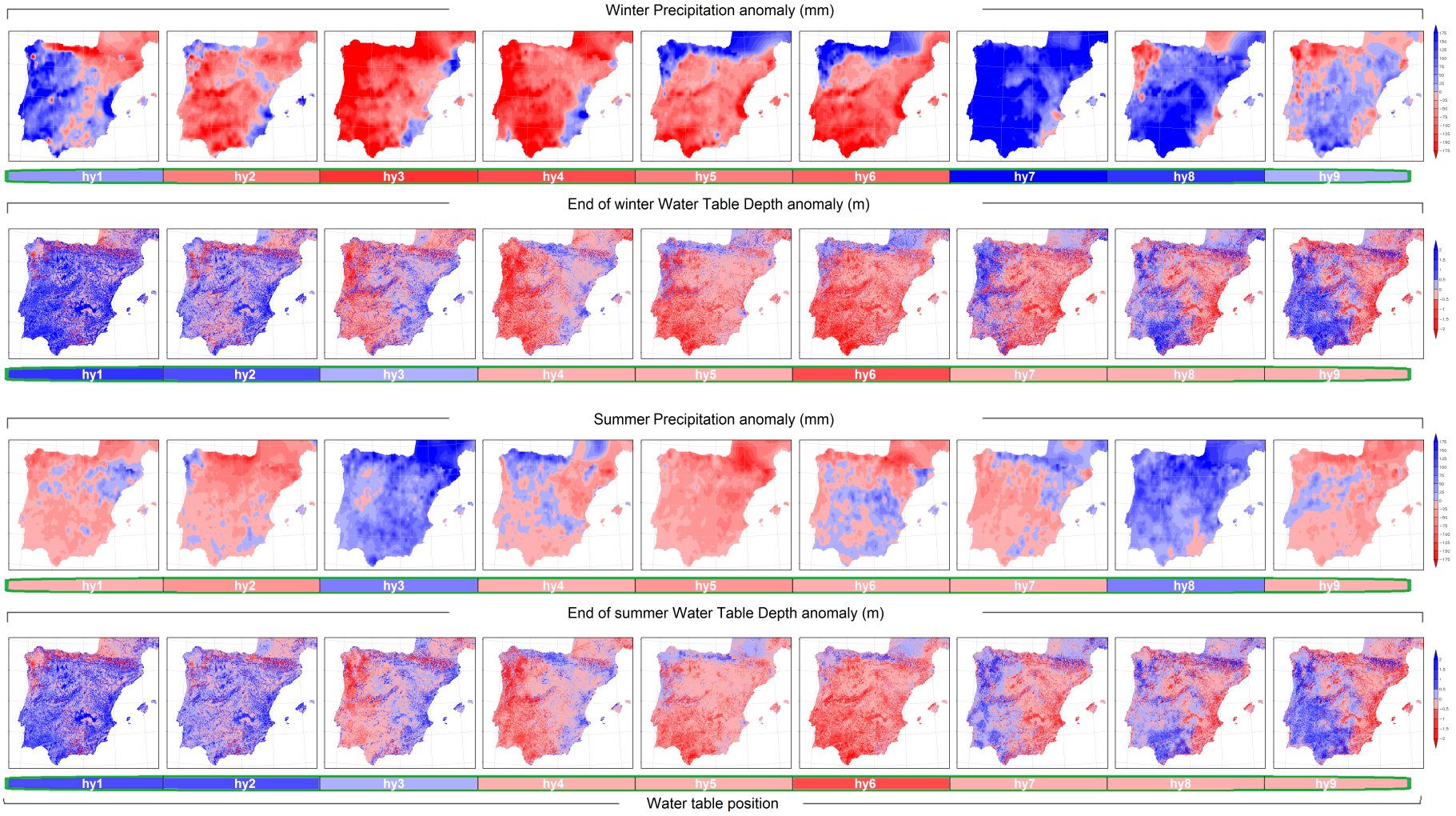

Figure 6.1: Seasonal anomaly plots for precipitation and *wtd*. Each column represents a whole hydrological year (hy1 to hy9) simulated. Rows from top to bottom: winter precipitation anomaly (mm), end of winter (March 1st) *wtd* anomaly (m), summer precipitation anomaly (mm) and end of summer (September 1st) *wtd* anomaly (m). Colour bars below each row represent the averaged anomaly value for the Iberian Peninsula.

6.2 The effects of water table persistence on soil moisture memory

The water table persistence and its connection to the soil through upward capillary fluxes are expected to induce certain memory of past atmospheric conditions into the soil. Over regions where the water table is shallow, the groundwater-soil link is more important as seen in Section 5.1, and the longer timescale of variation of the water table position affects soil moisture.

6.2.1 Analysis over the Iberian Peninsula

The plots in Figure 6.2 show, over the Iberian Peninsula and chronologically along the 9 complete hydrological years simulated; total yearly precipitation anomalies (top row), *wtd* anomalies at the end of the hydrological year (m; middle row), and top-2 m soil moisture difference between the WT and the FD simulations anomalies (bottom row). From the top and middle rows the water table persistence is made clear, and the bottom row of soil moisture difference between the WT and FD runs patterns can be understood as a measure of the water table influence on soil moisture and its spatial and time variabilities.

The soil moisture difference between the WT and FD runs is always positive along the experiment, since the soil is wetter in the WT run (see Section 5.1), but the anomaly plots in the bottom row Figure 6.2 tell how positive it is during the different hydrological years in comparison to the mean, and therefore how important the water table influence is under different climatic conditions and how such importance follows yearly changes in precipitation (top row) and water table position (middle row). Blue positive anomalies indicate stronger water table influence on soil moisture and red negative anomalies indicate weaker influence.

From Figure 6.2 the following is noted:

- Intense climate events at the surface (positive anomalies in blue or negative anomalies in red in the precipitation plots) cause responses in the water table position (shallower anomalies in blue and deeper anomalies in red)that are not immediate, and may last up to 1 or 2 years in time. For instance:
  - High precipitation in the Northern Sub-Plateau and the southern half of the peninsula during hy1 keeps the water table shallower than the mean during the next year at numerous zones in spite of clearly negative precipitation anomalies during hy2.
  - On the eastern coast, the hy1 positive precipitation anomaly is especially high, and the water table appears shallower than the mean during the next 3 years, even though the precipitation anomalies in the region keep changing.

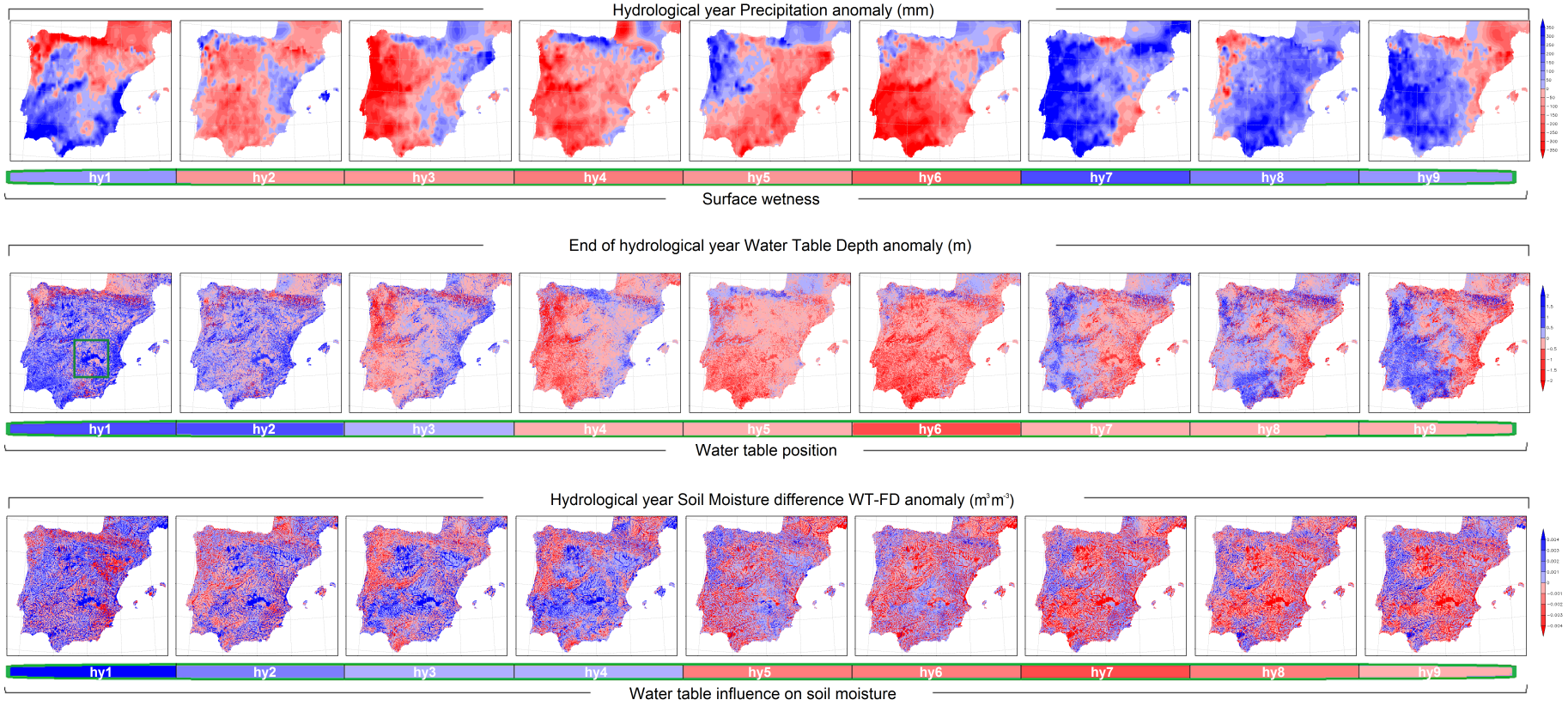

Figure 6.2: Hydrological year anomaly plots. Each column represents a whole hydrological year (hy1 to hy9) simulated. Rows from top to bottom: total yearly precipitation anomalies (mm), end of hydrological year (September 1st) *wtd* anomalies (m) and top-2 m soil moisture difference (WT-FD) anomalies (m^3 m^{-3}). Colour bars below each row represent the averaged anomaly value for the Iberian Peninsula.

  - Over the northern Cantabric coast, the very positive precipitation anomaly during hy4 translates into positive *wtd* anomalies in the region in hy4 and hy5 plots, in spite of negative precipitation anomalies during hy5 over large zones of the coast.
  - On the other hand, the positive precipitation anomaly during hy5 in the northwestern part of the peninsula is not enough to be reflected in the *wtd* plots as positive anomaly, since the region comes from 2 consecutive very dry years (hy3 and hy4), and therefore the water table stays deeper than the mean over most of the region after hy5.

- Following an initial overall wet year (wetter than the mean in the centre and south but drier in the north), the precipitation anomalies averaged for the Iberian Peninsula are clearly negative from hy2 to hy6, and then clearly positive during the last 3 years. However, this surface wetness regime is followed with 1-2 years delay in the water table position, that deepens slowly from a shallow initial position up to hy6 and then starts to rise up from the very wet hy7, but it never reaches the positive anomaly position. This water table delayed behaviour is made very visible by the colour bars below each row, showing the anomalies averaged for the whole peninsula.
- Looking at the bottom row, the very positive anomaly during hy1 can respond to a shallow initial water table position. Later on, the positive anomalies indicating stronger water table influence on soil moisture appear during dry years and regions where water table position "remembers" former wet events. The regions of more intense anomalies (positive and negative) are the shallow water table regions, where the mean soil moisture differences are greater.
- The overall wetter year at the surface, hy7, is the year with less water table influence on soil moisture, as expected, since the evapotranspiration demands are covered by precipitation.
- The colour bar (average for the Iberian Peninsula) in the bottom row follows with a 1-year delay the colour bar in the middle row, indicating how the water table depth memory is induced into the soil moisture.

A deeper understanding of the degree of the water table persistence influence on the soil can be reached analysing the time correlation indexes between the yearly soil moisture and the two players affecting its time evolution: precipitation and water table depth (Figure 6.3).

The time series of the hydrological year soil moisture anomalies in the FD simulation and the hydrological year precipitation anomalies are positively correlated at every point of the domain (left plot in Figure 6.3), with lower indexes over high northern regions where topography takes over. However, when the same time correlation is evaluated using the WT simulation soil moisture anomalies, the positive index decreases at shallow water table regions all over the Iberian Peninsula (middle plot in Figure 6.3), indicating that the soil moisture dependence on precipitation has

diminished. The averaged correlation index between yearly precipitation and soil moisture anomalies series over the Peninsula decreases from 0.81 to 0.72, and from 0.82 to 0.60 when averaging only over shallow water table regions ($wtd \leq 8$m).

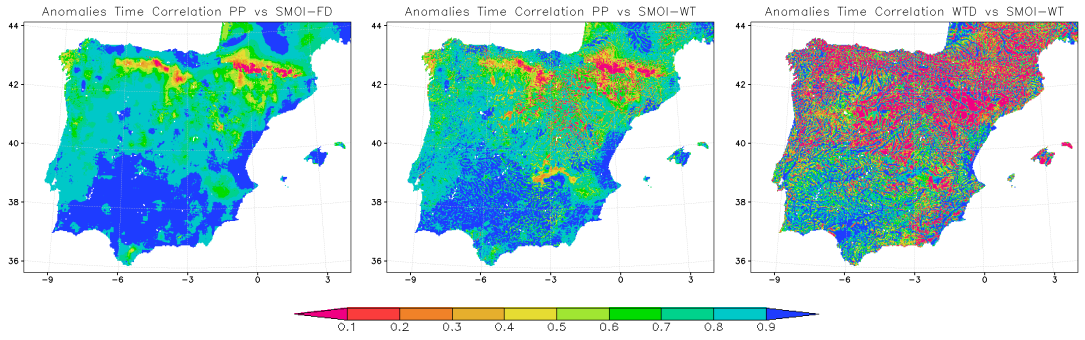

Figure 6.3: Yearly anomalies time series correlations for the Iberian Peninsula (along the 9 complete hydrological years simulated). Left: Precipitation (mm) vs. soil moisture in the WT simulation. Centre: Precipitation (mm) vs. soil moisture in the FD simulation. Right: Water table depth vs. soil moisture in the WT simulation.

Patterns of higher positive time correlation (over 0.5) in the Iberian Peninsula between the *wtd* anomalies and the soil moisture anomalies in the WT simulation (right plot in Figure 6.3) appear over many shallow water table regions in the southern half of the peninsula, the Northern Sub-Plateau or Galicia, precisely where the soil moisture anomalies correlation with the precipitation anomalies (middle plot) decrease. The averaged correlation index between yearly water table and WT soil moisture anomalies series is 0.43 over the whole peninsula, and 0.93 when averaging over shallow water table regions. Hence, the water table persistence enters into the system as a factor to explain partly the soil moisture anomalies.

To further understand how the precipitation influence on soil moisture decreases and the water table persistence influence increases, Figure 6.4 shows the time series along the 9 hydrological years of the spatial correlation indexes between the Iberian Peninsula fields of precipitation and soil moisture anomalies (left), and between water table depth and soil moisture anomalies over shallow water table points (right). The light blue columns represent the mean Iberian Peninsula precipitation for each hydrological year.

Figure 6.4 (left) illustrates how precipitation anomalies explain soil moisture anomalies in the FD simulation (dark blue line) to a higher degree that in the WT simulation (dark green line), mostly during wetter years.

Figure 6.4 (right) shows how the *wtd* anomalies explain to some degree the soil moisture anomalies in the WT simulation (dark orange line); the spatial correlation index increases during the early years as precipitation decreases, marking the greater influence of the *wtd* on soil moisture during droughts, then it decreases in hy5 with an increase of precipitation and goes up again in the wettest hy7, when

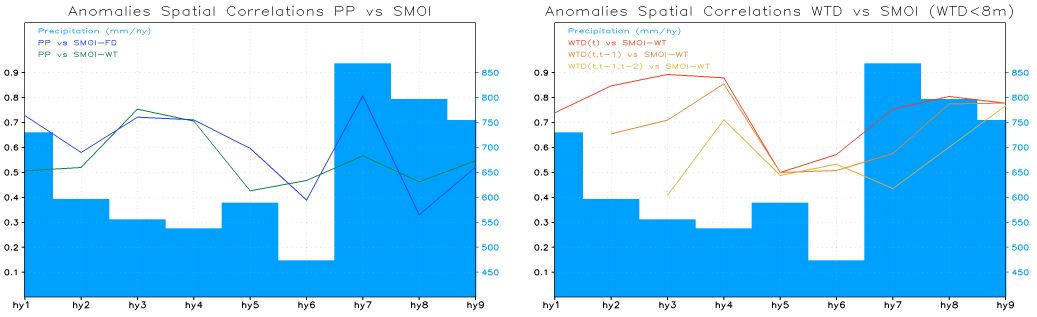

Figure 6.4: Anomalies spatial correlations for the Iberian Peninsula along the 9 complete hydrological years simulated and total yearly precipitation (mm; light blue columns). Left: Precipitation vs. soil moisture in the FD simulation (dark blue line) and precipitation vs. soil moisture in the WT simulation (dark green line). Right: *wtd* vs. soil moisture in the WT simulation (dark orange line), mean last 2 years *wtd* vs. soil moisture in the WT simulation (orange line), and mean last 3 years *wtd* vs. soil moisture in the WT simulation (dark yellow line). Only points with mean *wtd* above 8 m are considered for the spatial correlations between *wtd* and soil moisture anomalies.

precipitation anomalies do not explain soil moisture anomalies in the WT simulation as strongly as in the FD simulation (left).

The orange line in Figure 6.4 (right) represents the spatial correlation between the *wtd* anomalies for the past 2 years (hy_t, hy_{t-1}) and soil moisture anomalies at hy_t, whereas the dark yellow line represents the spatial correlation between the *wtd* anomalies for the past 3 years (hy_t, hy_{t-1}, hy_{t-2}) and soil moisture anomalies at hy_t. Their high value and their upper trend during the dry middle years and the last 2 years can be explained as soil moisture memory of water table positions during former years while precipitation follows a decreasing trend (hy2-hy4, hy7-hy9).

6.2.2 A closer look: *La Mancha Húmeda*

La Mancha Húmeda is a Biosphere Reserve situated in the upper Guadiana Basin. It comprises the Tablas de Daimiel National Park, which corresponds to the core area, the Alcázar Lake and the Lagunas de Ruidera National Park. The Equilibrium Water Table is found very shallow at this region (see Section 3.2.2), and therefore it is a marked wet spot that helps understand the water table influence on soil moisture memory at a finer scale.

6.2.2.1 Soil moisture memory induced over the localized shallow water table zone

In Figure 6.5 a series of plots represent a 250×225 km^2 area containing *La Mancha Húmeda*. The zoomed area is highlighted with a green contour in Figure 6.2

(middle row, first plot). The plots show, chronologically for the 9 hydrological years simulated; total yearly precipitation anomalies (top row, simple zoom of top row in Figure 6.2), soil moisture anomalies in the FD simulation (second row), soil moisture anomalies in the WT simulation (third row), and end of hydrological year *wtd* anomalies (bottom row, simple zoom of the middle row in Figure 6.2).

From Figure 6.5, the following is noted:

- Soil moisture anomalies in the FD simulation (second row) are a clear response to precipitation anomalies (top row).
- From hy1 the water table appears very shallow in the central wet area (bottom row), then the lack of precipitation (in this region the precipitation anomalies are negative or very slightly positive up to hy6) causes the water table to descend. However, the *wtd* anomalies persist positive and do not become negative until hy4.
- In the WT simulation soil moisture anomaly plots (third row), the central wet area follows *wtd* anomalies, with very positive anomaly in hy1 and then with a wetter soil wetter than the mean during the dry hy2 and hy3.
- From hy5, the negative *wtd* anomaly started in hy4 intensifies. In spite of higher precipitation during the last 3 years, the water table never recovers and the *wtd* anomalies in the central wet area are negative up to the end of the simulation.
- Soil moisture anomalies are negative in the central area from hy4 as a direct response to the *wtd* anomalies, and the soil also never recovers in the simulation, even though it can be clearly observed how in the last 3 years high precipitation causes positive soil moisture anomalies around the central area.
- The averaged soil moisture anomalies (colour bars below second and third row) change when considering the water table influence. For instance, the mean soil moisture anomaly over the zoomed area in hy7 results positive due to positive precipitation anomaly, whereas in the WT simulation it is negative due to water table persistence.

From Figure 6.5 it is concluded that soil moisture patterns in the FD simulation follow directly the evolution of precipitation patterns, whereas in the WT simulation soil moisture patterns reflect a combination of precipitation and *wtd* patterns. The FD approach, without groundwater representation, lacks the memory induced in the WT simulation by the groundwater implementation, which is very apparent over shallow water table areas. This memory is bimodal, since the water table persistence makes the soil "remember" dry and wet periods, and therefore drought effects are buffered but also last longer.

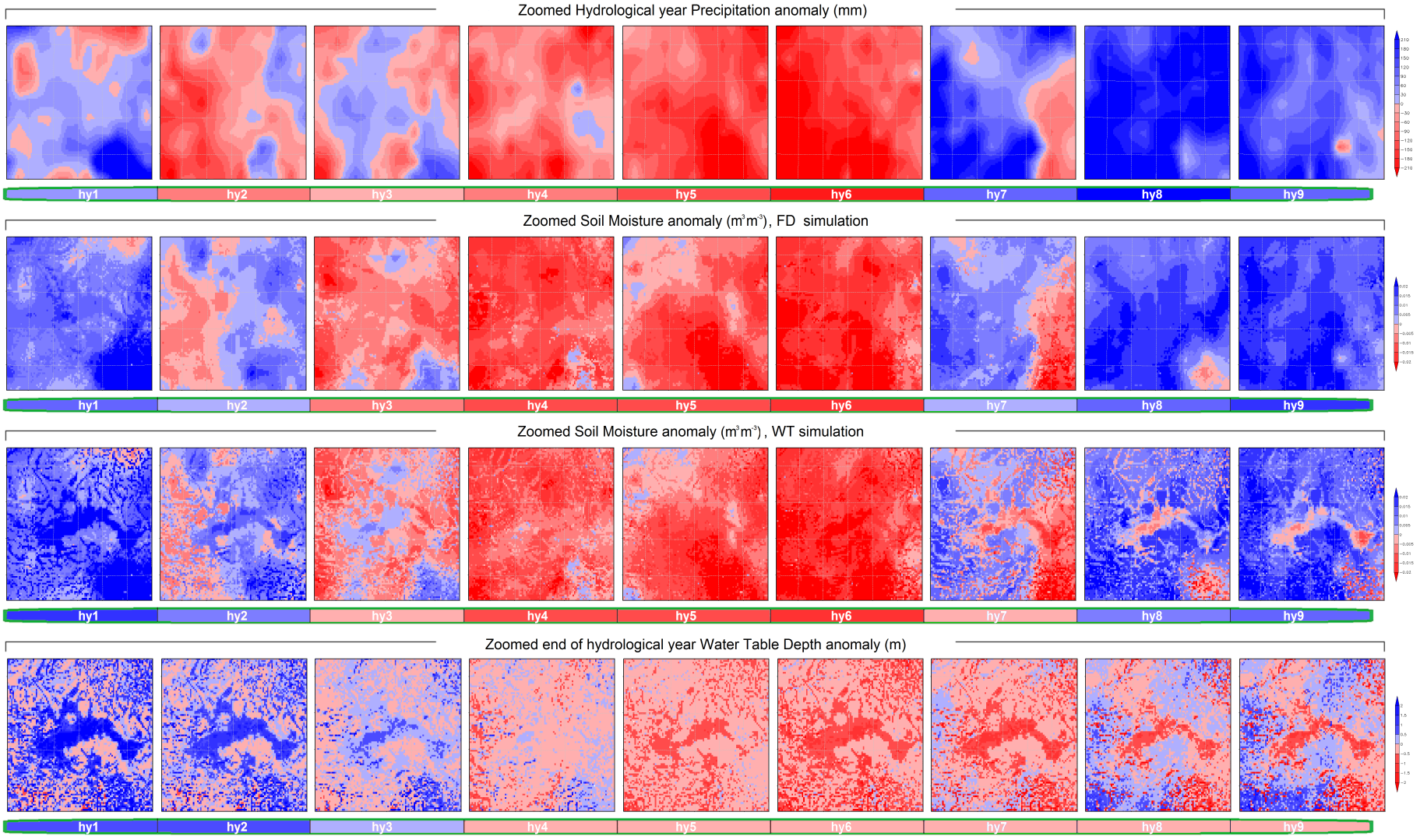

Figure 6.5: Zoomed hydrological year anomaly plots in the region highlighted with a green contour in Figure 6.2 (middle row, first plot). Each column represents a whole hydrological year (hy1 to hy9) simulated. Rows from top to bottom:: total yearly precipitation anomalies (mm), top-2 m soil moisture anomalies (m^3 m^{-3}) in the FD simulation, top-2 m year soil moisture anomalies (m^3 m^{-3}) in the WT simulation and end of hydrological year (September 1^{st}) *wtd* anomalies (m). Colour bars below each row represent the averaged anomaly value for zoomed area.

6.2.2.2 The effects of soil moisture memory on evapotranspiration (ET)

In Section 5.3, it was discussed an enhancement of ET fluxes to the atmosphere in the WT simulation. It was more significant over shallow water table regions and water scarcity periods, when analysing the seasonal means over the Iberian Peninsula. But, how will the increased soil moisture memory in the WT simulation affect land-atmosphere fluxes evolution in time?

The next set of plots in Figure 6.6 attempts to answer this question over the zoomed region, and focussing on summer ET, when the effects are clearer. The plots show, chronologically for the 9 hydrological years simulated; total yearly precipitation anomalies (top row), summer daily ET anomalies in the FD simulation (middle row), and summer daily ET anomalies in the WT simulation (bottom row).

From Figure 6.6, the following is pointed out:

- Summer ET anomalies in the FD simulation (middle row) reflect clearly the precipitation anomalies pattern for each year (top row), as do the soil moisture anomalies in the FD simulation in Figure 6.5.
- In the WT simulation, however, a new pattern of enhanced ET areas is superimposed to the precipitation induced pattern (bottom row). These enhanced ET areas correspond to shallow water table areas.
- Positive ET anomaly points (green and blue colours) are spotted in the central area during hy1 and hy2 in the WT plots, whereas the FD plots do not present these positive ET anomalies due to low precipitation rates in the area. This positive anomalies correspond to the initial shallow water table position and the soil moisture memory induced by the water table persistence.
- Other less significant positive summer ET anomalies are found in the WT plots following the Guadiana stream in the especially dry hy5, that are not observed in the FD simulation.
- The memory from the central dry years showed for soil moisture in Figure 6.5 is transferred to summer ET more clearly than the memory form the wet initialization, as the wet central area presents negative anomalies (yellow and brown colors) during the wet hy7, hy8 and hy9 in the WT simulation, whereas in the FD simulation the wet central area does not stand out and summer ET anomalies follow the precipitation anomalies pattern, being positive in nearly the whole region for the last 2 years.

From Figure 6.6 it is concluded that the increased soil moisture memory by the water persistence over the region of *La Mancha Húmeda* shown in the previous section is passed to the atmosphere in the form of ET memory from past wet or dry periods.

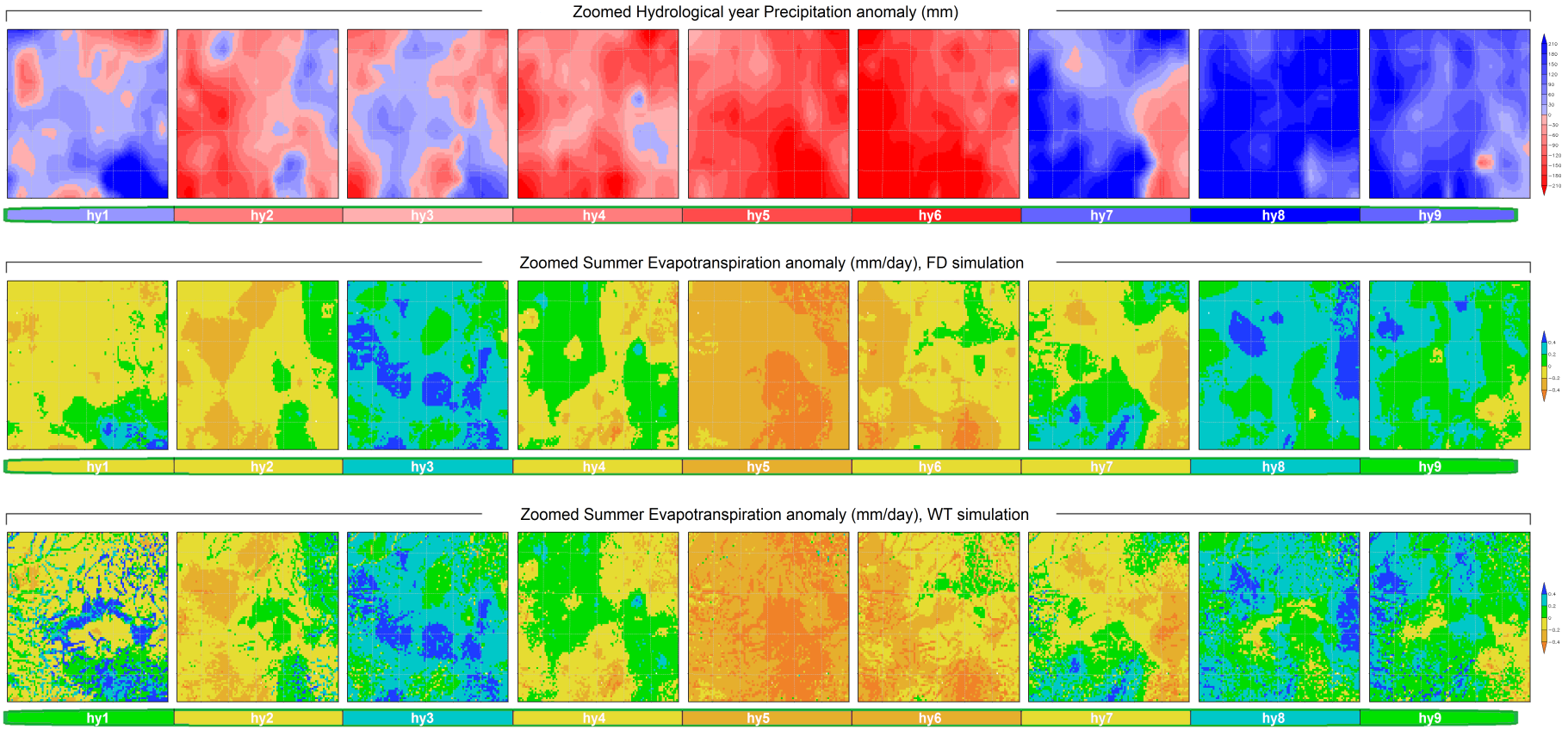

Figure 6.6: Zoomed hydrological year anomaly plots in the region highlighted with a green contour in Figure 6.2 (middle row, first plot). Each column represents a whole hydrological year (hy1 to hy9) simulated. Rows from top to bottom: total yearly precipitation anomalies (mm), summer ET anomalies (mm day^{-1}) in the FD simulation and summer ET anomalies (mm day^{-1}) in the WT simulation.

6.3 Discussion

Soil moisture memory refers to dry or wet anomalies of longer persistence in time, as compared to atmosphere conditions. The objective of this chapter is to study the water table persistence in the Iberian Peninsula and the soil moisture memory that it induces. In order to do so, hydrological year (September-August) anomalies from the 10-year WT and FD LEAFHYDRO simulations for water table depth, soil moisture, evapotranspiration and precipitation are used.

The water table shows seasonal and interannual persistence, the time evolution responds to long-term climatic conditions but not immediately to seasonal or annual peaks and lows in precipitation. The water table response to intense precipitation events and intense droughts is slow, keeping a 1-2 years delay from surface events.

The water table persistence has significant influence on soil moisture time evolution (0.43 correlation index between *wtd* and soil moisture anomalies time series, averaged for the whole peninsula), while precipitation influence decreases when the water table is considered (from 0.81 correlation between precipitation and soil moisture anomalies in the FD run to 0.72 in the WT run). But the higher influence on soil moisture is found over shallow water table regions ($wtd \leq 8$ m; groundwater and soil are hydraulically connected), where the averaged time correlation indexes with soil moisture anomalies in the WT run are 0.60 for precipitation and 0.93 for *wtd*. A closer look over the well known shallow water table region *La Mancha Húmeda* provides clearer evidences on the water table persistence influence on soil moisture and evapotranspiration fluxes memory:

- In the FD run, soil moisture patterns follow directly the time evolution of precipitation patterns.
- In the WT run, soil moisture patterns follow a combination of precipitation and *wtd* evolution patterns, reflecting the interannual water table persistence.
- The memory induced is bimodal; *1*) soil moisture "remembers" past wet conditions through the water table persistence at shallow positions, buffering drought effects, and *2*) soil moisture "remembers" past dry conditions through the water table persistence at deep positions, causing a delay in drought recovery.
- The soil moisture memory is passed to the atmosphere, as evapotranspiration time evolution patterns follow the soil moisture patterns in the WT run.

The water table persistence translates into soil moisture memory from past dry or wet periods over shallow water table regions. Then, the soil moisture memory is passed to the atmosphere as evapotranspiration memory.

Chapter 7

Water table integrated effects over the main Iberian river basins

The LEAFHYDRO WT simulation links the time evolution of the groundwater reservoir to soil moisture and water fluxes at the surface. *Miguez-Macho et al.* (2007) [83] analysed this linked behaviour using a 1-year simulation over 2 points where the water table was shallow for different reasons (lateral transport from surrounding mountains in a California site and high precipitation rate in a Mississippi site), in order to study the response of the initial version of LEAFHYDRO under different climate conditions. They found that shallow water tables can have different roles in the water cycle when the climate and topographic conditions are different; sustaining evapotranspiration (ET) during the dry season in the California site by lateral groundwater flow convergence, and delivering precipitation surplus to the rivers to maintain a steady streamflow in the Mississippi site.

The Iberian Peninsula presents different precipitation regimes. One of the goals in this work is to understand the effects of groundwater-soil interactions over different climatic regions and periods. In order to do so, the LEAFHYDRO simulations (WT and FD) results are integrated over the main Iberian basins and analysed in this chapter. River basins can be considered as independent topographically-driven regions integrating the hydrological system behaviour.

7.1 Main Iberian basins

The identification of the basins is performed using a routing scheme that follows the main rivers and all their tributaries upwards from the mouth to the sources. For

this scheme the river parameters A_d (m^2; accumulated drainage area) and fd (flow direction), calculated as detailed on Section 3.2.4, are used.

Figure 7.1 shows the river basins studied inside the Iberian Peninsula (left) and the seasonal distribution of the mean yearly precipitation over each basin for the 9 complete hydrological years simulated (right). Five basins discharge to the Atlantic Ocean; Miño, Duero, Tajo, Guadiana and Guadalquivir, and three basins discharge to the Mediterranean Sea; Ebro, Júcar and Segura.

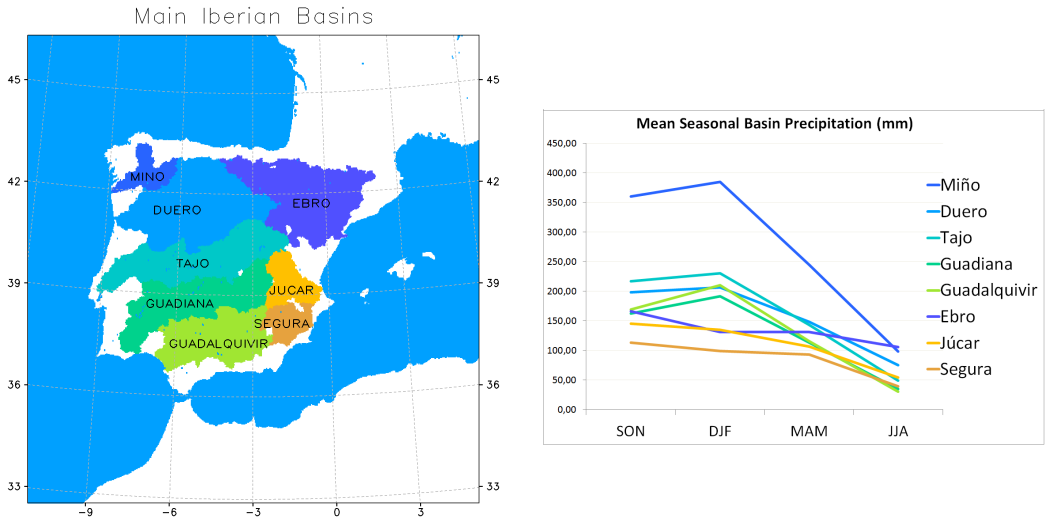

Figure 7.1: Left: Main river basins in the Iberian Peninsula, isolated using a routing scheme. Right: Mean seasonal precipitation (mm) distribution over the main Iberian basin for the 9 complete hydrological years simulated.

From Figure 7.1 (right) two distinctive precipitation regimes for the selected Iberian basins are observed:

1. **The open Atlantic basins** present a clear seasonal precipitation regime, with the wettest season in winter and the driest in summer. The total yearly precipitation decreases from north to south; the northern Miño basin reaches the maximum in the Peninsula (1088 mm yr^{-1}), then the Duero and Tajo basins in the north-centre reach similar values (628 and 640 mm yr^{-1}, respectively), and finally the southern Guadiana and Guadalquivir basins reach the minimum values (503 and 526 mm yr^{-1}, respectively).

2. **The Mediterranean basins** are drier and present a different and more moderate seasonal regime, with autumn as the wettest season and summer as the driest. However, the Ebro basin shows practically no dry season; 515 mm yr^{-1} evenly distributed through the year (only $\sim$ 50 mm difference between autumn and summer, due to high precipitation rates all throughout the year in the Pyrenees, see Figure 5.2). The Júcar and Segura basins show a clearer dry season in summer, accumulating only $\sim$ 10% of the yearly precipitation (441 and 345 mm yr^{-1}, respectively).

Based on these different precipitation regimes, in the next section an analysis of the effects of the groundwater-soil interactions and their time evolution under different climatic conditions is carried out.

7.2 Seasonal and long-term time evolution

The seasonal, annual and long-term behaviour of the groundwater-soil-atmosphere system is studied next over the main Iberian rivers basins (Figure 7.1).

The most significant influence on soil moisture and land-atmosphere fluxes within a basin takes place over shallow water tables regions ($wtd \leq 8m$), where groundwater is hydraulically connected to the upper soil crust through vertical fluxes. The shallow water table cells accumulate groundwater from the rest of the basin through lateral groundwater flux convergence and integrate its effects on soil moisture and land-atmosphere fluxes. The fraction of shallow water table cells is approximately one third of the total in the Atlantic basins – ranging from 31.6% in the Guadiana basin to 34.7% in the Miño basin –, and one fourth in the Mediterranean basins – 24.3% in the Ebro basin, 27.5% in the Júcar basin and 28.1% in the Segura basin –, as the eastern half of the peninsula presents an overall deeper water table (see Section 3.2.2). Therefore, to clearly show the impacts of groundwater, the time evolution of *wtd*, soil moisture and ET enhancement (ET difference between the WT and FD simulations) in this section is evaluated over shallow water table cells only.

7.2.1 Atlantic basins

Figures 7.2 and 7.3 show for each Atlantic basin two graphs; *1*) on the left, seasonal precipitation (blue bars) and the time series of area averaged *wtd* for the shallow water table cells (red line), WT-FD top-2 m soil moisture difference (orange line at the bottom) and WT-FD ET difference (turquoise bars at the bottom); and *2*) on the right, the power spectrum analyses for the time series of soil moisture (WT run in blue and FD run in red) and *wtd* (inside box), where again only shallow water table cells are used. Power spectrum graphs illustrate the water table effects on soil moisture for longer periods.

From Figures 7.2 and 7.3, the time evolution of the water table and its influence on soil moisture and ET under the Atlantic basins climatic conditions is evaluated, outlining the following points:

1. About *wtd* time evolution;
    - The *wtd* series (red lines in left graphs) presents a very clear annual cycle in all basins, following precipitation (blue bars in left graphs) and ET; upward trend during autumn and winter, since the surface balance

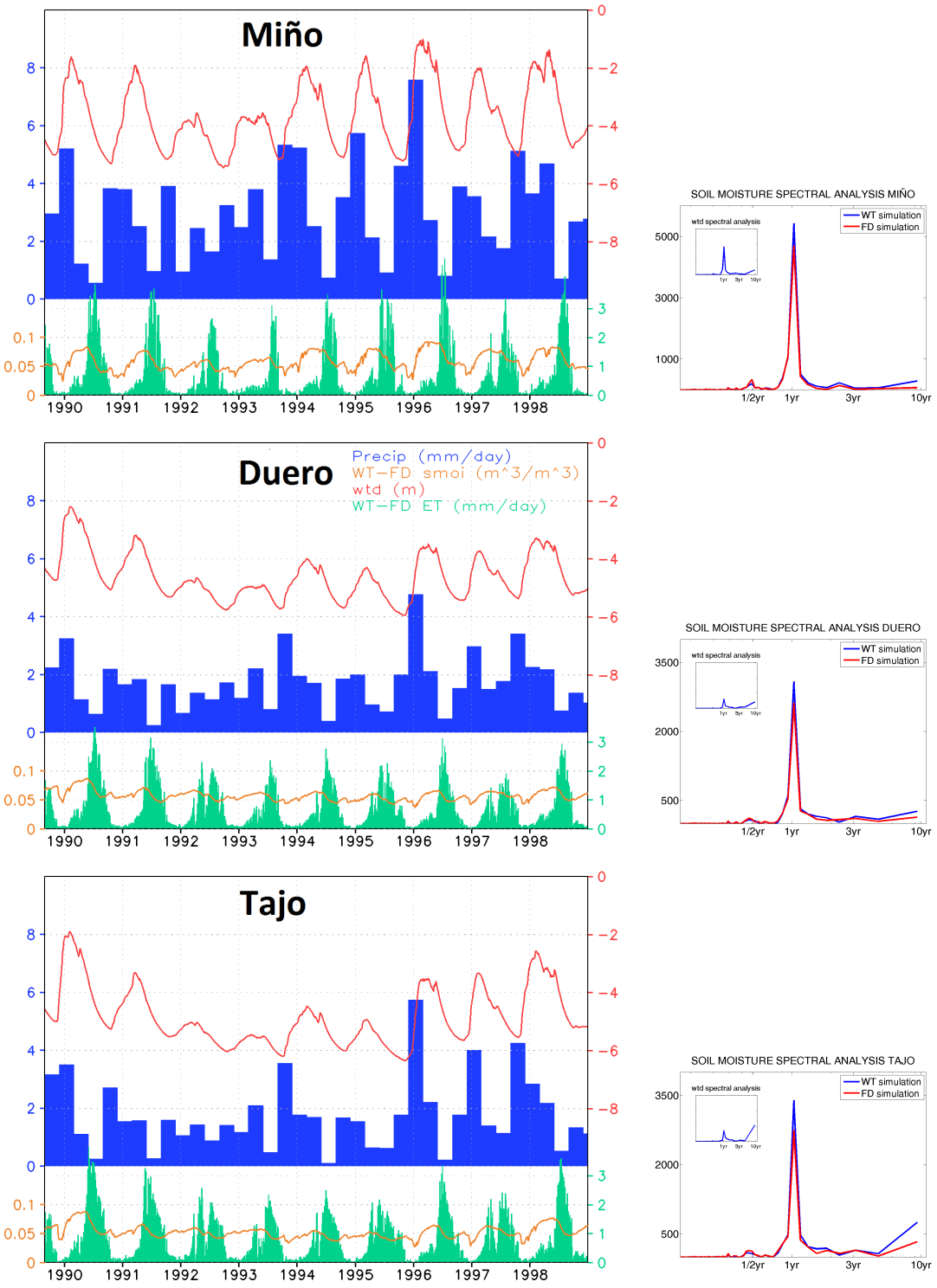

Figure 7.2: Atlantic basins time evolution, from top to bottom: Miño, Duero and Tajo. Left: Seasonal precipitation (mm day^{-1}; blue bars), and time series averaged over the shallow water table cells of *wtd* (m; red line), WT-FD top-2 m soil moisture difference (m^3 m^{-3}; orange line) and WT-FD ET difference (mm day^{-1}; turquoise bars). Right: Power spectrum analyses for top-2 m soil moisture (WT simulation in blue and FD simulation in red) and *wtd* (inside box), only shallow water table cells are used.

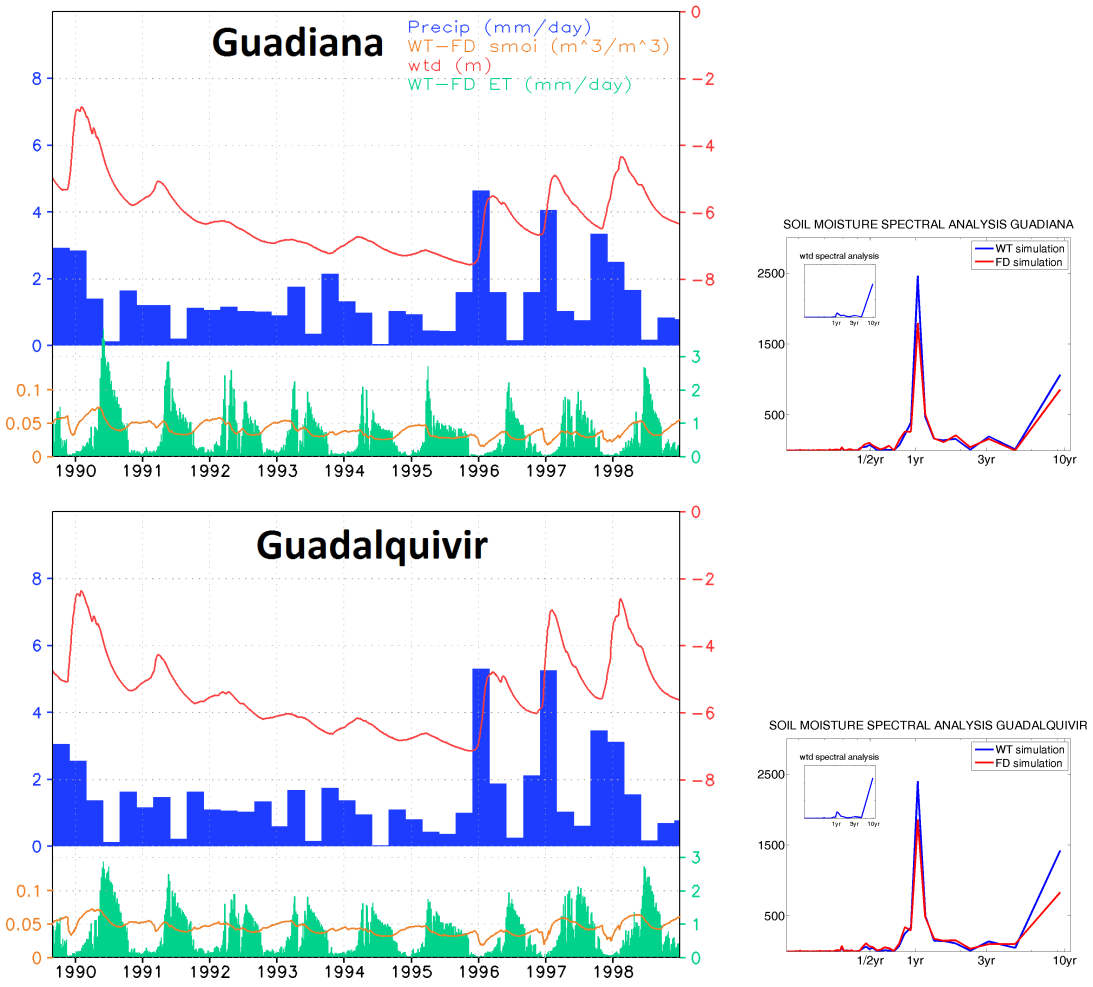

Figure 7.3: Atlantic basins time evolution (continuation from Figure 7.2): Guadiana (top) and Guadalquivir (bottom).

($P - ET$, precipitation minus evapotranspiration) is the highest, and deepening trend from late spring until the maximum depth is reached after summer, since precipitation decreases and ET demands groundwater resources through capillary rise.

- The reach of the *wtd* annual peaks and lows reflects the intensity of the rainy season.
- The long drought starting in summer 1990 and lasting until 1995/1996 is clear in the central and southern basins (a peak in autumn 1993 rainfall buffers somehow the drought in the Duero and Tajo basins). The water table follows these surface events, showing a long-term downward trend all along the drought and an upward trend after 1996, when precipitation increases significantly.
- The long-term *wtd* trends show the water table persistence. During the central drier years the deepening is slow, keeping the water table at relatively shallow positions that allow groundwater-soil interactions. Then it

takes 3 very wet rainy seasons from autumn 1996 for the water table to recover to shallower positions close to the depth it had before the drought.

2. The WT-FD soil moisture difference time series (orange lines at the bottom in left graphs) shows the water table influence on soil moisture;

   - Groundwater makes always the soil wetter in the WT run, as discussed in Chapters 5 and 6.
   - The difference in soil moisture presents lows during precipitation peaks because the soil is wet in both the FD and WT runs, and hence the water table presence is not as influential.
   - On top of the latter lows, there is a clear annual cycle in the soil moisture difference; increasing gradually from autumn towards spring since the water table presence slows down drainage during the rain season in the WT run, and then decreasing drastically in late spring or early summer.

3. The latter drastic decrease in soil moisture difference is explained by the annual peak of enhanced ET in the WT run (WT-FD ET difference; turquoise bars at the bottom in left graphs);

   - In spring ET demands are maximal and therefore ET enhancement reaches a peak; *a*) in the WT run, the water accumulated in the top soil during the rainy season due to slow drainage, plus the dominance of the upward capillarity flux later during the dry season, cover ET demands, whereas *b*) in the FD run, the top soil accumulated less water during the rainy season and there is no upward capillarity flux, resulting is less water availability to cover ET demands.
   - The timing of the enhanced ET is different for the different basins, depending on the soil water availability from precipitation. In the Miño basin the period of intense enhanced ET is short, only during summer. As water availability decreases towards the central and southern basins due to less intense and shorter rainy season, the ET enhancement period starts earlier, in early spring or even late winter (like during the central years of simulation in the Guadiana and Guadalquivir basins), and lasts longer if the dry season has been especially dry (like in 1995).
   - The amount of total yearly enhanced ET is similar for all Atlantic basins. However, the enhanced ET is more significant in relative terms as the basins are drier towards the south (see Figure 7.4), ranging from 13.3% in the Miño basin to 21.4% in the Guadalquivir basin.

     Note that data in Figure 7.4 is averaged for the whole basins (not only shallow water table cells)
   - ET is mostly energy limited in the Miño basin. In the rest of the basins ET is water limited, therefore the groundwater influence on ET enhancement over the shallow water table regions is stronger.

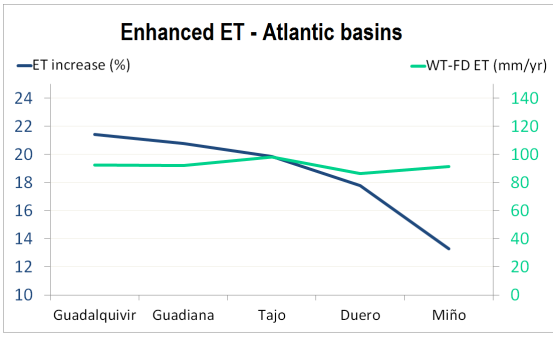

Figure 7.4: Mean yearly enhanced ET (mm yr^{-1}; turquoise line) and ET increase in the WT simulation (%) in the Atlantic basins.

4. About soil moisture memory;

   - The power spectrum (right graphs in Figures 7.2 and 7.3) show higher amplitude in the WT simulations for soil moisture at one year and longer periods, and this difference is explained by the *wtd* power spectrum (inside box), which shows most energy in the several years long fluctuations.
   - The left graphs in Figures 7.2 and 7.3 show the latter, more clearly towards the south (Guadiana and Guadalquivir basins). The soil moisture difference (orange lines) show long-term trends following the long-term *wtd* trends (red lines), and therefore the soil water availability and its potential contribution to ET keep memory from past dry or wet years. For instance, in the Guadiana basin, the WT-FD ET fluxes (turquoise bars) during the year 1996 are clearly lower than during the year 1990, even though there is higher precipitation in the previous wet season. This is explained by the soil moisture memory, showing less soil moisture difference during 1996 due to a long-term trend induced by the water table persistence.

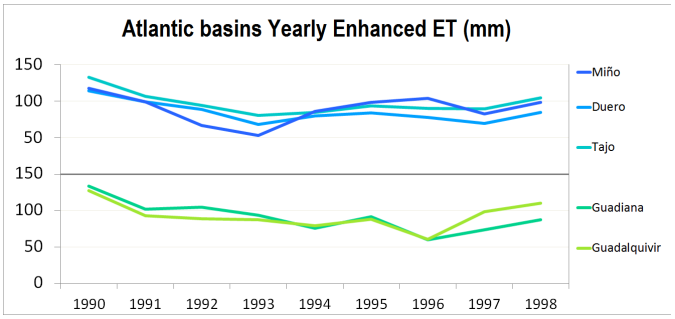

Figure 7.5: Time series for yearly Enhanced ET (WT-FD ET difference; mm) along the 9 hydrological years for the Atlantic basins.

   - The total enhanced ET yearly evolution in Figure 7.5 gives a measure of this memory for the five Atlantic basins, reflecting the long-term *wtd* trends. Hence, the ET enhancement during the dry season depends not

only on the previous wet season precipitation but also on the water table position.

7.2.2 Mediterranean basins

A different precipitation regime is observed for the Mediterranean basins (Figure 7.1); moderate with precipitation all year in the Ebro basin, and moderate wet season with a marked dry summer in the Júcar and Segura basins. The total rainfall amount decreases significantly towards the south.

Figure 7.6 shows the time evolution of the water table and its influence on soil moisture and ET under the Mediterranean basins climatic conditions. The following is noted:

1. About *wtd* time evolution;
    - The *wtd* annual cycle and the reach of its peaks and lows follow the rain and ET seasons as described for the Atlantic basins, but the intensity of the cycle is lower due to the lower accumulated precipitation during the wet season.
    - The severity of the drought (growing from north to south) is as intense as seen in the southern Atlantic basins, but its effects on the long-term water table evolution are intensified by the moderate precipitation during the last 3 years, which stops the depression of the water table during the drought but it is not enough to rise the water table position to shallower depths as seen in the Atlantic basins.
2. The annual cycle of the WT-FD soil moisture difference is lees intense than in the Atlantic basins because the wet season is more moderate. In the Ebro basins where summer is nearly as wet as winter, the cycle is harder to detect.
3. About ET enhancement in the WT run;
    - The annual cycle of the WT-FD ET is the same as seen for the Atlantic basins. However, the differences between basins are not so strong; the reach of the maximum ET enhancement is very similar every year and the intense enhancement period starts slightly earlier in the basins with less intense rainy season.
    - As observed for the Atlantic basins, the enhanced ET is more significant in relative terms as the basins are drier towards the south: 14.1% in the Ebro basin, 20.3% in the Júcar basin and 28.4% in the Segura basin.
4. About soil moisture memory;
    - The power spectrum (right graphs in Figure 7.6) shows the increase of soil moisture memory as the WT simulation present higher amplitudes for longer periods. The memory grows from north to south.

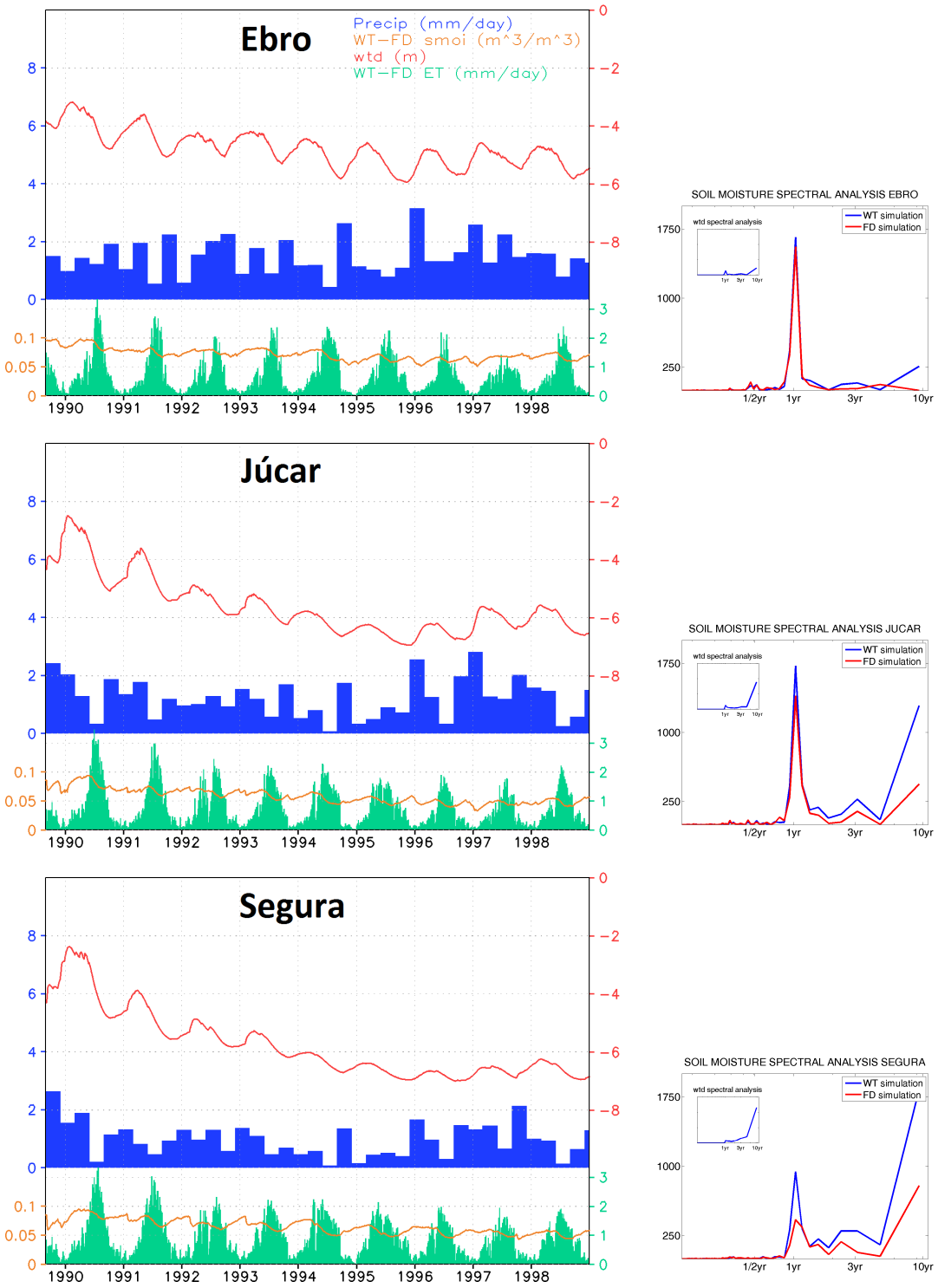

Figure 7.6: Mediterranean Basins Time Evolution, from top to bottom: Ebro, Júcar and Segura. As Figure 7.2.

- The soil moisture difference presents a long-term deepening trend during the drought and then a steady position during the last 3 years, translating the water table persistence into soil moisture memory, since the water table never recovers initial depths after the drought.

- The total enhanced ET yearly evolution in Figure 7.7, however, do not reflect the *wtd* and soil moisture difference long-term trends as clearly as seen in Figure 7.5 for the Atlantic basins. On top of the long-term trend imposed by the soil moisture difference, it reflects a different cycle imposed by summer precipitation; ET enhancement peaks during the years of lower summer precipitation (1994 in the 3 basins or 1990 in the Segura basin), and ET enhancement lows during the years of higher summer precipitation (1997 in the 3 basins or 1992 in the Ebro basin), when the dry season is absent or less clear. Hence, the ET fluxes memory is constrained in the Mediterranean basins by the intensity of the dry season, more still in the northern Ebro basin that presents less marked dry season.

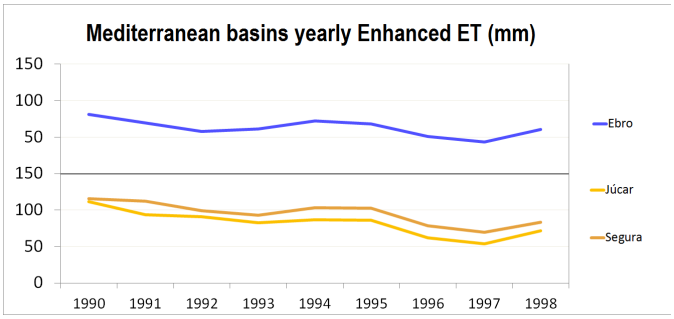

Figure 7.7: Time series for yearly Enhanced ET (mm) along the 9 hydrological years for the Mediterranean basins.

7.3 Discussion

The strength of the groundwater-soil coupling depends on the water table depth, but the effects of the coupling differ under different climatic conditions. In this chapter, the effects of the water table on soil moisture and land-atmosphere fluxes are evaluated as area averages over the main Iberian basins. Lateral flow convergence, driven by topography, distributes groundwater resources within a basin, and therefore the groundwater role in the hydrological cycle integrates the climatic conditions over the whole basin.

The Atlantic basins (Miño, Duero, Tajo, Guadiana and Guadalquivir) and the Mediterranean basins (Ebro, Júcar and Segura) present distinctive precipitation regimes; *a*) in the Atlantic, marked wet season (winter) and marked dry season (summer); *b*) in the Mediterranean, moderate wet season (autumn) with practically no dry season in the Ebro basin, and moderate wet season (autumn) and marked dry season (summer) in the Júcar and Segura basins.

During the wet season (autumn-winter) the water table rises due to drainage of precipitation, but its presence (WT run) slows down the drainage as compared to the

FD run, and therefore the soil moisture difference between both runs also follows an upward trend. Then, when the ET season begins in spring, the soil moisture difference is maximal and there is more soil water availability to meet ET demands in the WT run, causing a marked peak in the ET difference (WT-FD; ET enhancement) evolution. During spring and summer the higher soil water availability in the WT run continues due to capillary rise and there is ET enhancement until the next wet season, when the cycle starts again. The ET enhancement is more significant in the drier southern basins, where ET is more water limited (21.4% ET enhancement in the Atlantic Guadalquivir basin and 28.4% in the Mediterranean Segura basin). In the northern Miño basin where ET is not so much water limited as energy limited, the ET enhancement is less significant (13.3%).

The 10-year period of simulation presents a long drought from 1990 to 1995/1996 in all basins except the Miño basin. The water table follows the long-term precipitation trend with a slow *wtd* depression along the drought, and then gradually recovering to shallower a position during the last 3 years when precipitation is high. This long-term *wtd* trend is passed to the soil moisture difference time evolution, and therefore the soil moisture potential contribution to ET "remembers" past dry and wet years. In the Atlantic basins, the soil moisture memory induces ET memory, more clearly in the southern drier basins, where the water table influence on the land-atmosphere fluxes depends not only on the previous wet season intensity but also on the long-term *wtd* evolution. In the Mediterranean basins, this ET memory is constrained by the intensity of the dry season, since during years of especially dry summer ET enhancement increases above the *wtd* trend, and during years of especially wet summer ET enhancement decreases below the *wtd* trend.

Chapter 8

Conclusions

Land-atmosphere coupling is a key factor in climate modeling research. In this context, it is essential for the scientific community to achieve a correct representation of the processes and storages that affect land-atmosphere interactions in GCM and RCM land surface schemes. Groundwater plays an important role in the water cycle, interacting with the land surface via vertical fluxes through the water table surface and distributing water resources spatially via lateral transport, driven by topography. This thesis is intended as a step forward in the model representation of groundwater dynamics and their influence on the land-atmosphere system. To carry out the task, the Land Surface and Groundwater Model LEAFHYDRO is presented and evaluated. The model represents groundwater dynamics through 3 different interactions; *1*) two-way groundwater-soil fluxes, *2*) groundwater lateral flow, and *3*) two-way groundwater-streams exchange. 10-year simulations (WT run, with the groundwater scheme switched on, and FD run, with the groundwater scheme switched off) are performed over the Iberian Peninsula in order to study the influence of groundwater dynamics on soil moisture and evapotranspiration (ET) fluxes at seasonal and interannual timescales. The model is forced with daily analysis precipitation (0.2° spatial resolution). The water table initial condition is a high resolution Equilibrium Water Table Depth, obtained in the USC *Non-Linear Physics Group* [47] with a simple groundwater model [42], as a balance between the atmospheric influence in the form of climatic groundwater recharge ($R = P - ET - Q_h$, recharge R equals precipitation P minus evapotranspiration ET minus surface runoff Q_h) and the topographic influence in the form of gravity-driven lateral convergence. The main findings and conclusions of this research work are summarized next:

1. LEAFHYDRO is a solid tool to asses the groundwater-land surface link. Validation with observational water table depth (wtd) data shows that the model simulates a realistic water table position and time evolution; *a*) 66.0% of the observations with shallow mean water table ($wtd \leq 8$ m), which are hydraulically connected to the soil, are well represented in the model, *b*) the model captures the mean water table position along the simulated period (less than

2 m difference between observed and simulated mean *wtd* in 14.0% of the observation sites, 33.0% if only shallow observation sites are considered), and *c*) the model represents realistically the seasonal cycle and interannual trends in the *wtd* observations (32.3% of the observation sites present a correlation greater than 0.5 between observed and simulated time series).

2. The representation of streamflow closes the water budget in LEAFHYDRO, discharging ultimately to the ocean. The simulated dry season stream baseflow is maintained by groundwater, that accumulates recharge during the wet season and feeds the streams during the dry season where the water table is above the riverbed. Then, when the rainy season begins again in autumn, the streamflow recovers quickly due to surface runoff and groundwater flux. When comparing to streamflow observations, this seasonal behaviour improves the *free-drain* approach (represented by the FD run, where the water draining through the deeper soil layer in the model flows directly to the streams), that dries out the streams in summer and then takes longer to recover when the rainy season begins, since there is no gruoundwater flux.

3. Groundwater-soil exchange fluxes can be positive (upward capillary flux) to meet ET demands, since topographically-driven lateral groundwater flow and river infiltration (when the water table is below the riverbed) represent a groundwater source different to vertical fluxes. A yearly Long-Term Recharge estimation is presented that localizes zones of strong groundwater-soil coupling, as positive recharge regions, over *a*) extended interior semiarid regions of shallow water table and insufficient precipitation to meet ET demands, and *b*) river valleys of strong lateral groundwater convergence. The positive groundwater recharge, and therefore the groundwater-soil coupling, follows seasonal cycle of the surface water balance ($P-ET$, precipitation minus evapotranspiration); it is strong in spring, when ET demands are the highest in the peninsula, maximal in summer, when ET demands are lower than in spring but the precipitation is at a minimum, moderate in autumn, when precipitation is enough to cover ET demands, and minimal in winter, the season of highest precipitation and lowest ET demands.

4. The groundwater-soil coupling over shallow water table regions results in soil moisture increase with respect to the FD run. Hence, the soil moisture fields present a new wet pattern of shallow water table regions superimposed to the soil texture and climatic conditions patterns. Groundwater interactions reduce soil moisture seasonality, since the soil moisture increase ($100\Delta\eta/\eta_{FD}$, where $\Delta = \eta_{WT} - \eta_{FD}$) is greater at water scarcity seasons (spring and summer; negative $P-ET$ balance, due mostly to high ET demands in spring and minimum precipitation in summer). On average over shallow water table regions ($wtd \leq 8$ m; 31.4% of the Iberian Peninsula territory), the soil moisture increase is 24.4% in spring and 23.9% in summer, whereas in winter and autumn it is 19.3% and 20.9%, respectively.

5. The soil moisture increase translates to the atmosphere as ET enhancement (positive ET difference between the WT and FD runs). The spatial patterns of ET enhancement over the peninsula resemble the shallow water table and strong groundwater-soil coupling patterns. On average over the peninsula and comparing to the FD run, ET results 17.4% higher in the WT run (0.24 mm dαy^{-1}). ET reaches the maximum enhancement in summer (34.9%, 0.54 mm dαy^{-1}). Analysing this ET enhancement over different river basins in the peninsula, the greater values and therefore greater groundwater-soil coupling are found over the southern drier basins, where the ET is water limited (21.4% yearly ET enhancement in the Atlantic Guadalquivir basin and 28.4% in the Mediterranean Segura basin), whereas the northern Miño basin presents the weakest coupling (13.3% yearly ET enhancement), since the ET there is less water limited and more energy limited. This ET enhancement will have an important impact on precipitation recycling and seasonal forecasting in fully coupled groundwater-land-atmosphere modeling studies.

6. The water table shows strong seasonal and interannual persistence, responding to long-term climatic conditions but not immediately to seasonal or yearly peaks and lows in precipitation. Over shallow water table regions, this water table persistence induces a new pattern in soil moisture long-term evolution. Analysing yearly soil moisture anomalies over the 10-year period simulated, the new pattern of soil moisture evolution reflecting the water table pattern is captured as induced soil moisture memory. This soil moisture memory is bimodal; *1*) soil moisture "remembers" past wet conditions through the water table persistence at shallow positions, buffering drought effects, and *2*) soil moisture "remembers" past dry conditions through the water table persistence at deep positions, causing a delay in drought recovery.

7. The soil moisture memory is passed to the atmosphere as ET enhancement memory in the WT run. Analysing the integrated water table effects on the land-atmosphere system and their long-term evolution over the Iberian river basins, the *wtd* long-term evolution is reflected by the soil moisture difference (WT-FD) evolution, or in other words, the water table persistence is reflected by the long-term evolution of the soil moisture potential contribution to ET enhancement in the WT run. Hence, ET enhancement "remembers" past dry and wet years. This ET memory is strong in the Atlantic basins, but in the Mediterranean basins it is constrained by the intensity of the dry season; in years of especially dry summer ET enhancement increases above the *wtd* trend, and in years of no dry season (summer nearly as wet as winter) ET enhancement decreases below the *wtd* trend.

Future work

The line of research followed in the USC *Non Linear Physics Group* during recent years, producing initial conditions for the water table depth in the Iberian Peninsula [47], the Amazon [41], or even global patterns [40], in order to later evaluate the groundwater influence on LSM simulations as done in this thesis, has a very clear final goal: to perform fully coupled land surface and climate simulations where a dynamic water table scheme accounts for the groundwater influence on climate. Work is ongoing in this direction coupling the groundwater scheme in LEAFHYDRO to the RCM WRF. Results in convective precipitation enhancement through recycling of local water vapour evapotranspirated as enhanced ET, higher cloudiness, summer surface cooling and overall improvement of seasonal forecast are expected, contributing to the growing efforts in the scientific community to improve the model representation of the land-atmosphere system (see Section 1.3).

The LEAFHYDRO Land Surface and Groundwater Model has demonstrated to be a simple but robust tool for groundwater hydrology research, and its continuous development is planned in the USC *Non Linear Physics Group*. Some of the lines of development are; *a*) representation of the deep soil-groundwater linkage, below the soil crust resolved by the model, since deep soil properties (porosity, conductivity, capillary potential) might be misrepresented by the bottom soil layer properties, leading to slow drainage and accumulation of water in the deep soil, *b*) representation of surface runoff, triggered by heavy rainstorms or snowcover depletion from high mountainous areas, *c*) subgrid scale geological features representation, since rocks less permeable than the cell soil type in localized zones also trigger surface runoff, or *d*) dynamic vegetation representation.

Work is ongoing to elaborate a high resolution Equilibrium Water Table Depth for the Iberian Peninsula, which will reproduce the spatial distribution of the water table in the peninsula more realistically than the one used as initialization in this thesis [47], since the atmospheric influence in the form of climatic groundwater recharge will be a long-term estimation from LEAFHYDRO several decades simulation.

Bibliography

[1] Corine land cover (http://eea.europa.eu/publications/cor0-landcover). *Commission of the European Communities* (1995).

[2] Era-interim: New ecmwf reanalysis products from 1989 onwards. *ECMWF Newsletter 110* (2006).

[3] Plan especial ante situaciones de alerta y eventual sequía en la cuenca del segura [in spanish]. Tech. rep., Confederación Hidrográfica del Segura, 2006.

[4] Update on era-interim. *ECMWF Newsletter 111* (2007).

[5] Towards a climate data assimilation system: Status update of era-interim. *ECMWF Newsletter 115* (2008).

[6] *Libro Blanco del Agua en España [in Spanish]*. Centro de Publicaciones del Ministerio de Medio Ambiente, Spain, 2010.

[7] Adams, E. E., and Pielke-Sr., R. A. A parameterization of heterogeneous land surfaces for atmospheric numerical models and its impact on regional meteorology. *Monthly Weather Review 117* (1989), 2113–2136.

[8] AEMET/IMP. *Iberian Climate Atlas*. AEMET, 2011.

[9] Anyah, R. O., Weaver, C. P., Miguez-Macho, G., Fan, Y., and Robock, A. Incorporating water table dynamics in climate modeling: 2. simulated gruondwater influence on coupled land-atmosphere variability. *Journal of Geophysical Research 113* (2008).

[10] Arnold, J. C., and Allen, P. M. Automated methods for estimating baseflow and ground water recharge from streamflow records. *Journal of the American Water Resources Association 5*, 2 (1999), 411–424.

[11] Avissar, R., Avissar, P., Mahrer, Y., and Bravdo, B. A. A model to simulate response of plant stomata to environmental conditions. *Agricultural and Forest Meteorology 34*, 1 (1985), 21–29.

[12] Avissar, R., and Piel, R. A. Empirical equations for some soil hydraulic properties. *Water Resources Research 14* (1978), 601–604.

[13] Avouac, J. P. Earthquakes human-induced shaking. *Nature Geoscience 11*, 5 (2012), 763–764.

[14] Baron, J. S., Hartman, M. D., Kittel, T. G. F., Band, L. E., Ojima, D. S., and Lammers, R. B. Effects of land cover, water redistribution, and temperature on ecosystem processes in the south platte basin. *Ecological Aplications 8* (1998), 1037âĂŞ1051.

[15] Beljaars, A. C. M., Viterbo, P., Miller, M. J., and Betts, A. K. The anomalous rainfall over the united states during july 1993: Sensitivity to land surface parameterization and soil moisture. *Monthly Weather Review 1085* (1996).

[16] Belo-Pereira, M., Dutra, E., and Viterbo, P. Evaluation of global precipitation data sets over the iberian peninsula. *Journal of Geophysical Research 116* (2011).

[17] Betts, A. K. Understanting hydrometeorology using global models. *Bullentin of the American Meteorological Society 11*, 85 (2004).

[18] Brier, G. W., and Allen, R. A. Verification of weather forecast. *Compendium of Meteorology, American Meteorological Society* (1951), 841–848.

[19] Brubaker, K. L., Entekhabi, D., and Eagleson, P. S. Estimation of continental precipitation recycling. *Journal of Climate 6* (1993), 1077–1089.

[20] Burde, G. I., and Zangvil, A. The estimation of regional precipitation recycling. part 1: Review of recycling models. *Journal of Climate 14*, 12 (2001), 2497–2508.

[21] Burde, G. I., and Zangvil, A. The estimation of regional precipitation recycling. part 2: A new recycling model. *Journal of Climate 14*, 12 (2001), 2509–2527.

[22] Chanson, H., Ed. *The Hydraulics of Open Channel Flow : An Introduction.* Butterworth-Heinemann, Oxford, UK, 2nd Edition, 2004.

[23] Chase, T. N., Pielke-Sr., R. A., Kittel, T. G. F., Baron, J. S., and Stohlgren, T. J. 1998: Potential impacts on colorado rocky mountain weather and climate due to land use changes on the adjacent great plains. *Journal of Geophysical Research 104* (1999), 16673–16690.

[24] Clapp, R. B., and Hornberger, G. M. Empirical equations for some soil hydraulic properties. *Water Resources Research 14*, 4 (1978), 601–604.

[25] David, T. S., Henriques, M. O., Kurz-Besson, C., Nunes, J., Valente, F., Vaz, M., Pereira, J. S., Siegwolf, R., Chaves, M. M., Gazarini, L. C., and David, J. S. Water-use strategies in two co-occurring mediterranean evergreen oaks: surviving the summer drought. *Tree Physiology 27* (2007), 793–803.

[26] de la Torre, A. M., and Miguez-Macho, G. Groundwater influence on soil moisture memory and land-atmosphere interactions over the iberian peninsula. *In Preparation*.

[27] de Luis, M., Brunetti, M., González-Hidalgo, J. C., Longares, L. A., and Martín-Vide, J. Changes in seasonal precipitation in the iberian peninsula during 1946-2005. *Global and Planetary Change 74* (2010).

[28] de Quervain, M. R. Snow structure, heat, and mass flux through snow. *IAHS Report 107, WMO 1* (1973).

[29] de Vries, J. J. Dynamics of the interface between streams and groundwater systems in lowland areas, with reference to stream net evolution. *Journal of Hydrology 155* (1994), 39–56.

[30] de Vries, J. J. Seasonal expansion and contraction of stream networks in shallow groundwater system. *Journal of Hydrology 170* (1995), 15–26.

[31] Decharme, B., Alkama, R., Douville, H., Becker, M., and Cazenave, A. Global evaluation of the isba-trip continental hydrological system. part ii: Uncertainties in river routing simulation related to flow velocity and groundwater storage. *Journal of Hydrometeorology 11* (2010), 601–617.

[32] Decharme, B., Douville, H., Boone, A., Habets, F., and Noilhan, J. Impact of an exponential profile of saturated hydraulic conductivity within the isba lsm: Simulations over the rhone basin. *Journal of Hydrometeorology 7* (2006), 61–80.

[33] Dickinson, R. E. Land-atmosphere interaction. *Reviews of Geophysics 33* (1995), 917–922.

[34] Dingman, S. L. *Physical Hydrology. Second edition*. Waveland Prss Inc., USA, 2002.

[35] Dirmeyer, P. A., and Brubaker, K. L. Characterization of the global hydrologic cycle from a back-trajectory analysis of atmospheric water vapor. *Journal of Hydrometeorology 8* (2007), 20–37.

[36] Eltahir, E. A. B., and Bras, R. L. Precipitation recycling in the amazon basin. *Quarterly Journal of the Royal Meteorological Society 120* (1994), 861–880.

[37] Eltahir, E. A. B., and Yeh, P. J.-F. On the asymmetric response of aquifer water level to floods and droughts in illinois. *Water Resources Research 35*, 4 (1999), 1199–1217.

[38] Essenwanger, O. M. *General Climatology 1C: Classification of Climates*. Elsevier Science, 2001.

[39] et al., M. J. Recent decline in the global land evapotranspiration trend due to limited moisture supply. *Nature 467* (2011), 951–954.

[40] Fan, Y., Li, H., and Miguez-Macho, G. Global patterns of groundwater table depth. *Science 339* (2013), 940–943.

[41] Fan, Y., and Miguez-Macho, G. Potential groundwater contribution to amazon evapotranspiration. *Hydrology and Earth System Science 14* (2010), 2039–2056.

[42] Fan, Y., Miguez-Macho, G., Weaver, C. P., Walko, R., and Robock, A. Incorporating water table dynamics in climate modeling: 1. water table observations and equilibrium water table simulations. *Journal of Geophysical Research 112* (2007).

[43] Feth, J. H. Water facts and figures for planners and managers. *US Geological Survey Circular 601-I* (1973).

[44] Fetter, C. W. *Applied Hydrogeology*. Prentice-Hall, 1942.

[45] García-Hidalgo, J. F., Temino, J., and Segura, M. Holocene aeolian development in central spain; chronology, regional correlations and causal processes. *Quaternary Science Reviews 26* (2007), 2661 – 2673.

[46] Garrido, A., Martínez-Santos, P., and Llamas, M. R. Groundwater irrigation and its implications for water policy in semiarid countries: the spanish experience. *Hydrogeology Journal 14* (2006), 340–349.

[47] Gestal-Souto, L., de la Torre, A. M., and Rios-Entenza, A. The role of groundwater on the iberian climate, precipitation regime and land-atmosphere interactions. *Revista Real Academia Galega de Ciencias [In Galician] 29* (2010), 89–128.

[48] Gestal-Souto, L., Miguez-Macho, G., Fan, Y., and de la Torre, A. M. Water table depth and potential capillary flux to the land surface in the iberian peninsula. *Submitted*.

[49] Gimeno, L., Nieto, R., Trigo, R. M., Vicente-Serrano, S. M., and López-Moreno, J. I. Where does the iberian peninsula moisture come from? an answer based on a lagrangian approach. *Journal of Hydrometeorology 11* (2010), 421–436.

[50] Giorgi, F., Bi, X., and Pal, J. S. Mean, interannual variability and trends in a regional climate change experiment over europe. ii: climate change scenarios (2071âĂŞ2100). *Climate Dynamics 23* (2004).

[51] González, P. J., Tiampo, K. F., Palano, M., Cannavo, F., and Fernández, J. The 2011 lorca earthquake slip distribution controlled by groundwater crustal unloading. *Nature Geoscience 11*, 5 (2012), 821–825.

[52] Gutman, G., and Ignatov, A. The derivation of the green vegetation fraction from noaa/avhrr data for use in numerical weather prediction models. *International Journal of Remote Sensing 19*, 8 (1998), 1533–1543.

[53] Harding, R. J., Blyth, E. M., Tuinenburg, O. A., and Wiltshire, A. Land atmosphere feedbacks and their role in the water resources of the ganges basin. *Science of the Total Environment 468-469*, 3 (2013), S85–S92.

[54] Herrera, S., Gutiérrez, J. M., Ancell, R., Pons, M. R., Frías, M. D., and Fernández, J. Development and analysos of a 50-year high-resolution daily gridded precipitation dataset over spain (spain02). *Journal of Climatology* (2010).

[55] J., T., and Piel, R. A. Estimating the soil surface specific humidity. *Journal of Applied Meteorology 31* (1992), 480–484.

[56] Jarvis, A., Reuter, H. I., Nelson, A., and Guevara, E. Hole-filled seamless srtm data v4, international centre for trapical agriculture (ciat), available from http://srtm.csi.cgiar.org.

[57] Jiménez, P. A., de Arellano, J. V. G., González-Rouco, J. F., Navarro, J., Montávez, J. P., García-Bustamante, E., and Dudhia, J. The effect of heat waves and drought on surface wind circulations in the northeast of the iberian peninsula during the summer of 2003. *Journal of Climate 24* (2010), 5416–5422.

[58] Johansen, O. *Thermal conductivity of soils*. PhD thesis, Trondheim, Norway. (CRREL Draft Translation 637, 1977). ADA 044002, 1975.

[59] Koster, R. D., Dirmeyer, P. A., Guo, Z., Bonan, G., Chan, E., Cox, P., Gordon, C. T., Kanae, S., Kowalczyk, E., Lawrence, D. M., Liu, P., , Lu, C. H., Maleysev, S., McAvaney, B., Mitchell, K., Mocko, D., Oki, T., Oleson, K. W., Pitman, A., Sud, Y. C., Taylor, C. M., Verseghy, D., Vasic, R., Xue, Y., and Yamada, T. Regions of strong coupling between soil moisture and precipitation. *Science 305* (2004), 1138–1140.

[60] Koster, R. D., Mahanama, S. P. P., Yamada, T. J., Balsamo, G., Berg, A. A., Boisserie, M., Dirmeyer, P. A., Doblas-Reyes, F. J., Drewitt, G., Gordon, C. T., Guo, Z., Jeong, J. H., Lawrence, D. M., Lee, W. S., Li, Z., Luo, L., Maleysev, S., Merryfield, W. J., Seneviratne, S. I., Stanelle, T., van den Hurk, B. J. J. M., Vitart, F., and Wood, E. F. Contribution of land surface initialization to subseasonal forecast skill: First results from a multi-model experiment. *Geophysical Research Letters 37* (2010).

[61] Koster, R. D., and Suarez, M. J. Soil moisture memory in climate models. *Journal of Hydrometeorology 2* (2001), 558–570.

[62] Landsberg, H. E. Climatic aspects of droughts. *Bullentin of the American Meteorological Society 63* (1982), 593–598.

[63] Lee, T. J. *The impact of vegetation on the atmospheric boundary layer and convective storms*. PhD thesis, Colorado State Univ., Fort Collins, CO (United States), 1992.

[64] Lee, T. J., Pielke-Sr., R. A., and Mielke-Jr., P. W. Modeling the clear-sky surface energy budget during fife 1987. *Journal of Geophysical Research 100* (1995), 25585–25593.

[65] Lehner, B., Verdin, K., and Jarvis, A. New global hydrography derived from spaceborne elevation data. *EOS, Transactions: AGU 89*, 10 (2008), 93–94.

[66] Leung, L. R., Huang, M., and Qian, Y. Climate-soil-vegetation control on groundwater table dynamics and its feedbacks in a climate model. *Climate Dynamics 36* (2011), 57–81.

[67] Lo, M., and Famiglietti, J. S. Effect of water table dynamics on land surface hydrologic memory. *Journal of Geophysical Research 115* (2010).

[68] Lorenz, R., Jaeger, E. B., and Seneviratne, S. I. Persistence of heat waves and its link to soil moisture memory. *Geophysical Research Letters 37*, 9 (2010).

[69] Lorenzo-Lacruz, J., Morán-Tejeda, E., Vicente-Serrano, S. M., and López-Moreno, J. I. Streamflow droughts in the iberian peninsula between 1945 and 2005: spatial and temporal patterns. *Hydrology and Earth System Sciences 17* (2013), 119–134.

[70] Louis, J. F., Tiedtke, M., and Geleyn, J. F. A short history of the pbl parameterization at ecmwf. *Proceedings from the ECMWF Workshop on Planetary Boundary Layer Parameterization (25-27 November 1981)* (1981), 59–79.

[71] Lubczynski, M. W. The hydrogeological role of trees in water-limited environments. *Hydrogeology Jounal 17*, 1 (2009).

[72] Lucas-Pilcher, P., Arora, V. K., Caya, D., and Laprise, R. Implementation of a large-scale variable velocity river flow routing algorithm in the canadian regional climate model (crcm). *Atmosphere-Ocean 41*, 2 (2003).

[73] Mahrer, Y., and Pielke-Sr., R. A. A numerical study of the airflow over irregular terrain. *Contributions to Atmospheric Physics 50* (1977), 98–113.

[74] Martín-Vide, J., and López-Bustins, J. A. The western mediterranean oscillation and rainfall in the iberian peninsula. *International Journal of Climatology 26* (2006).

[75] Martínez-Cortina, L., Mejías-Moreno, M., Díaz-Munoz, J. A., Morales-García, R., and Ruiz-Hernández, J. M. Estimation of groundwater resources in the upper guadiana basin together with some observations concerning the definitions of renewable and available resources. *Boletin Geológico y Minero [In Spanish] 112*, 1 (2011), 17–36.

[76] Martínez-Gil, F. J. *La nueva cultura del agua en España [in Spanish]*. Bakeaz-Coagret, 1997.

[77] Maxwell, R. M., and Kollet, S. J. Interdependence of groundwater dynamics and land-energy feedbacks under climate change. *Nature Geoscience 1* (2008), 665–669.

[78] Maxwell, R. M., and Miller, N. L. Development of a coupled land surface and groundwater model. *Journal of Hydrometeorology 6* (2005).

[79] McCumber, M. C., and Pielke-Sr., R. A. Simulation of the effects of surface fluxes of heat and moisture in a mesoscale numerical model, part i: Soil layer. *Journal of Geophysical Research 86* (1981), 9929–9938.

[80] Mejías-Moreno, M., López-Gutiérrez, J., and Martínez-Cortina, L. Hydrogeological characteristics and groundwater evolution of the western la mancha unit: the influence of the wet period 2009-2011. *Boletin Geológico y Minero [In Spanish] 132*, 2 (2012), 91–108.

[81] Miguez-Macho, G., and Fan, Y. The role of groundwater in the amazon water cycle: 1. influence on seasonal streamflow, flooding and wetlands. *Journal of Geophysical Research 117* (2012).

[82] Miguez-Macho, G., and Fan, Y. The role of groundwater in the amazon water cycle: 2. influence on seasonal soil moisture and evapotranspiration. *Journal of Geophysical Research 117* (2012).

[83] Miguez-Macho, G., Fan, Y., Weaver, C. P., Walko, R., and Robock, A. Incorporating water table dynamics in climate modeling: 2. formulation, validation and soil moistur simulation. *Journal of Geophysical Research 112* (2007).

[84] Morales, A., Olcina, J., and Rico, A. M. The different perceptions about droughts in spain: adaptations and correction systems. *Investigaciones Geográficas [in Spanish] 23* (2000), 5–46.

[85] Moriasi, D. N., Arnold, J. G., Liew, M. W. V., Bingner, R. L., Harmel, R. D., and Veith, T. L. Model evaluation guidelins for systematic quantification of accuracy in watershed simulations. *American Society of Agricultural and Biological Engineers 50*, 3 (2007), 885–900.

[86] Naranjo, L., and Pérez-Mununzuri, V., Eds. *A variabilidade natural do clima en Galicia [in Galician]*. Xunta de Galica, Fundación Caixagalicia, 2006.

[87] Nash, J. E., and Sutcliffe, J. V. River flow forecasting through conceptual models part i – a discussion of principles. *Journal of Hydrology 10*, 3 (1970), 282–290.

[88] Niu, G., Yang, Z., Dickinson, R. E., and Gulden, L. E. Development of a simple groundwater model for use in climate models and evaluation with gravity recovery and climate experiment data. *Journal of Geophysical Research 112* (2007).

[89] Orth, R., Koster, R. D., and Seneviratne, S. I. Inferring soil moisture memory from journal of hydrometeorologystreamflow observations using a simple water balance model. *Journal of Hydrometeorology* (2013), Ahead of Print.

[90] Paredes, D., Trigo, R. M., García-Herrera, R., and Franco-Trigo, I. Understanding predipitation changes in iberia in early spring: Weather typing and storm-tracking approaches. *Journal of Hydrometeorology 7* (2006).

[91] Pielke-Sr., R. A., Avissar, R., Raupach, M., Dolman, H., Zeng, X., and Denning, S. Interactions between the atmosphere and terrestrial ecosystems: Influence on weather and climate. *Global Change Biology 4* (1998), 101–115.

[92] Prudhommea, C., Giuntoli, I., Robinson, E. L., Clark, D. B., Arnell, N. W., Dankers, R., Fekete, B. M., Franssen, W., Gosling, D. G. N., Hagemann, S., Hannah, D. M., Kim, H., Masaki, Y., Satoh, Y., Stacke, T., Wada, Y., and Wisser, D. Hydrological droughts in the 21st century, hotspots and uncertainties from a global multimodel ensemble experiment. *Proceedings of the National Academy of Sciences of the United States of America (PNAS)* (2013), Early Edition.

[93] Rios-Entenza, A., and Miguez-Macho, G. Moisture recycling and the maximum of precipitation in spring in the iberian peninsula. *Climate Dynamics* (2013).

[94] Roads, J., and Betts, A. Ncep-ncar and ecmwf reanalysis surface water and energy budgets for the mississippi river basin. *Journal of Hydrometeorology 1* (1999).

[95] Robock, A., Vinnikov, K. Y., Srinivasan, G., Entin, J. K., Hollinger, S. E., Speranskaya, N. A., and Namkhai, A. The global soil moisture data bank. *Bullentin of the American Meteorological Society 6*, 81 (1999).

[96] Rodell, M., Houser, P. R., Jambor, U., Gottshalck, J., Mitchell, K., Meng, C. J., Arsenault, K., Cosgrove, B., Radakovich, J., Bosilovich, M., Entin, J. K., Walker, J. P., Lohmann, D., and D, D. T. The global land data assimilation system. *Bullentin of the American Meteorological Society 85* (2004).

[97] Ruíz, J. M. *Desarrollo de un Modelo Hidrológico Conceptual - Distribuido de Simulación continua integrado con un sistema de información geográfica*. PhD thesis, E.T.S. Ing. de Caminos, Canales y Puertos, Universidad Politécnica de Valencia, 1998.

[98] Sánchez, N., Martínez-Fernández, J., Calera, A., Torres, E., and Pérez-Gutiérrez, C. Combining remote sensing and in situ soil moisture data for the application and validation of a distributed water balance model (hidromore). *Agricultural Water Management 98* (2010), 69–78.

[99] Schär, C., Lüthi, D., and Beyerle, U. The soil-precipitation feedback: A process study with a regional climate model. *Journal of Climate 12*, 3 (1999), 722–741.

[100] Schär, C., Vidale, P. L., Lüthi, D., Frei, C., Häberli, C., Liniger, M. A., and Appenzeller, C. The role of increasing temperature variability in european summer heatwaves. *Nature 427* (2004).

[101] Schlosser, C. A., and Milly, P. C. D. A model-based investigation of soil moisture predictability and associated climate predictability. *Journal of Hydrometeorology 3*, 4 (2002).

[102] Sellers, P. J., Sud, Y. M. Y. C., and Dalcher, A. A simple biosphere model (sib) for use within general circulation models. *Journal of the Atmospheric Sciences 43*, 6 (1986), 505–531.

[103] Seneviratne, S. I., and Koster, R. D. A revised framework for analyzing soil moisture memory in climate data: Derivation and interpretation. *Journal of Hydrometeorology 13*, 1 (2012).

[104] Seneviratne, S. I., Koster, R. D., Guo, Z., Dirmeyer, P. A., Kowalczyk, E., Lawrence, D., Liu, P., Lu, C. H., Mocko, D., Oleson, K. W., and Verseghy, D. Mean, interannual variability and trends in a regional climate change experiment over europe. ii: climate change scenarios (2071–2100). *Journal of Hydrometeorology 7* (2006).

[105] Seneviratne, S. I., Lüthi, D., Litschi, M., and Schär, C. Land-atmosphere coupling and climate change in europe. *Nature 443* (2006).

[106] Serrano, L., and Zunzunegui, M. The relevance of preserving temporary ponds during drought: hydrological and vegetation chandes over a 16-year period in the doñana national park (south-west spain). *Aquatic Conservation: Marin and Freshwater Ecosystems 18* (2008), 261–279.

[107] Shiklomanov, I. A., and Rodda, J. C., Eds. *World water resources at the beggining of the 21st century*. Press Syndicate of the University of Cambridge, 2003.

[108] Sobrino, J. A., Gómez, M., Jiménez-Munoz, J. C., and Olioso, A. Application of a simple algorithm to estimate daily evapotranspiration from noaa-avhrr images for the iberian peninsula. *Remote Sensing of Environment 110*, 2 (2007), 139–148.

[109] Sutanudjaja, E. H., de Jong, S. M., van Geer, F. C., and Bierkens, M. F. P. Using ers spaceborne microwave soil moisture observations to predict groundwater head in space and time. *Remote Sensing Environment 138* (2013).

[110] Tremback, C. J., and Kessler, R. A surface temperature and moisture parameterization for use in mesoscale models. *Seventh Conference on Numerical Weather Prediction, Montreal, PQ, Canada, American Meteorological Society* (1985), 355–358.

[111] Vergnes, J. P., Decharme, B., Alkama, R., Martin, E., Habets, F., and Douville, H. A simple groundwater scheme for hydrological and climate applications: Description and offline evaluation over france. *Journal of Hydrometeorology 13* (2012), 1149–1171.

[112] Vicente-Serrano, S. M. Spatial and temporal analysis of droughts in the iberian peninsula (1910-2000). *Hydrological Sciences Journal 51* (2006), 83–97.

[113] Vidale, P. L., Lüthi, D., Wergmann, R., and Schär, C. The anomalous rainfall over the united states during july 1993: Sensitivity to land surface parameterization and soil moisture. *Climate Change 81* (2006).

[114] Vincke, C., and Thiry, I. Water table is a relevant source for water uptake by a scots pin (pinus silvestris l.) stand: Evidences from continuous evapotranspiration and water table monitoring. *Agricultural and Forest Meteorology 148* (2008).

[115] Walko, R. L., Band, L. E., Baron, J. S., Kittel, T. G. F., Lammers, R., Lee, T. J., Ojima, D., Pielke-Sr., R. A., Taylor, C., Tague, C., Tremback, C. J., and Vidale, P. L. Coupled atmosphere-biophysics-hydrology models for environmental modeling. *Journal of Applied Meteorology and Climatology 39* (2000), 934–944.

[116] Wilhite, S. A., and Glantz, M. H. Understanding the drought phenomenon: the role of definitions. *Water International 10* (1985), 111–120.

[117] Yeh, P. J.-F., and Eltahir, E. A. B. Representation of water table dynamics in a land surface scheme. part i: Model development. *Journal of Climate 18* (2004), 1861–1880.

[118] Yeh, P. J.-F., and Eltahir, E. A. B. Representation of water table dynamics in a land surface scheme. part ii: Subgrid variability. *Journal of Climate 18* (2004), 1881–1901.

[119] Yuan, X., Xie, Z., Zheng, J., Tian, X., and Yang, Z. Effects of water table dynamics on regional climate: A case study over east asian monsoon area. *Journal of Geophysical Research 113* (2008).

[120] Zaitchik, B. F., Santanello, J. A., Kumar, S. V., and Peters-Lidard, C. D. Representation of soil moisture feedbacks during drought in nasa unified wrf (nu-wrf). *Journal of Hydrometeorology 14*, 1 (2013).

[121] Zeng, X., Zhao, M., and Dickinson, R. E. Intercomparison of bulk aerodynamic algorithms for the computation of sea surface fluxes using the toga coare and tao data. *Journal of Climate 11* (1998), 2628–2644.